JYU DISSERTATIONS 323

Xin Ding

Halogen Bond in Crystal Engineering

Structural Studies on Crystals with Neutral Ruthenium Centered Complexes and 1-(4-pyridyl)-4-thiopyridine Zwitterion as Halogen Bond Acceptors

UNIVERSITY OF JYVÄSKYLÄ
FACULTY OF MATHEMATICS
AND SCIENCE

JYU DISSERTATIONS 323

Xin Ding

Halogen Bond in Crystal Engineering

Structural Studies on Crystals with Neutral Ruthenium Centered Complexes and 1-(4-pyridyl)-4-thiopyridine Zwitterion as Halogen Bond Acceptors

Esitetään Jyväskylän yliopiston matemaattis-luonnontieteellisen tiedekunnan suostumuksella
julkisesti tarkastettavaksi joulukuun 17. päivänä 2020 kello 12.

Academic dissertation to be publicly discussed, by permission of
the Faculty of Mathematics and Science of the University of Jyväskylä,
on December 17, 2020, at 12 o'clock noon.

JYVÄSKYLÄN YLIOPISTO
UNIVERSITY OF JYVÄSKYLÄ

JYVÄSKYLÄ 2020

Editors
Matti Haukka
Department of Chemistry, University of Jyväskylä
Päivi Vuorio
Open Science Centre, University of Jyväskylä

Permanent link to this publication: http://urn.fi/URN:ISBN:978-951-39-8420-5

ISBN 978-951-39-8420-5 (PDF)
URN:ISBN:978-951-39-8420-5
ISSN 2489-9003

ABSTRACT

Ding, Xin
Halogen bond in crystal engineering: structural studies on crystals with neutral ruthenium centered complexes and 1-(4-pyridyl)-4-thiopyridine zwitterion as halogen bond acceptors
Jyväskylä: University of Jyväskylä, 2020, 59 p.
(JYU Dissertations
ISSN 2489-9003; 323)
ISBN 978-951-39-8420-5 (PDF)

This work focuses on using both ruthenium complexes and a newly synthesized organic zwitterion as halogen bond (XB) acceptors to construct a series of crystal structures and to investigate the selectivity of halogen bond. *p*-Diiodotetrafluorobenzene (*p*-DITFB) was used as the halogen bond donor to co-crystalize with $[Ru(bpy)(CO)_2X_2]$ (X=Cl, Br, I), yielding a series of crystals **1-3**. The strength of X···I in **1-3** follows the order of Ru-Cl>Ru-Br>Ru-I, indicating electrostatic nature of the XBs. Isomorphic $[Ru(bpy)(CO)_2Cl_2]$•*p*-DITFB (**1)** and $[Ru(bpy)(CO)_2Br_2]$•*p*-DITFB (**2)**, with both halido ligands involved in XB, form zig-zag chains, which expand into 3D network with solvent accommodating voids. $[Ru(bpy)(CO)_2I_2]$•*p*-DITFB (**3**) forms linear chains with only one of the two iodo ligands involved in XB. The neighboring linear chains are further linked together *via* F···O interaction to form 3D networks.

The XB preference for S over N in the sulfur coordinated thiocyanate ligand of $[Ru(bpy)(CO)_2(S\text{-}NCS)_2]$ was studied with I_2 as XB donor. The computational analysis results, which demonstrate no major energy differences between SCN···I and NCS···I system, suggest the pivotal role of packing effect. Moreover, because of the narrower energy gap between HOMO and LUMO in $[Ru(bpy)(CO)_2(S\text{-}NCS)_2]$•$2I_2$ than in $[Ru(bpy)(CO)_2(S\text{-}NCS)_2]$•$I_2$ (**4**), the singly interacting adduct (**4**) was the only experimentally obtained structure, regardless of the amount of I_2 used.

A new bidentate XB acceptor, 1-(4-pyridyl)-thiopyridine (PTP), incorporating both bidentate sp^3-S and monodentate sp^2-N, has been synthesized. Three crystals (**5-7**) were obtained from co-crystalizing the PTP with *p*-diiodobenzene (DIB), *p*-DITFB, and iodopentafluorobenzene (IPFB), respectively. The structure of **5-7** demonstrate the selectivity of XB between S and N as well. All the results from this study prove that XB is a viable tool in constructing extended metal networks with $[Ru(bpy)(CO)_2X_2]$, and, however, indicate that all the other intermolecular interactions, along with XB, also exert unneglectable impact on the crystal formation.

Keywords: crystal engineering, halogen bond, electrostatic, selectivity

TIIVISTELMÄ

Ding, Xin
Halogeenisidos kiderakenteiden muokkauksessa: neutraalien ruteniumkompleksien ja halogeneenisidosakseptorikahtaisionin 1-(4-pyridyyli)-4-tiopyridiinin kiderakennetutkimuksia
Jyväskylä: Jyväskylän yliopisto, 2020, 59 s.
(JYU Dissertations
ISSN 2489-9003; 323)
ISBN 978-951-39-8420-5 (PDF)

Väitöskirjassa keskitytään erityisesti ruteniumkompleksien ja työssä syntetisoidun kahtaisionin käyttäytymiseen halogeenisidosakseptorina. Käyttämällä *p*-dijododetrafluorobentseeniä (*p*-DITFB) halogeenisidosdonorina ja ruteniumyhdisteitä [Ru(bpy)(CO)$_2$X$_2$] (X=Cl, Br, I) akseptoreina valmistettiin sarja halogeenisidoksia sisältäviä kiderakenteita (**1-3**). Tässä sarjassa halogeenisidoksen ,X···I, sidosvoimakkuuden osoitettiin kasvavan järjestyksessä Ru-Cl>Ru-Br>Ru-I, mikä osoittaa halogeenisidoksen olevan luonteeltaan pääasiassa elektrostaattinen. Isomorfisissa [Ru(bpy)(CO)$_2$Cl$_2$]•*p*-DITFB (**1**) ja [Ru(bpy)(CO)$_2$Br$_2$] •*p*-DITFB (**2**) rakenteissa molemmat halidoligandit osallistuvat halogeenisidokseen. Rakenteen ”siksak”-ketjut muodostavat 3D-verkostoja liuottimen täyttäessä rakenteen aukkoja. [Ru(bpy)(CO)$_2$I$_2$]•*p*-DITFB (**3**) muodostaa lineaarisia ketjuja, joissa vain yksi kahdesta jodiligandista osallistuu halogeenisidokseen. Vierekkäiset lineaariset ketjut kytkeytyvät edelleen toisiinsa F···O – vuorovaikutuksella ja muodostavat 3D-verkoston.

Rikin ja typen taipumusta muodostaa halogeenisidoksia I$_2$:n kanssa tutkittiin tarkastelemalla rikkikoordinoitunutta tiosyanaattia sisältävän [Ru(bpy)(CO)$_2$(S-NCS)$_2$] yhdisteen ja I$_2$:n muodostamaa rakennetta. Teoreettisten laskennallisten tulosten perusteella suuria energiaeroja SCN···I ja NCS···I vuorovaikutusten välillä ei ole. Kuitenkin kokeellisesti vain NCS···I [Ru(bpy)(CO)$_2$(S-NCS)$_2$]•I$_2$ (**4**) rakenne onnistuttiin valmistamaan. Tulokset viittaavat siihen, että syy NCS···I muodon suosimiseen löytyy kiderakenteessa olevien heikkojen vuorovaikutusten yhteisvaikutuksesta yksittäisen halogeenisidoksen sijaan. Vertaamalla laskennallisesti rakenteita, joissa vain toinen tiosyanaattiligandi on muodostanut halogeenisidoksen rakenteisiin, joissa molemmat SCN-ligandit osallistuvat halogeenisidoksiin, on osoitettu, että niiden rajaorbitaaleista korkeimman miehitetyn molekyyliorbitaalien (HOMO) energiat ovat hyvin lähellä toisiaan. Sitä vastoin alin miehittämätön orbitaali (LUMO) on stabiilimpi [Ru(bpy)(CO)$_2$(S-NCS)$_2$]•I$_2$ (**4**) yhdisteellä, jonka johdosta [Ru(bpy)(CO)$_2$(S-NCS)$_2$]•I$_2$ on ainut kokeellisesti saatu rakenne riippumatta synteesissä käytetyn I$_2$:n määrästä.

Väitöskirjatutkimuksessa syntetisoitiin uusi kaksihampainen XB-akseptori, 1-(4-pyridyyli)-tiopyridiini (PTP), jossa on kaksihampainen sp^3-S ja yksihampainen sp^2-N. Työssä saatiin kolme kiderakennetta (**5-7**) kiteyttämällä XB-akseptori *p*-dijodibentseenin (DIB), *p*-DITFB:n, ja jodopentafluorobentseenin (IPFB) kanssa. Rakenteet (**5-7)** osoittavat myös XB:n selektiivisyyden rikin ja typen välillä. Tämän tutkimuksen tulokset osoittavat, että XB on käyttökelpoinen vuorovaikutus, jonka avulla on mahdollista liittää yhteen halogeeniligandeja sisältäviä yhdisteitä, kuten [Ru(bpy)(CO)$_2$X$_2$], laajemmiksi verkostoiksi. Pelkkä halogeenisten tarkastelu ei kuitenkaan riitä selittämään muodostuvia rakenteita vaaan kaikki vuorovaikutukset on otettava huomioon. vuorovaikutuksilla halogeenisidokset mukaan lukien on myös vaikutusta kiteiden muodostumiseen.

Author's address

Xin Ding
Department of Chemistry
University of Jyväskylä
P.O. Box 35
FI-40014 University of Jyväskylä
Finland
xin.x.ding@jyu.fi

Supervisors

Professor Matti Haukka
Department of Chemistry
University of Jyväskylä
Jyväskylä, Finland

Dr. Elina Laurila
Department of Chemistry
University of Jyväskylä
Jyväskylä, Finland

Reviewers

Docent Sirpa Jääskeläinen
Department of Chemistry
University of Eastern Finland
Joensuu, Finland

Assoc. Prof. Giancarlo Terraneo
Department of Chemistry, Materials, and Chemical Engineering "Giulio Natta"
Politecnico di Milano
Milan, Italy

Opponents

Assoc. Prof. Dominik Cinčić
Faculty of Science
Department of Chemistry
University of Zagreb
Zagreb, Croatia

ACKNOWLEDGEMENTS

This thesis work was carried out at the Department of Chemistry, University of Jyväskylä. Financial support from Academy of Finland, grant number 130571 and 295881, is greatly acknowledged.

I want to express my sincerest gratitude to my supervisor, Professor Matti Haukka, for his unreserved guidance and enlightenment to me during the whole study. His unconditional support and trust have been the most treasured and the most appreciated. I thank Professor Kari Rissanen for his advices. I want to thank Dr. Matti Tuikka for introducing me to the wonderful world of crystal engineering and great experiences of working together. I thank Docent Pipsa Hirva for the great collaboration. I also want to show my gratitude to Dr. Elina Laurila for both her advices and friendship.

Also, a great appreciation goes to my dear friend Dr. Kalle Kolari for his countless helps. I also thank Dr. Laura Koskinen, a great friend, for all the encouragement and friendship. I am also grateful for Lauri Kivijärvi for all merry conversations and helps.

Lastly, I want to thank my family for always being there for me. All of you mean everything to me.

Stockholm 14.07.2020
Xin Ding

LIST OF ORIGINAL PUBLICATIONS

This dissertation is based on the original publications listed below.

I. Xin Ding, Matti Tuikka, Pipsa Hirva and Matti Haukka, Halogen Bond Preferences of Thiocyanate Ligand Coordinated to Ru (II) via Sulphur Atom, *Solid State Sci.* **2017**, 17, 8-13.

II. Xin Ding, Matti Tuikka, Kari Rissanen and Matti Haukka, Extended Assemblies of $Ru(bpy)(CO)_2X_2$ (X=Cl, Br, I) Molecules Linked by 1, 4-Diiodotetrafluoro-Benzene (DITFB) Halogen Bond Donors, *Crystals*. **2019**, 9, 319.

III. Xin Ding, Matti Tuikka and Matti Haukka, A Novel Halogen Bond Acceptor: 1-(4-Pyridyl)-4-Thiopyridine (PTP) Zwitterion, Xin Ding, Matti Tuikka and Matti Haukka, *Crystals*. **2020**, 10, 165.

The author carried out all the experimental synthesis, crystallization, and initial X-ray structure characterization for the publication of I-III, except the computational calculation of paper I. The author drafted all the three papers.

Other publications, but not included in the thesis

I. Xin Ding, Matti Tuikka and Matti Haukka, Halogen Bonding in Crystal Engineering. DOI: 10.5772/48592.

II. Xin Ding, Matti J. Tuikka, Pipsa Hirva, Vadim Yu. Kukushkin, Alexander S. Novikov and Matti Haukka. Fine-tuning Halogen Bonding Properties of Diiodine through Halogen-Halogen Charge Transfer – Extended $[Ru(2,2'\text{-bipyridine})(CO)_2X_2]\bullet I_2$ Systems (X=Cl, Br, I), *CrystEngComm,* **2016**, 18, 1987-1995.

III. Maria V. Chernysheva, Margrita Bulatova, Xin Ding, and Matti Haukka, Influences of Substituents in the Aromatic Ring on the Strength of Halogen Bonding in Iodobenzene Derivatives. *Cryst. Growth Des.* **2020**, 20, 11, 7197-7210.

CONTENTS

1 INTRODUCTION

Halogen bond (XB), one of the noncovalent interactions, has risen to a prominent role in crystal engineering[1-5] due to its strong directionality[6-9] and comparable strength to that of hydrogen bond (HB)[10], another widely utilized noncovalent interaction in crystal engineering.

XB is defined as a net attractive interaction between an electron-poor region on a halogen atom (XB donor) in a molecular entity and an electron-rich region (XB acceptor) on another or the same molecular entity.[6] A typical halogen bonded complex is denoted as R-X···Y, where R-X is the XB donor and Y is the acceptor. The nature of XB is mainly electrostatic, [11-13] but charge transfer, polarization and dispersion forces all contribute to the formation of XB. [14-15]

Commonly used XB donors include neutral dihalogens, organic halogens (C-X, X=Br, I), and halonium ions.[6] However, due to the redox property of neutral halogens and sometimes ion-free requirement in a system, organic XB donors have drawn intensive interests.[16-20] The strength of XB donor can be tuned by introducing substituents of various electronegativities to the moiety where the halogen atom is. The larger the electronegativity of the substituents, the stronger the XB donor becomes.

The scale of XB acceptors, compared with that of XB donors, is significantly broader. Oxygen[21-24], sulfur[25-27] and nitrogen[28-31], along with halide anions[6], are the widely used XB acceptors. Moreover, phosphorus[32] and even selenium[33] have also been reported as XB acceptors.

Though the directionality and the strong strength of XB afford the predictability in crystal engineering, these features are unable to guarantee the success of constructing the desired architecture without the inclusion of the selectivity of XB. Numerous studies have been focusing on competition between XB and HB.[34-37] However, very limited researches have been reported on the choice of XB interactive sites.[38]

1.1 The nature of halogen bond (XB)

Extensive studies have confirmed the primary force in XB is electrostatic,[39-44] a feature of XB acknowledged in the definition of XB proposed by IUPAC.[6] Moreover, several other researches have revealed that both charge transfer and dispersion, along with electrostatic force, contribute to the formation of XB.[45-48]

1.1.1 Electrostatic force

The electrostatic force model, proposed by Politzer et al. [39], is built on the anisotropic distribution of the electrostatic potential $V_s(r)$ around a halogen atom (X, X=Cl, Br, I) in a moiety (R-X).

It is commonly accepted that the electrostatic potential of a free halogen atom at ground state is positive everywhere due to the dominance of the effect of the nucleus over that of the dispersed electrons.[49, 50] However, when a free halogen atom (X) interacts through a covalent bond with a moiety (R) of strong electronegativity to form a new moiety (R-X), the electron distribution around the halogen atom becomes anisotropic. Such change in electrostatic potential generates a region of negative electrostatic potential belt around the halogen atom perpendicular to the R-X axis, leaving the positive region, the σ–hole, on the outmost position of the electrostatic potential surface of the halogen atom along the R-X axis, shown in **Figure 1**[39]. It is worth mentioning that a XB donor can simultaneously interact with another XB donor on the negative 'belt' surrounding the σ-hole, functioning as a XB acceptor.[49]

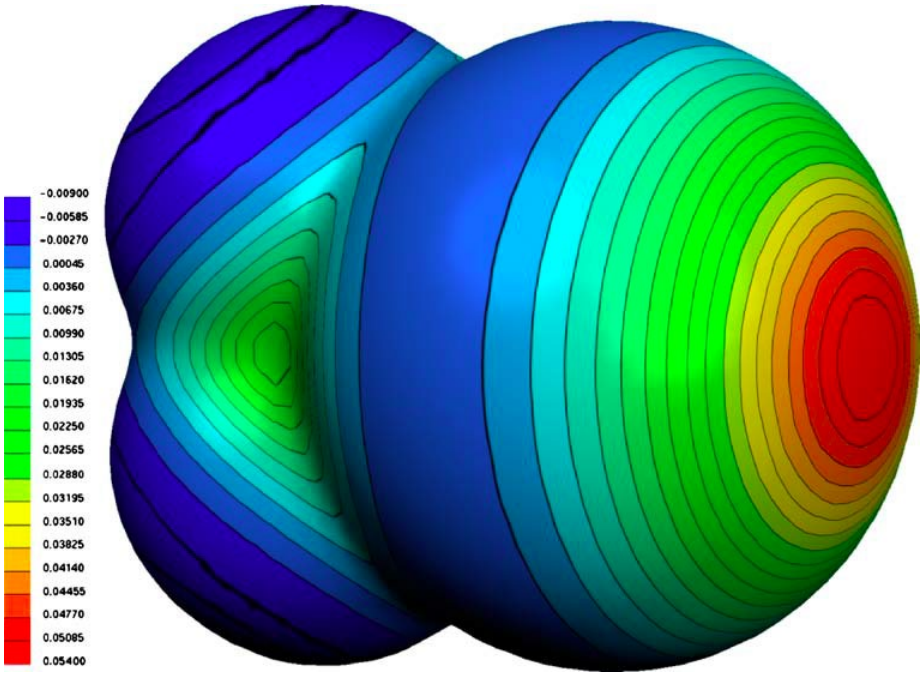

Figure 1. The molecular electrostatic potential, in Hartrees, at the 0.001 electron Bohr^{-3} isodensity surface of CF_3I. Figure is readapted from **Ref. 39.** Copyright **2007** Springer.

A variable temperature (VT) single crystal X-ray analysis of 3, 4-dichlorophenol and 4-bromo-3-chlorophenol revealed the rapid increase in XB length, indicating the short-range-effective nature of electrostatic force, and, in turn, confirming the significance of electrostatic force in XB.[50]

Clearly, the existence and the strength of the σ–hole dictate the electrostatic force model.[40, 41] The σ–hole is the product of the electron withdrawing competition between the halogen atom X and its connected moiety R.[39] If the electron withdrawing ability of X is stronger than that of R, the X can lose the σ–hole due to the neutralization of the positive electrostatic potential region by gained electrons from R. Thus, the strength of XB donor is correlated to the magnitude of the σ-hole, which is negatively correlated with the electronegativity of the X. As a result, the order of XB donor strength is R-Cl < R-Br < R-I.[39, 42]

This electrostatic force perspective provides sufficient explanations on strong directionality of XB, which is from the existence of the σ-hole and its peripheral location along the R-X axis on a halogen atom. Moreover, this model shows that by increasing the electronegativity of the R of R-X, *ceteris paribus*, the magnitude of the σ-hole on the X increases as well, indicating tunability of the XB.[42, 43]

Though the electrostatic model successfully explained the directionality and the strength of XB, this model fails to reason the elongation of R-X bond once it participates in XB. Besides, this interpretation of XB is insufficient in some cases where a poor correlation occurs between the strength of XB donors and the electrostatic potentials. To understand the cause of such "outliers", charge transfer has been revealed in some studies as the major cause.[51-54]

1.1.2 Charge Transfer

Charge transfer (CT), an attractive interaction, is rationalized as the transferring of electrons from the highest occupied molecular orbital (HUMO) of a XB acceptor to the lowest unoccupied molecular orbital (LUMO) of the XB donor upon the formation of a XB. The CT theory was proposed by Mulliken to reason the UV-vis observations and the polarity of the adducts formed by interactions between the electron acceptor (dihalogens) and the electron donor (benzene or oxygen containing organic compounds).[55]

The elongation of C-I bond in XB caused by CT was confirmed experimentally by X-ray analysis of a series of cocrystals with *p*-DITFB as XB donor.[51] Similarly, the elongation of the C-Br bond was also observed in XB formed with bromocarbons as XB donor and bromometalates as XB acceptor.[52] In the same study, Rosokha et al.[52] noticed that, despite the overlap of LUMOs and the σ-hole on bromocarbons, the overlap of HOMOs and the most negative electrostatic potential does not exist on bromometalates, and concluded that such divergence lead to the deviation from linearity of the formed XBs.

The CT contribution in XB was further confirmed in a research featuring an unexpected trend in the strength of CY_3I (Y=F, Cl, Br, I) as XB donors when

both chloride and trimethylamine are XB acceptors.[53] Based on the electrostatic model, the strength of XB donor reduces from CF_3I to CI_4 upon forming XB with chloride. However, the interaction energies of the obtained adducts suggested the opposite trend. Such trend was due to the significant contribution of CT, which was proven by the strong correlation between both electrostatic and CT contributions and the interaction energies, and such correlation was absent when only electrostatic contribution was included. Moreover, another strong linear correlation was also found between the CT and the total interaction energies in the study of the nature of XB in 55 adducts, suggesting the importance of CT in XBs.[54] Lastly, the increased negative charge on I_B in the system of $RuX\cdots I_A\text{-}I_B$ (X=Cl, Br, I) clearly demonstrates the contribution of CT.[56]

1.1.3 Dispersion

Dispersion in XB is mainly caused by the high polarizability of both XB donor and acceptor atoms and the short distance between them, which is shorter than the sum of van der Waals radii of the two atoms.[49]

Studies on the strength of XB have revealed the indispensable contribution of dispersion.[57, 58] Moreover, the prediction of the existence of adduct $CH_3Cl\cdots O{=}CH_2$ is validated by incorporating dispersion,[59] which is caused by the strong polarization of both Cl atom and the O atom, resulting in the σ-hole on the Cl, whose electrostatic potential is negative everywhere around the Cl in an isolated CH_3Cl.[60]

To conclude, the electrostatic force, to a great extent, dictates the strong directionality of the XB, meanwhile, both CT and dispersion, together with the electrostatic force, contribute to the strength of XB.

1.2 XB in Crystal Engineering

The key to utilize XB in crystal engineering is the controllability. Therefore, the nexus of XB is to 'match' the XB donor and acceptor in a desired manner. This section presents structures in dimensionality —0D, 1D, 2D and 3D — formed *via* XB and each dimensional structure is discussed in two parts: metal-containing systems is firstly reviewed, and then is followed by organic-compounds-only systems. The dimensionality here refers to the structure formed *via* XB only. All the crystal structures use the CCDC code, the identity of crystal structures deposited in the Cambridge Crystallographic Data Centre (CCDC).

1.2.1 Zero-dimensional System (0D)

In general, a monotopic XB donor with a mono- or polytopic XB acceptor affords a 0D structure, and vice versa. Meanwhile, the size of both XB donor and XB acceptor influence the final polymeric structure significantly. When

both XB donor and XB acceptor are of small size, all the possible XB bonding sites can be utilized, forming polymeric structure. However, if either XB donor or XB acceptor, or both, are of large size, due to the tendency to avoid voids of large volume in crystals, less available XB binding sites will be occupied.[61]

1.2.1.1 0-D Metal Containing System (0D MX)

In this system, the XB acceptors are metal complexes and organic halogens (C-X) are XB donors. Including metal complexes with organic molecules has great potential in materials with sensing, guest uptake/release, optical and catalysis properties.[62-66]

I_2 is a common XB donor in the MX system. A trimeric structure (**Figure 2**, FIQFUG[67]) is formed *via* XB with iodo[phthalocyaninato(2-)]iron (III) (FePcI) interacting with I_2, which bridges two FePcI molecules. A isostructural trimer (**Figure 2**, EXOXUK[68]) is obtained from iodo[phthalocyaninato(2-)]manganese (III) (MnPcI) interacting with I_2. The length of I-I bond (d_{I2}) in both FIQFUG and EXOXUK is 2.766Å and 2.783Å, respectively, longer than that in pure I_2, 2.715Å[69]. The lengthening of I-I bond suggests the CT contribution to the XB. Similarly, a trimeric structure (**Figure 2**, ABAPOJ[132]) is afforded *via* XB from I_2, a bitopic XB donor, co-crystallizing with iodo[tri(2-tolyl)phosphine]gold (Au[(2-$MeC_6H_4)_3P$]I), a monodentate XB acceptor.

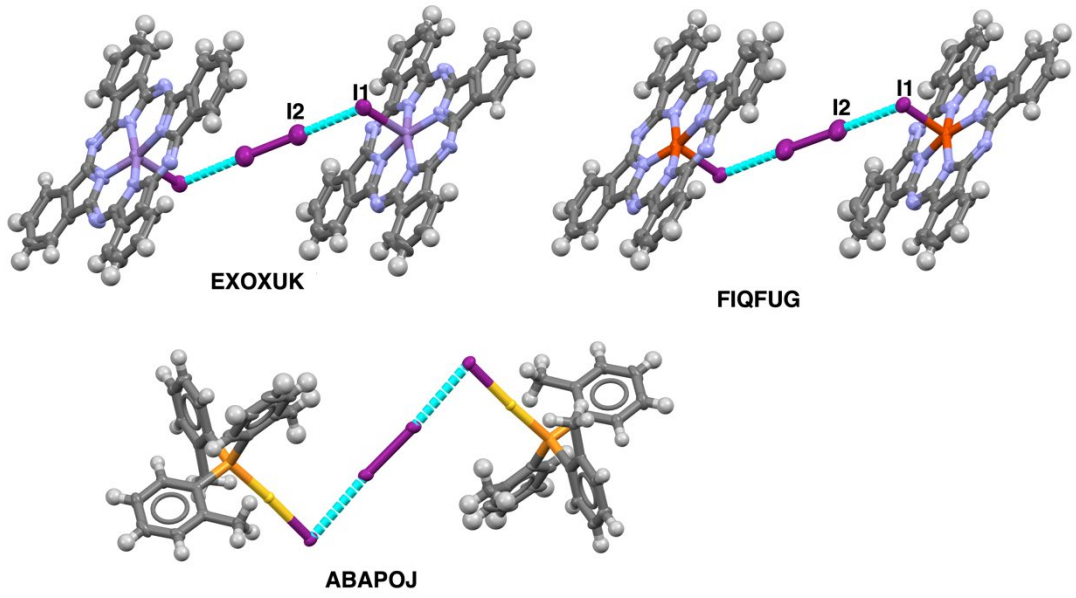

Figure 2. Halogen bonded discrete crystal structures, featuring metal coordinated iodo ligand as XB acceptor. EXOXUK[68]: iodo[phthalocyaninato(2-)]manganese and diiodine; FIQFUG[67]: iodo[phthalocyaninato(2-)]iron and diiodine; ABAPOJ[132]: iodo[tri(2-tolyl)phosphine]gold (Au[(2-$MeC_6H_4)_3P$]I) and diiodine.

Only discrete structures are available in some cases, even though XB donor or acceptor, or both, are multitopic, due to the occupation of potential XB bonding sites by HB, hindering the extension of the structure *via* XB. In the trimmer

EDIXEU[70], **Figure 3**, only I1 atom of diiodo-[1-(2-N, N-dimethylaminophenyl)-2, 3, 4, 5- tetramethylcyclophentadienyl]cobalt (III) participates in the XB formation with I_2, while I3 of the cobalt complex engages in HB. JOYDIK[71], **Figure 3**, exhibits such structural limitation as well. Even though both I1 and I2 of $[AuDI_2]^+$ (D=N, N'-dimethylperhydrodiazepin-2, 3-dithione) are potential XB accepting sites and I_3^- is able to function as a ditopic XB donor, only a dimmer is formed between them, as other I atoms participate in HB formation. Clearly, HB competes with XB and exerts great influence on structure formation.

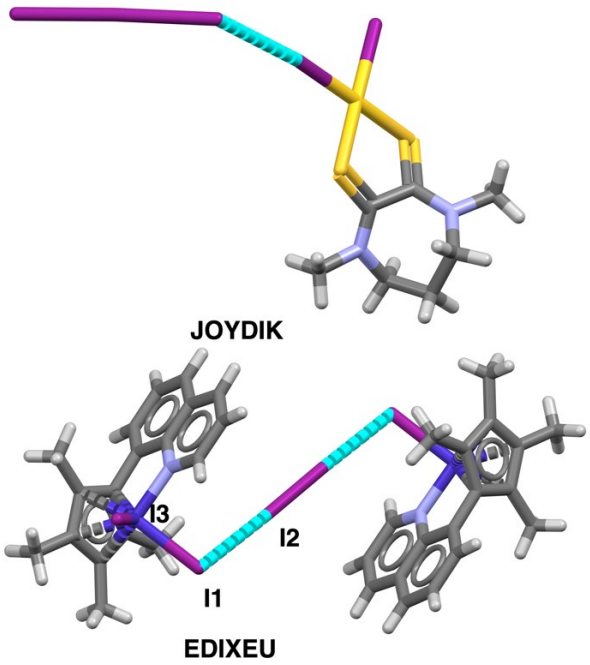

Figure 3. Discrete halogen bonded trimeric structures with halido ligand as XB acceptor. JOYDIK[71]: $[AuDI_2]^+$ (D=N, N'-dimethylperhydrodiazepin-2, 3-dithione) and I_3^-; EDIXEU[70]: diiodo-[1-(2-N, N-dimethylaminophenyl)- 2, 3, 4, 5- tetramethylcyclophentadienyl]cobalt and diiodine.

1.2.1.2 0-D Organic-Compound-Only Systems

Fluorinated halogen containing benzene ($C_6F_mX_n$, X=Br, I, n=6-m) is a common XB donor to form discrete structures with organic XB acceptors. A dimmer (IWONAL[72], **Figure 4**) *via* XB between 4-[(2-hydroxy-3-methoxybenzylidene) amino] benzonitrile and *o*-DITFB is formed ($d_{I1\cdots N2}$: 3.158Å, $<_{C\text{-}I1\cdots N2}$: 176.58°). When *p*-DITFB replaces *o*-DITFB to interact with the same XB acceptor in IWONAL[72], a trimmer (IWONOZ[72], **Figure 4**) is afforded ($d_{I1\cdots N8}$: 3.053Å, $<_{C\text{-}I1\cdots N8}$: 177.95°; $d_{I2\cdots N6}$: 3.019Å, $<_{C\text{-}I2\cdots N6}$: 176.45°). The shorter XB distance in IWONOZ[72] suggests that *p*-DITFB is a stronger XB donor than *o*-DITFB. In both cases, XB takes place on the sp-N.

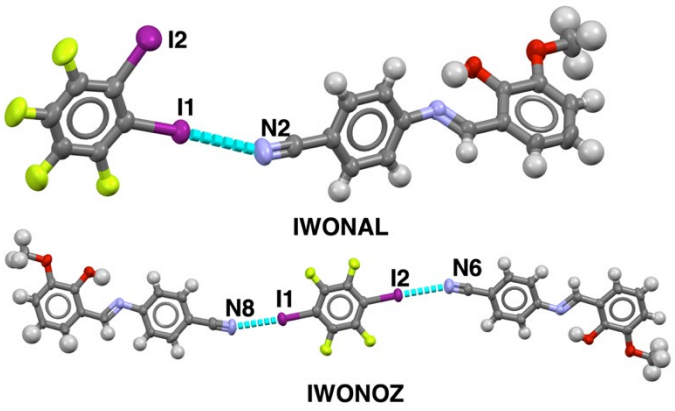

Figure 4. Halogen bonded discrete crystal structures featuring sp²-N as XB acceptor. IWONAL[72]: 4-[(2-hydroxy-3-methoxybenzylidene) amino] benzonitrile and *o*-DITFB; IWONOZ[72]: 4-[(2-hydroxy-3-methoxybenzylidene) amino] benzonitrile and *p*-DITFB.

sp²-N is also found as a XB acceptor with discrete structures. A *p*-DITFB bridges two 2-[(1E-[(pyridin-3-yl)imino]methyl]phenol molecules *via* XB into a trimmer (ODIQOK[73], **Figure 5**) ($d_{N2...I1}$: 2.902Å, $<_{N1...I1-C}$: 169.70°). Interestingly, when the XB donor changes to *m*-DITFB, a tetramer ((ODIQIE[73], **Figure 5**) is harvested *via* HO···I ($d_{O1...I2}$: 3.004Å, $<_{O1...I2-C}$: 172.32°) and N···I ($d_{N2...I1}$: 2.873Å, $<_{N2...I1-C}$: 171.60°). Moreover, when the tritopic XB donor 1, 3, 5-triiodotrifluorobenzene (*sym*-TITFB) is introduced to the same XB acceptor, a hexamer (ODIQAW[73], **Figure 5**) is obtained *via* I1···N4 ($d_{I1...N4}$: 2.896Å, $<_{C-I1...N4}$: 173.33°), I2···N2 ($d_{I2...N2}$: 2.932Å, $<_{C-I2...N2}$: 170.60°), and I3···O1 ($d_{I3...O1}$: 3.368Å, $<_{C-I3...O1}$: 149.16°). The HO···I in both ODIQIE and ODIQAW demonstrates that hydroxyl (-OH), a common HB donor, can act as XB acceptor as well.

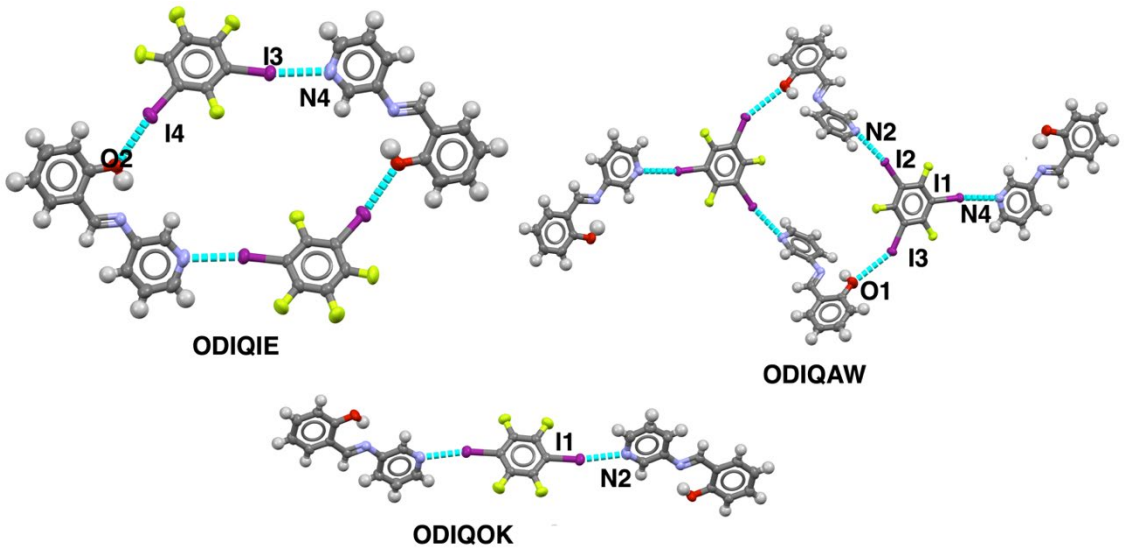

Figure 5. Halogen bonded discrete crystal structures featuring sp²-N and hydroxyl O. ODIQIE[73]: 2-[(1E-[(pyridin-3-yl)imino]methyl]phenol and *m*-DITFB; ODIQOK[73]: 2-[(1E-[(pyridin-3-yl)imino]methyl]phenol and *p*-DITFB; ODIQAW[73]: 2-[(1E-[(pyridin-3-yl)imino]methyl]phenol and *sym*-TITFB.

Oxygen atom engaged in XB is not only in hydroxyl but also in carbonyl (C=O) and ether (C-O-C) groups. IWOMUE[72], shown in **Figure 6**, is a trimmer formed by *p*-DITFB bridging two 1-4-[(2-hydroxy-3-methoxybenzylidene)amino]phenyl ethenone through two bifurcated O1···I1···O2, where O1 is in the hydroxyl group and O2 is in the ether group ($d_{O1...I1}$: 3.378 Å, $<_{O1...I1-C}$: 155.42°; $d_{O2...I1}$: 3.218 Å, $<_{O2...I1-C}$: 151.42°; $<_{O1...I1...O2}$: 46.1°). When *o*-DITFB interacts with the same XB acceptor in IWOMUE, a tetramer is yielded (IWONUF[72], **Figure 6**) linked by I1···O3 ($d_{I1...O3}$: 2.977 Å, $<_{C-I1...O3}$: 177.73°) and the bifurcated O2···I2···O1 ($d_{I2...O1}$: 3.206Å, $<_{C-I2...O1}$: 152.79°; $d_{I2...O2}$: 3.367Å, $<_{C-I2...O2}$: 154.04°;). Clearly, the bifurcated XB in both structures are quite similar in both strength and directionality due to the exact same synthon, containing carbonyl and ether, in the XB acceptors. Moreover, the shorter distance between O3 in carbonyl and I1 in *o*-DITFB indicates that O atom in carbonyl is a relatively stronger XB acceptor compared with tin hydroxyl and ether. O atom in carbonyl in XB is also found in trimmer WEDWUA[74], shown in **Figure 6**, in which *p*-DBTFB bridges two lidocaine molecules *via* Br···O ($d_{O...Br}$: 3.101Å, $<_{O...Br-C}$: 169.86°).

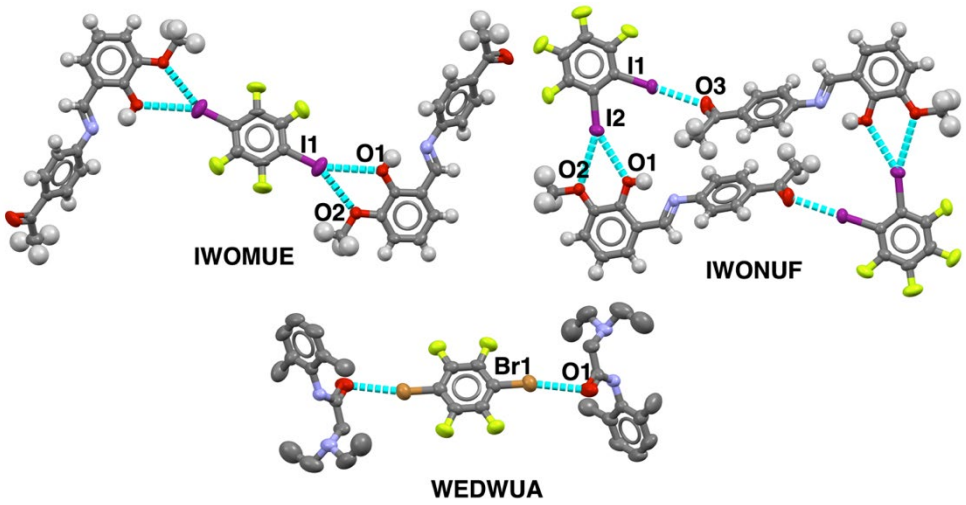

Figure 6. Halogen bonded discrete structures featuring hydroxyl O and carbonyl O as the XB donor. IWOMUE[72]: 1-4-[(2-hydroxy-3-methoxybenzylidene)amino]phenyl ethenone and *p*-DITFB; IWONUF[72]: 1-4-[(2-hydroxy-3-methoxybenzylidene)amino]phenyl ethenone and *o*-DITFB; WEDWUA[74]: lidocaine and *p*-DBTF.

Sulfur atoms in different synthons are also reported as XB acceptors. HIZQOY[75], shown in **Figure 7**, is a trimmer between 1, 4-dithiane and 4-iodotetrafluorobenzoic acid. In addition, S in thione (C=S) can also form XB. MIXYUQ[76], shown **Figure 7**, is a homomeric dimmer formed by the self-complementary 3-(3-iodophenyl)-1, 3-thiazole-2-thione.

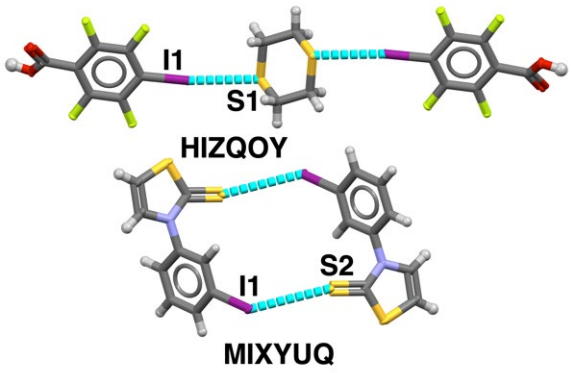

Figure 7. Halogen bonded discrete structures featuring sulfur as the XB donor. HIZQOY[75]: 1, 4-dithiane and 4-iodotetrafluorobenzoic acid; MIXYUQ[76]: 3-(3-iodophenyl)-1, 3-thiazole-2-thione.

1.2.2 One-dimensional System (1D)

The general rule governing the construction of 1-D structure is that such architecture is achieved through either self-complementary compound, which contain both XB donor and acceptor sites, or bitopic XB donors and bitopic XB acceptors.

1.2.2.1 1-D Metal Containing System (1D M-X)

A collection of metal complexes as monotopic XB acceptors with bitopic XB donors have been reported to form 1D chain structures, in which the monotopic XB acceptor is capable of forming bidentate XB.[77-79] A zigzag chain is formed through I2···I1···I3 bifurcated XB ($d_{I2...I1}$: 3.436Å, $<_{I3\text{-}I2...I1}$:176.88°; $d_{I3...I1}$: 3.578Å, $<_{I2\text{-}I3...I1}$: 171.40°) between iodo-triphenylphosphine-gold (I) and diiodine, ABAPEZ[78], shown in **Figure 8**. Assemblies with 1D chain structures are also formed *via* XBs between coordinated Cl or Br, bidentate XB acceptors, and bitopic XB donors. SEZREX[79], shown in **Figure 8**, is formed through I1···Br1···I2 between bromo-dicarbonyl-(cyclopentadienyl)-iron and *p*-DITFB ($d_{I1...Br1}$: 3.311Å, $<_{C\text{-}I1...Br1}$: 172.02°, $<_{I1...Br1\text{-}Fe}$: 107.61°; $d_{I2...Br1}$: 3.294Å, $<_{C\text{-}I2...Br1}$: 175.03°, $<_{I2...Br1\text{-}Fe}$: 109.22°; $<_{I2...Br1...I1}$: 142.76°). Similarly, SEZQIA[78] (**Figure 8**), the isomorphic structure of SEZREX, forms 1D zigzag chain as well through I1···Cl1···I2 ($d_{I1...Cl1}$: 3.220Å, $<_{C...I1}$: 175.76°, $<_{I1...Cl1\text{-}Fe}$: 110.01°; $d_{I1...Cl1}$: 3.229 Å, $<_{C\text{-}I2...Cl1}$: 173.38°, $<_{I2...Cl1\text{-}Fe}$: 108.33°). Interestingly, however, in iodo-dicarbonyl-(cyclopentadienyl)-iron, only a trimmer, SEZRAT[79], is obtained with the same XB donor, despite the two available "docking" sites for the electrophilic I on the *p*-DITFB[79].

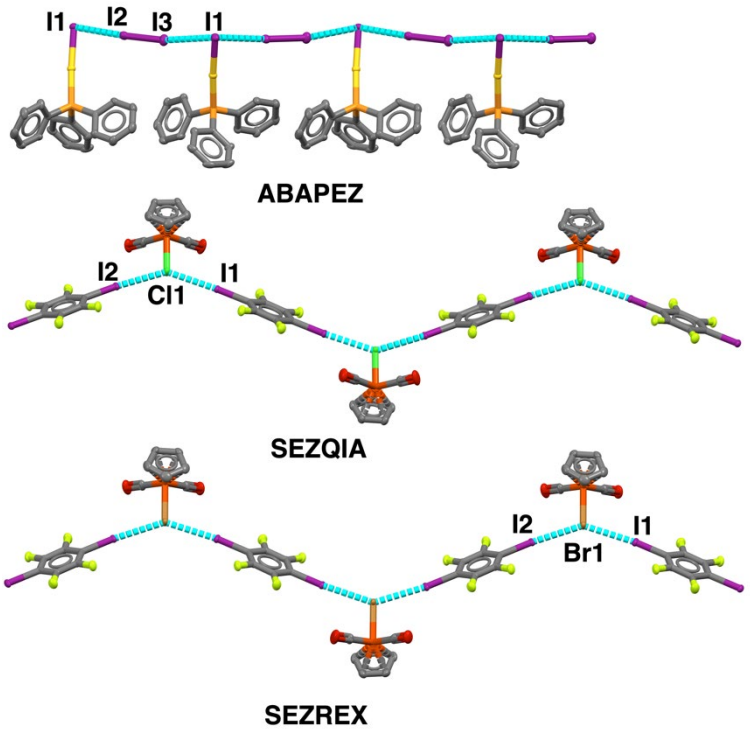

Figure 8. Halogen bonded chain structures featuring bidentate halido ligand as the XB acceptor. ABAPEZ[78]: iodo-triphenylphosphine-gold and diiodine; SEZQIA[78]: chloro-dicarbonyl-(cyclopentadienyl)-iron and *p*-DITFB; SEZREX[79]: bromo-dicarbonyl-(cyclopentadienyl)-iron and *p*-DITFB.

Numerous bitopic metal complexes have been studied to build chain structure with bitopic XB donors.[80-82] A zigzag chain structure (CILZEF[81], **Figure 9**) is formed by dichloro-bis(1, 10-phenanthroline)-cobalt (II) interacting with *p*-DITFB *via* I1···Cl2 ($d_{I1...Cl2}$: 3.137Å, $<_{C\text{-}I1...Cl2}$: 169.66°, $<_{I1...Cl2\text{-}Co}$: 117.18°) and I2···Cl1 ($d_{I2...Cl1}$: 3.145Å, $<_{C\text{-}I2...Cl1}$: 172.93Å, $<_{I2...Cl1\text{-}Co}$: 130.45°). The wide range of I···Cl-Co angle and the large deviation from 90° suggests that Cl as an XB acceptor lacks strong dictation on the directionality of XB, and that is likely due to the more isotropic negative electrostatic potential distribution around the Cl.[73] A linear chain (MIRHUT[81], **Figure 9**) is formed by chloro-[dimethyl sulfoxide]-[3-(pyridine-2-yl)-1-benzofuran-2-yl]-platinum and *p*-DITFB through Cl1···I1 ($d_{I1...Cl1}$: 3.264Å, $<_{C\text{-}I1...Cl1}$: 174.35Å) and O1···I2 ($d_{I2...O1}$: 2.980Å, $<_{C\text{-}I2...O1}$: 155.35°). A "ring-and-stick" chain structure (GABLAX[83], **Figure 9**) is formed with one dibromo-gold connecting three tris(2, 7-diiodo-1, 6-dithiaprene) *via* I1···Br1 ($d_{I1...Br1}$: 3.301Å, $<_{C\text{-}I1...Br1}$: 174.58°) and I2···Br2···I3 ($d_{I2...Br2}$: 3.618Å, $<_{C\text{-}I2...Br2}$: 167.91°; $d_{I3...Br2}$: 3.536Å, $<_{C\text{-}I3...Br2}$: 172.86°). In this structure four membered rings are formed and further extended into a linear structure by the "stick" — tris(2, 7-diiodo-1, 6-dithiaprene). Some XB acceptors have more than two docking sites for XB donor,[84, 85] but only behave as a bitopic acceptor due to insufficient space to accommodate more XB donor molecules. KARFEQ[83], shown in **Figure 9**, has similar zigzag chain structure to CILZEF[81]. However, only two of the three I atoms in the XB acceptor, (benzo-15-crown-5)-tri(iodo)-bismuth, engage in XB formation, leaving one I idle.

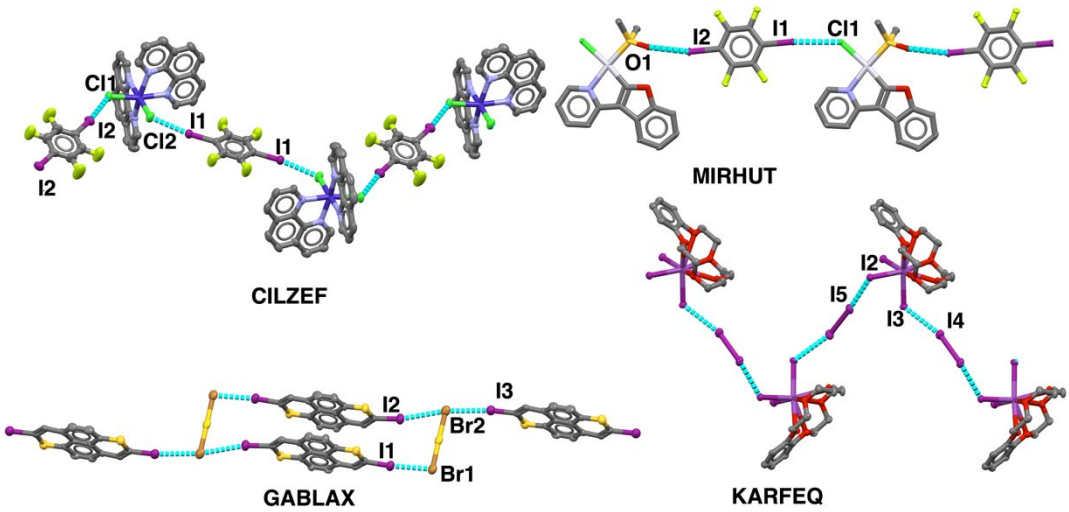

Figure 9. Halogen bonded chain structures featuring bitopic XB acceptors. CILZEF[81]: dichloro-bis(1,10-phenanthroline)-cobalt and *p*-DITFB; MIRHUT[81]: chloro-[dimethyl sulfoxide]-[3-(pyridine-2-yl)-1-benzofuran-2-yl]-platinum and *p*-DITFB; GABLAX[83]: dibromo-gold and three tris(2, 7-diiodo-1, 6-dithiaprene); KARFEQ[83]: (benzo-15-crown-5)-tri(iodo)-bismuth and diiodine.

In addition, self-complementary compounds are also viable building blocks for 1-D chain structure *via* XB. Assemblies (LORYIB[86], **Figure 10**) of linear structure is formed *via* Cl1···I1 ($d_{Cl1...I1}$: 3.423Å, $<_{Cl1...I1-C}$:169.47°). Both XB donor I and XB acceptor Cl are part of the copper complex molecule: dichloride-(2-[(4-iodophneyl)iminomethyl]pyridine-N, N′-copper (II). Moreover, only one Cl forms XB in LORYIB is probably due to the limited space caused by the *cis*-position of both Cl. Another linear chain structure (PEWHOR[87], **Figure 10**) is formed from another copper complex with *trans* positioned chloro ligand *via* two equivalent I···Cl ($d_{Cl...I}$: 3.413Å, $<_{Cl...I-C}$: 170.09°).

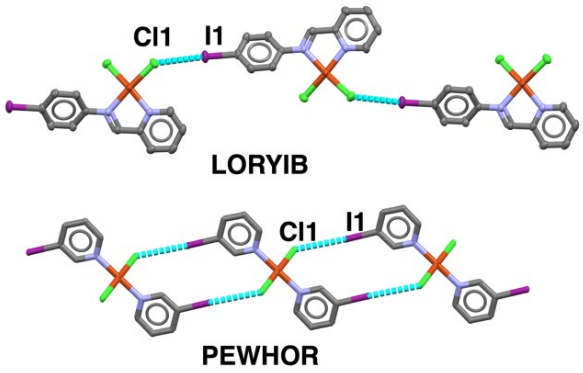

Figure 10. Halogen bonded chain structure featuring self-complementary metal complexes. LORYIB[86]: dichloride-(2-[(4-iodophneyl)iminomethyl]pyridine-N, N′-copper; PEWHOR[87]: dichloro-bis(3-iodopyridine)-copper.

1.2.2.2 1-D Organic-Compound-Only System

Nitrogen containing multitopic XB acceptors have been widely used in constructing 1D chain structures. [88] A zigzag chain (ANUPUV[23], **Figure 11**) is constructed with phenazine and *o*-DITFB *via* two equivalent N···I ($d_{I...N}$: 3.009 Å, $<_{N...I-C}$: 169.01°). Assemblies of helix structure (VENRAK[89], **Figure 11**) is formed with 4, 4′, 4″, 4‴-{methanetetrayltetrakis[(4, 1-phnylene)ethane-2, 1-diyl)]}tetrapyidine (TetraA) and *sym*-TITFB *via* I1···N3 ($d_{I1...N3}$: 2.741Å, $<_{C-I1...N3}$: 176.00°) and I2···N4 ($d_{I2...N4}$: 2.768Å, $<_{C-I2...N4}$: 177.63°). Only two N of the TetraA participate in XB formation, leaving one N idle and one engaged in HB. Nicotine and *p*-DITFB form linear structure (LAZXES[90], **Figure 11**) *via* I1···N4 ($d_{N4...I1}$: 3.015Å, $<_{C-I1...N4}$: 167.64°) and I2···N3 ($d_{N3...I2}$: 2.873Å, $<_{C-I2...N3}$: 174.78°). Two N at different hybridization state are the XB accepting sites. The much shorter XB distance on N3 than on N4 indicates sp^2-N is a stronger XB acceptor than sp^3-N. The asymmetric ditopic XB acceptor, pentoxifylline, interacts with *p*-DITFB, yielding assemblies with wavy chain structure (WEDXIP[91], **Figure 11**) *via* I2···N3 ($d_{I2...N3}$: 2.949Å, $<_{C-I2...N3}$: 172.21°) and I1···O3 ($d_{I1...O3}$: 2.934Å, $<_{I1...O3}$: 170.00°). Here both N and O are in sp^2 hybridization.

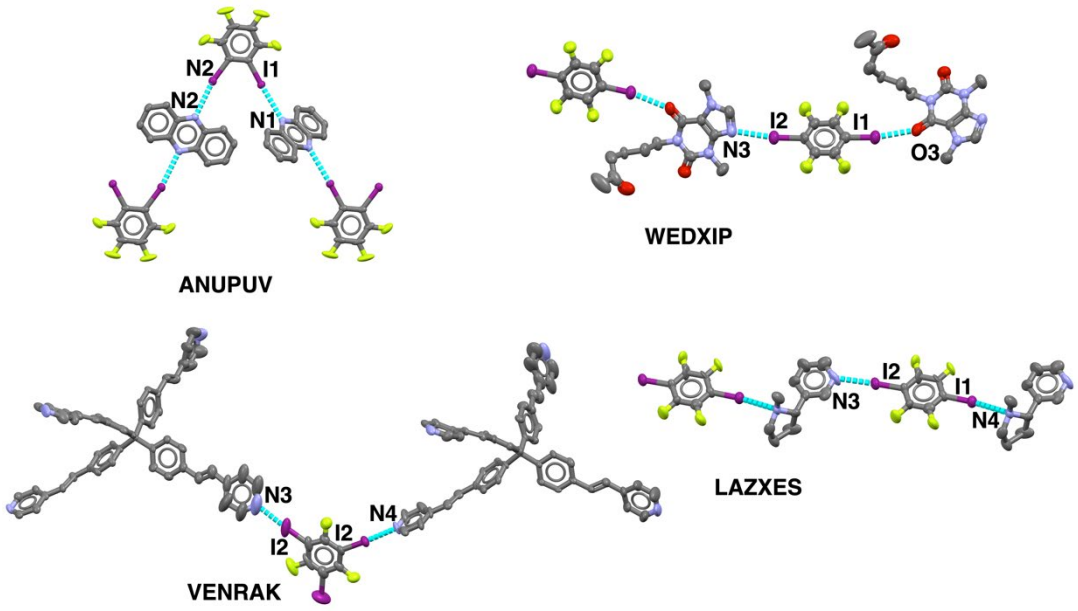

Figure 11. Halogen bonded chain structures featuring nitrogen and oxygen as XB acceptors. ANUPUV[23]: phenazine and *o*-DITFB; VENRAK[89]: 4, 4′, 4″, 4‴-{methanetetrayltetrakis[(4, 1-phnylene)ethane-2, 1-diyl)]}tetrapyridine and *sym*-TITFB; WEDXIP[91]: pentoxifylline and *p*-DITFB; LAZXES[90]: Nicotine and *p*-DITFB.

sp^3-O, sp^2-S and sp^3-S are all used in 1D structure construction as well. 1, 4-dioxane, a bitopic XB acceptor, interacts with *p*-DITFB, forming assemblies (DIVAO[92], **Figure 12**) with linear structure *via* N···I ($d_{N...I}$: 2.913 Å, $<_{N...I-C}$: 176.55°). In DIVAO the sp^3-O is a monodentate XB acceptor. Different from in DIVAO, in AFUHAN[24], shown in **Figure 12**, each sp^3-O is a bidentate XB

acceptor, interacting with two *p*-DITFB to form symmetric I···O···I ($d_{I...N}$: 2.662 Å, $<_{C\text{-}I...N}$: 176.17°). Similarly, sp^3-S is capable of forming XB as a bidentate XB acceptor due to lone pairs. ANUPIJ[23], shown in **Figure 12**, demonstrates a ladder structure formed by 1, 4-dithane and *p*-DITFB *via* symmetric I···S···I ($d_{I...S}$: 3.384Å, $<_{C\text{-}I...S}$: 164.83°). Furthermore, sp^2-S is a bidentate XB acceptor as well. Thiourea interacts with *p*-DITFB *via* I1···S···I2 ($d_{I1...S}$: 3.154 Å, $<_{C\text{-}I1...S}$: 178.33°; $d_{I2...S}$: 3.363 Å, $<_{C\text{-}I2...S}$: 175.97°), yielding assemblies of linear structure (OQIJIJ[133], **Figure 12**).

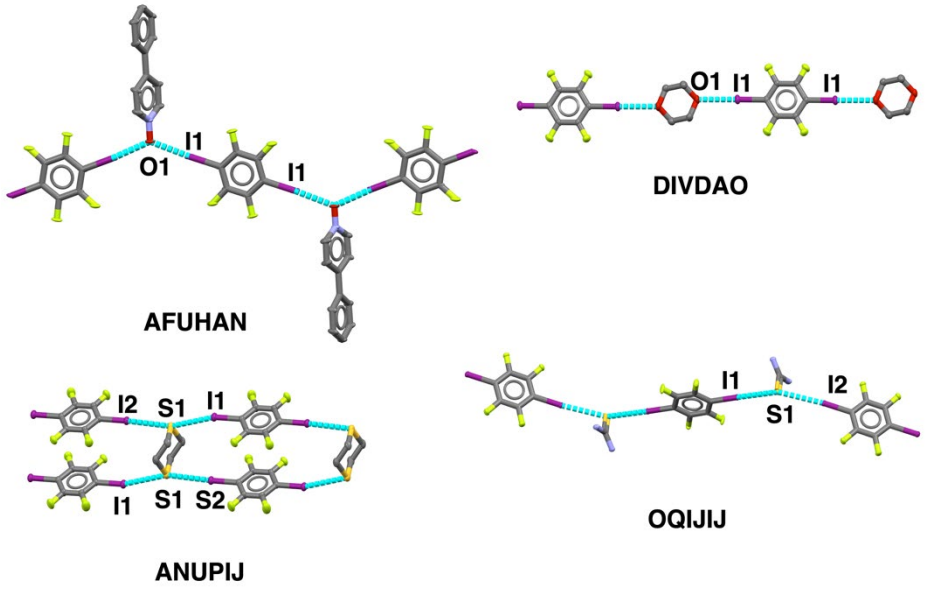

Figure 12. Halogen bonded chain structures featuring oxygen and sulfur as the XB acceptors. AFUHAN[24]: 4-phenylpyridine N-oxide and *p*-DITFBZ; ANUPIJ[23]: 1, 4-dithane and *p*-DITFB; DIVDAO[92]: 1, 4-dioxane and *p*-DITFB; OQIJIJ[133]: Thiourea and *p*-DITFB.

1.2.3 Two- and Three-dimensional Systems (2D and 3D)

A common method to afford high dimensional structures *via* XB is to increase the number of interacting sites on both XB donors and XB acceptors. The key to success of such method is to have functioning sites on each molecule orientated in a such way that ensures the availability of the desired binding sites. Usually, the higher the dimensionality is in desire, the more demanding the design becomes.

1.2.3.1 2D and 3D Metal Complex Containing System (2D and 3D M-X)

When either of the two interacting moieties, or both, forms at least three XBs, 2D architecture is obtained. Diiodine (I_2) is a common tecton used in building 2D layered structures due to the two available σ-holes on each end of the extension of the covalent bond and the negative electrostatic potential belt orthogonal to the covalent bond. AFUSOJ[93], shown in **Figure 13**, demonstrates the 2D layered structure of square grid type. Each square grid is formed *via*

I3···I1···I2, I1···I4, and I3···I5 ($d_{I3...I1}$: 3.585Å, $<_{I2\text{-}I3...I1}$: 174.36°; $d_{I2...I1}$: 3.272 Å, $<_{I3\text{-}I2...I1}$: 172.42°; $d_{I4...I1}$: 3.289Å, $<_{I5\text{-}I4...I1}$: 175.53°; $d_{I5...I3}$: 3.649Å, $<_{I4\text{-}I5...I3}$: 174.40°). It is worth noting that I1 of the palladium complex (2, 6-bis(dimethylaminomethyl)phenyl-C, N, N′)-iodo-palladium (II)) interacts with three I_2 simultaneously, and that I_2 is amphoteric in that it functions as both XB donor and acceptor. A quasi-honeycomb architecture (ABAPAV[94], **Figure 13**) is formed by I_2 interacting with iodo-(triisopropylphosphine)-gold (I) *via* I1···I2 ($d_{I1...I2}$: 3.647Å, $<_{I1...I2\text{-}I2C}$: 174.60°), I1···I3 ($d_{I1...I3}$: 3.863Å, $<_{I1...I3\text{-}I4}$: 161.69°), and I1···I4 ($d_{I1...I4}$: 3.615Å, $<_{I1...I4\text{-}I3}$: 167.32°). Clearly, the Au-I1 is a tridentate XB acceptor, while I_2 here only behaves as a XB donor.

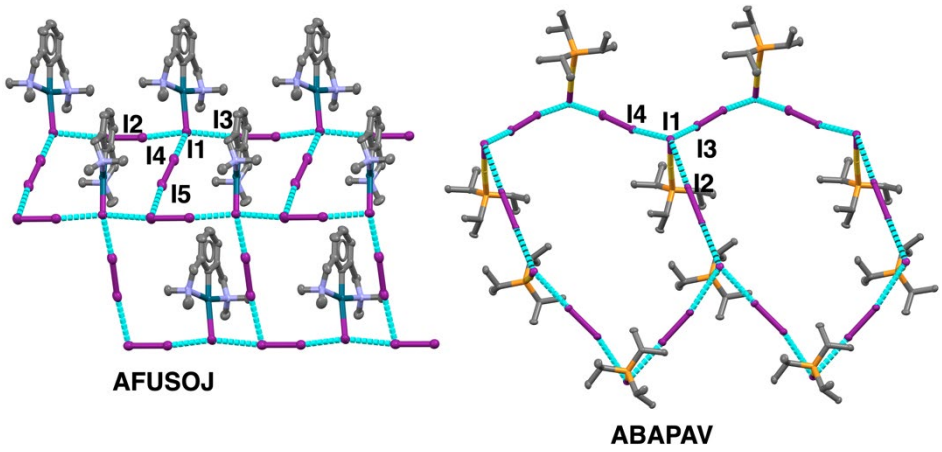

Figure 13. Halogen bonded two-dimensional networks. AFUSOJ[93]: (2, 6-bis(dimethylaminomethyl)phenyl-C, N, N′)-iodo-palladium and diiodine; ABAPAV[94]: iodo-(triisopropylphosphine)-gold and diiodine.

3D architecture can be constructed by using octahedral interacting moieties. DEJCAX[95], shown in **Figure 14**, is a 3D cubic architecture formed by the self-complementary trans-diiodo-bis(4-iodopyridine)-palladium (II). The Pd coordinated iodine atom (Pd-I), the XB acceptor, interacts with the pyridyl-I (py-I), the XB donor, forming Pd-I···I-py ($d_{Pd\text{-}I...I\text{-}py}$: 3.670 Å, $<_{I...I\text{-}C}$: 172.06°). Moreover, Pd-I···I-Pd takes place between adjacent Pd-complex molecules due to dispersion. Thus, combined with the Pd-I···I-Pd interaction, this palladium complex can be perceived as a pseudo-octahedral building block. Similarly, tris(m-3-oxo-1,3-bis(pyridine-4-yl)prop-1-en-1-olato)-iron (III), an iron complex of octahedral orientation, interacts with the ditopic *p*-DITFB, yielding a 3D cadge structure *via* N···I (FEZDIA[134], **Figure 14**).

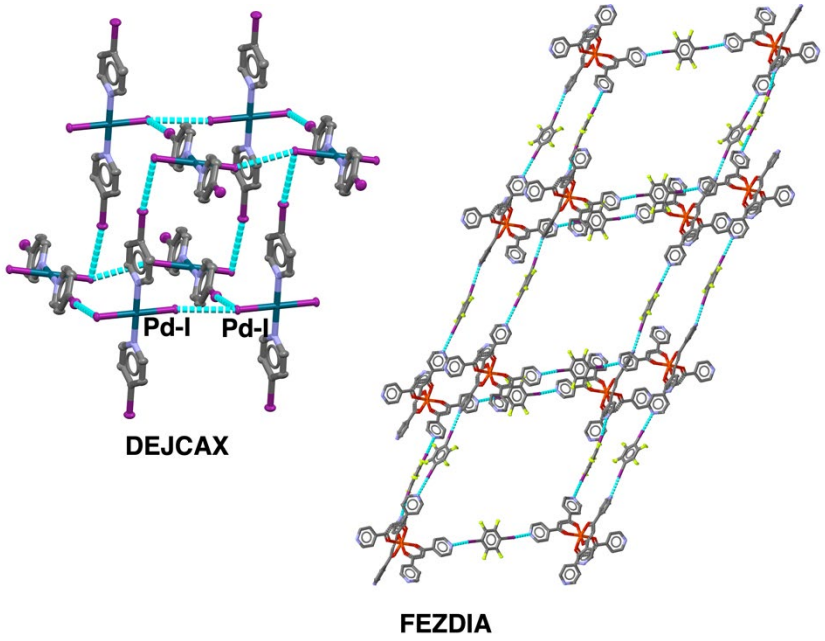

Figure 14. Halogen bonded three-dimensional cage structures. DEJCAX[95]: trans-diiodo-bis(4-iodopyridine)-palladium; FEZDIA[134]: tris(m-3-oxo-1,3-bis(pyridine-4-yl)prop-1-en-1-olato)-iron.

1.2.3.2 2-D and 3-D Organic-Compound-Only System

Methods of constructing 2D and 3D architectures in M-X system, to a large extent, apply to the organic-compound-only system as well. Multitopic sp^2-N containing XB acceptors are ideal building blocks in constructing high dimensional architectures due to the high controllability afforded by the monodentate nature of sp^2-N.[96] A 2D layer of square grid pattern (VENPAI[97], **Figure 15**) is formed with a tetratopic XB acceptor, 4, 4′, 4′′, 4′′′-{methanetetrayltetrakis[(4, 1-phenylene)ethene-2, 1-diyl]}tetrapyridine (TPTP) , and a bitopic XB donor, *p*-DITFB, *via* N1···I2 ($d_{N1...I2}$: 2.752Å, $<_{N1...I2-C}$: 176.49°) and N2···I1 ($d_{N2...I1}$: 2.925Å, $<_{N2-I1-C}$: 176.96°). Thiocyanide anion (SCN^-) is capable of offering three XB interactive sites. AHAJID[98], shown in **Figure 15**, is a 2D layer structure of quasi-honeycomb pattern. In this structure SCN^- and *sym*-TITFB are connected *via* I1···S1···I2 ($d_{I1...S1}$: 3.288Å, $<_{C-I1...S1}$: 171.75°; $d_{I2...S1}$: 3.245Å, $<_{C-I2...S1}$: 177.07°) and I3···N1($d_{I3...N1}$: 2.929Å, $<_{C-I3...N1}$: 176.48°). Another common type of tectons used in building high dimensional structures is anionic halogen.[61] MAHCIJ[135], eliciting herringbone 2D layer structure, shown in **Figure 15**, is formed by interaction between iodine anions and *p*-DITFB *via* I1···I4 ($d_{I1...I4}$:3.628Å, $<_{C-I1...I4}$: 175.85°) and I2···I4···I3 ($d_{I2...I4}$: 3.470Å, $<_{C-I2...I4}$:174.80°; $d_{I3...I4}$: 3.535Å, $<_{C-I3...I4}$: 175.18°). Here the iodine anion is a tridentate XB acceptor.

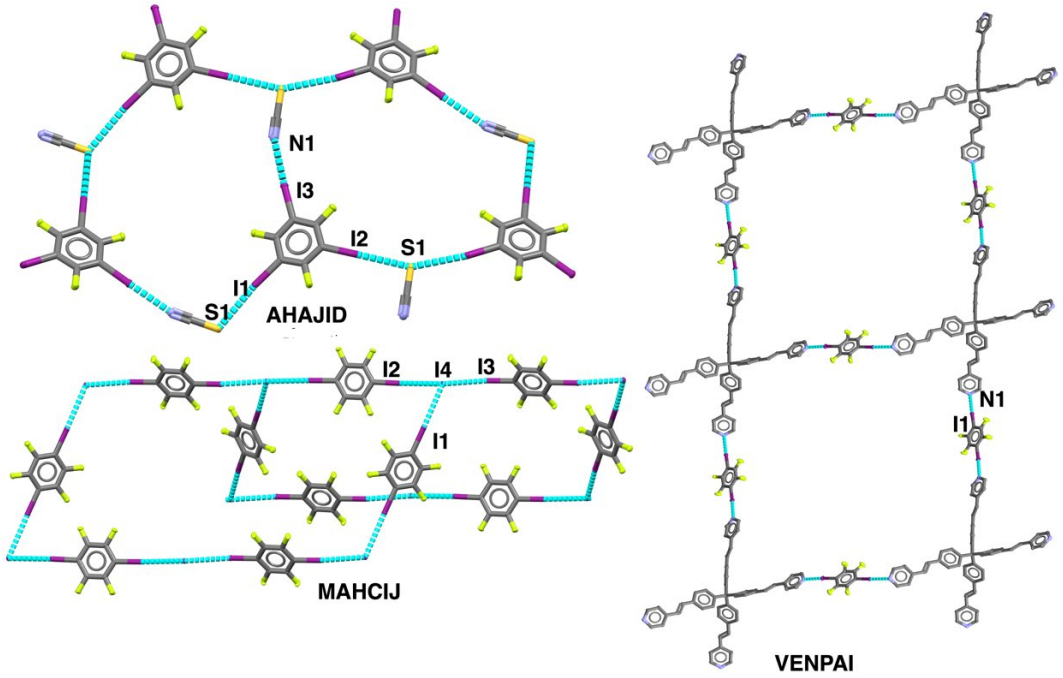

Figure 15. Halogen bonded two-dimensional networks. AHAJID[98]: thiocyanate and *sym*-TITFB; MAHCIJ[135]: iodine anion and *p*-DITFB; VENPAI[97]: 4,4′,4′′,4′′′-{methanetetrayltetrakis[(4,1-phenylene)ethene-2,1-diyl]}tetrapyridine and *p*-DITFB.

The common organic tectons used in building 3D structures are of tetrahedral orientation. The tetratopic XB acceptor, TPTP, used in VENPAI[97] interacts with 2, 3, 5, 6-tetraiododifluorobenzene (TIDFB), yielding a network of quasi-primitive cubes (VENREO[97], **Figure 16**) *via* I1···N2 ($d_{I1...N2}$: 2.814Å, $<_{C\text{-}I1...N2}$: 171.36°) and I2···N1 ($d_{I2...N1}$: 2.838Å, $<_{C\text{-}I2...N1}$:176.09°). The difference in those two architectures caused by different XB donors indicates the versatility of TPTP as a XB acceptor, and that to achieve a desired architecture the right match of building blocks is vital. Halogen anions, discussed previously, is also a good candidate for 3D construction, due to the ability to form four XBs orientated in tetrahedral position. VAPVOY[136], Shown in **Figure 16**, a rhombododecahedron network, is obtained from interactions between chlorine anion and tetrabromomethane *via* Cl···Br ($d_{Br...Cl}$:3.090Å, $<_{C\text{-}Br...Cl}$: 174.96°).

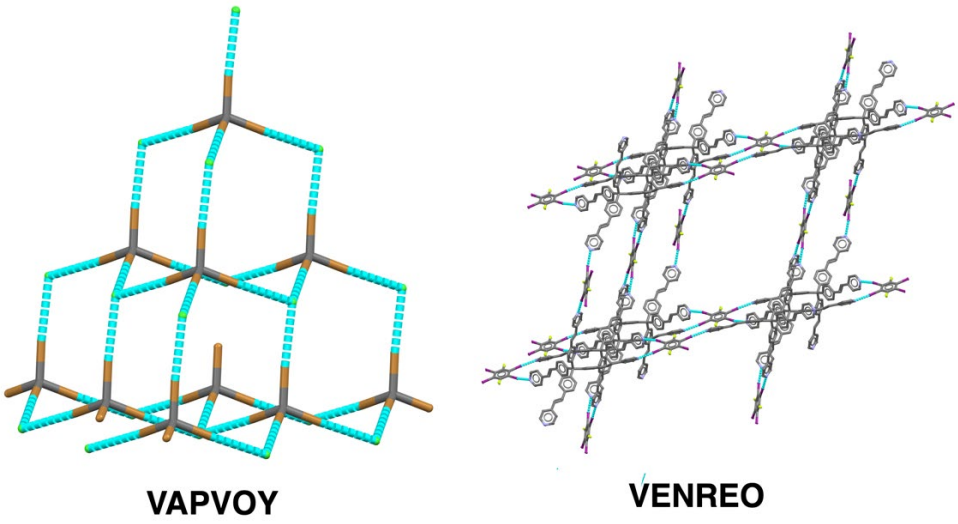

Figure 16. Halogen bonded three-dimensional structures. VAPVOY[136]: chlorine anion and tetrabromomethane; VENREO[97]: 4, 4′, 4′′, 4′′′-{methanetetrayltetrakis[(4, 1-phenylene)ethene-2, 1-diyl]}tetrapyridine and *p*-DITFB.

1.3 Selectivity of Halogen Bond

The selectivity of XB refers two aspects: first, whether the interactive site involves in XB or HB; second, the hierarchy of interactive sites in XB formation. The understanding of the selectivity of XB enhances the predictability in the construction of architectures, as the choice of those non-covalent interactions and the interactive sites affects both the conformation of molecules and consequently the structure of afforded assemblies.[35, 40]

1.3.1 Competition between XB and HB

Both XB and HB are primarily electrostatic interaction, and share great similarities in strength and directionality.[9, 10, 99] Thus, the investigation into the choice of XB and HB on an interactive site is necessary to avoid "synthon crossover".[100]

Aakeröy *et al.*[99] used a series of bromine substituted 2-aminopyrazine (**Scheme 1a**) and *p*-DITFB to construct assemblies of infinite chain structure by employing both XB and HB. They noticed that the self-complementary homo synthon N···H-N (amine) of the 2-aminonpryazine (**Scheme 1b**) was robust, and that I···N(pyrazine) was strong enough to compete over the proton on amine group despite the reduction in electrostatic potential on the N4 caused by the substitution of bromine. Thus, they concluded that both HB and XB had geometric bias in that HB preferred two-points interaction while XB chose single-point one, indicating the role of geometric complementarity in the competition of XB and HB, a conclusion which was also drawn by Gunawardana *et al.*[101] from their study on the competition between HB and XB

using three isomeric 1-(pyridylmethyl)-2, 2′-biimidazole and three perfloroiodobenzenes (IPFB, *p*-DITFB, and 2, 3, 5-TITFB) (**Scheme 1c**). However, the geometric preference provides little guidance to systems where only one-point interaction can take place.

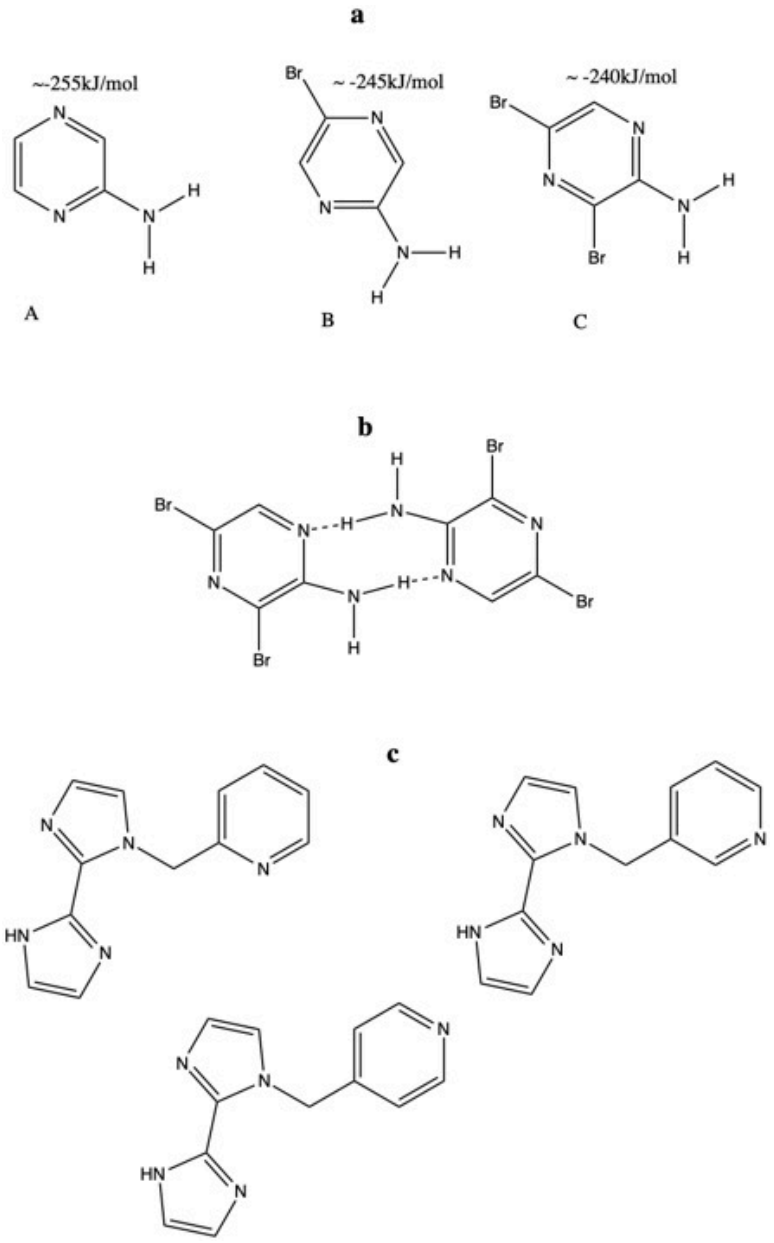

Scheme 1. Schematic structure of 2-Aminopyrazines and the homosynthon. a: 2-Aminopyrazine, A; 2-Amino-5-bromopyrazine, B; 2-Amino-3, 5-dibromopyrazine, C; b: homosynthon linked by HB; c: isomeric structures of 1-(pyridylmethyl)-2, 2′-biimidazole.

Focusing on one-point interaction, Nayak *et al.*[102] investigated the hierarchy of XB and HB with 4-iodophenol as donor and a series of N containing ditopic acceptors (**Scheme 2a**). By studying the 9 obtained crystal structures, they concluded that planar acceptors only formed either HB or XB exclusively, but that acceptors with twisted conformation formed both HB and XB. Such

conformation effect was confirmed by the results obtained from the study of Gamekkanda *et al.*[36]. They found that *trans*-1, 4-bis(iodoethynyl)cyclohexane-1, 4-diol formed both XB and HB with sp^2-N containing symmetric ditopic acceptors, whereas the *cis* form of the diol only afforded HB with the nitrogen containing acceptors, leaving XB on the hydroxyl oxygen atom of the *cis*-diol (**Scheme 2b**). Clearly, the conformation of acceptor molecules influences significantly the choice of the type of non-covalent interaction, but no clear preference was indicated regarding the acceptors of the same conformation.

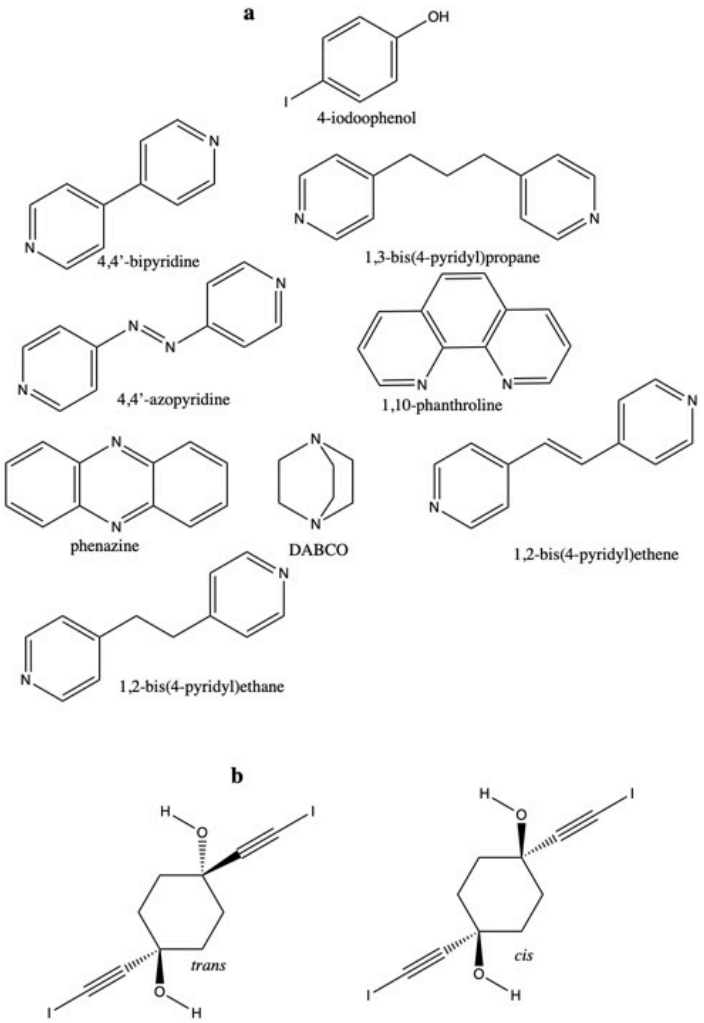

Scheme 2. Schematic structure of donors and acceptors used in study of the competition of XB and HB. a: 4-iodophenol and nitrogen containing molecules. b: *trans*- and *cis*-1, 4-bis(iodoethynyl)cyclohexane-1, 4-diol.

To further understand when XB prevails in competition with HB, Aakeröy *et al.*[34] used a group of phenyl-containing molecules with both XB (Br, I) and HB donors (-COOH, -OH, -CH=NOH) to co-crystalize with various monotopic, symmetric ditopic, and asymmetric ditopic acceptors (sp^2-N, sp^2-O, and sp^3-O). With the obtained 24 crystals, differences in electrostatic potential between the HB donor and the XB donor (Q value) were calculated and correlated to the selectivity between HB and XB. They found that: a) HB was present in all the 24

structures and XB was in only 13, and thus, HB was more competitive than XB; b) in structures involving monotopic and symmetric ditopic acceptors where both XB and HB formed, the average Q value was 142 kJ/mol, while in the structures where only HB was present, the average Q value was 175 kJ/mol. The Q value was further validified by correctly yielding 16 synthons out of 18 structures.[34] Clearly, the Q value provides a straightforward and applicable guide. However, it does not indicate any preferences for interactive site when only one type of non-covalent interaction takes place.

1.3.2 Selectivity of the XB Interactive Site

In cases where several XB interactive sites are available on one acceptor, sometimes puzzles can arise which site will engage in the formation of XB. Aakeröy *et al*.[43] confirmed the applicability of Etter's best donor-best acceptor rule in XB by calculating the electrostatic potentials on interactive sites of obtained co-crystals from a series of biimidazole as XB acceptor and phenyl containing halogens as XB donor (**Scheme 3**). Moreover, the importance of electrostatic potential in predicting the XB location was revealed and addressed.

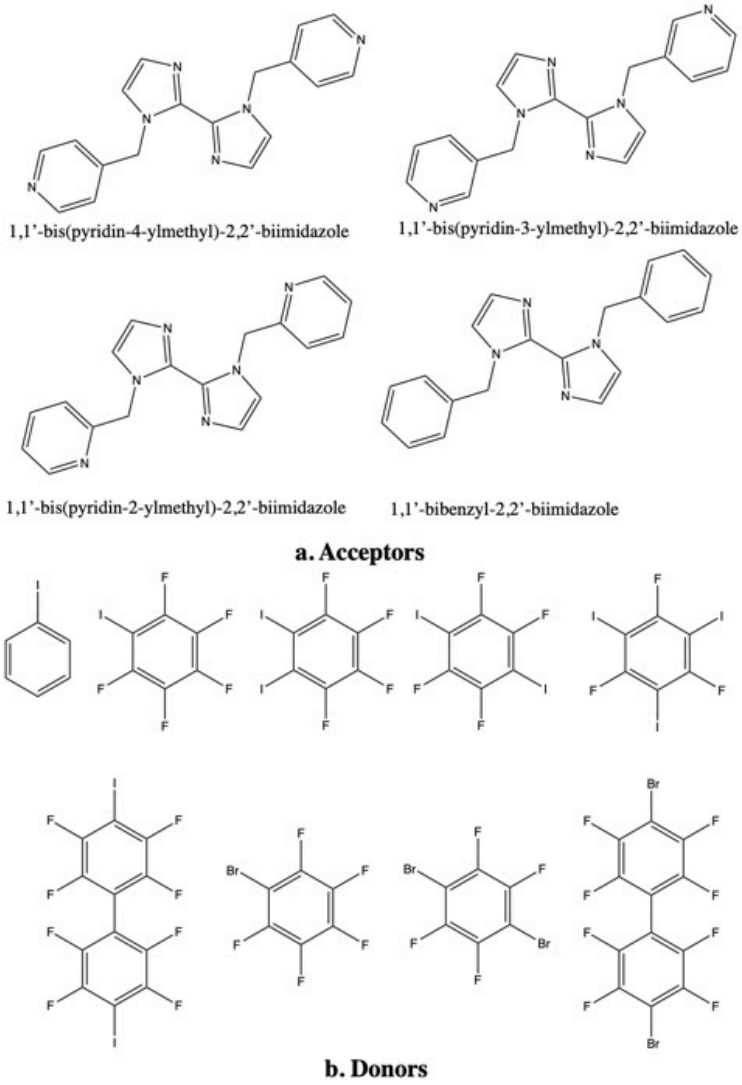

Scheme 3. Schematic structure of halogen bond donors and acceptors used in the studies of halogen bond selectivity by Aakeröy *et al.* **a**: N-(pyridinylmethyl)-2, 2′-biimidazole acceptors; **b:** phenol containing donors.

To further prove the pivotal role of electrostatic potential in the selectivity in XB, Aakeröy *et al.*[103] used fluoro-aliphatic organic halogens (**Scheme 4**) as the XB donor to co-crystalize with the same biimidazole XB acceptors in **Scheme 3**. The calculated electrostatic potentials yielded the same conclusion that the best XB docking site for XB donor was the pyridyl-N, which was of larger electrostatic potential than the imidazole-N.

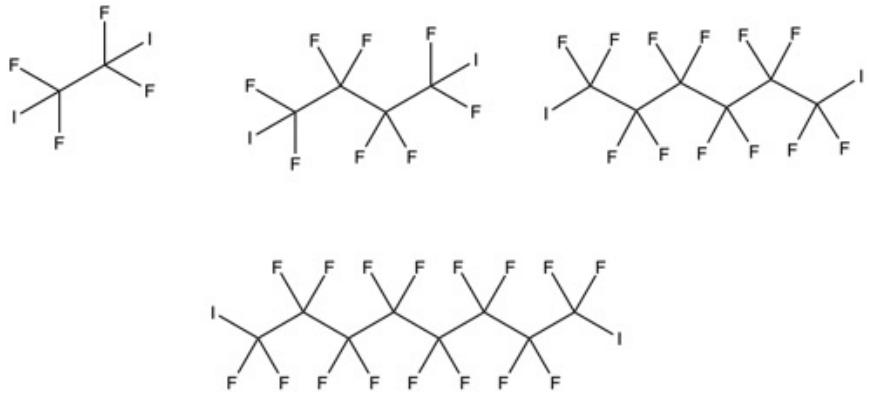

Scheme 4. Schematic of aliphatic halogen bond donors.

Similar to Etter's best donor-best acceptor rule, the hard-soft acid-base (HSAB) theory was proposed to predict and explain the selectivity of XB. This theory stresses that when several XB acceptors are available, the soft ones (atoms which are large and strongly polarizable) are the preferred XB acceptors. Cauliez *et al.*[38] noticed the prevalence of S···I in all the 6 crystals obtained from SCN^- and perfluoroiodobenzenes (*o*-DITFB, *m*-DITFB, *p*-DITFB, *sym*-TITFB). HSAB was employed to reason the stronger competitiveness of S than that of N: the soft S was the preferred XB acceptor when soft I was the donor. Moreover, they found that adjusting the strength of XB donors was effective in differentiating the XB accepting ability of S and N. Such application of HSAB to XB was later supported by Riel *et al.*[104], who investigated the halogen bond HSAB complementarity experimentally by co-crystalizing SCN^- with a bisethynyl benzene containing bitopic XB donor (**Scheme 5**) in methane and DCM, respectively. They argued that when both strong XB donor and strong HB donor were present, the soft S engaged in XB and the hard N formed HB, but that when only XB donor was available without the presence of strong HB donor, both N and S were able to form XB.

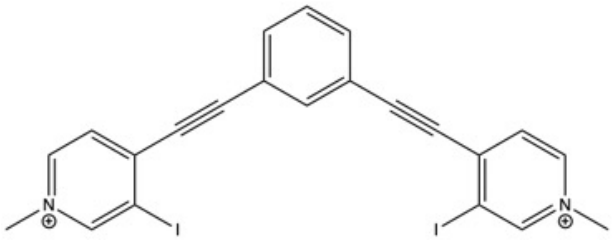

Scheme 5. Schematic structure of 4, 4′-[1, 3-phenylenebis(ethyne-2, 1-diyl)]bis(3-iodo-1-methylpyridine-1-ium).

1.4 Aim of the Study

The aim of the study was to utilize halogen bond as the primary force in crystal engineering. In our previous work I_2 was used to bridge $[Ru(bpy)(CO)_2X_2]$ (X=Cl, Br, I) compounds (**Scheme 6a**).[56] However, due to the redox property of I_2, organic iodine in some cases is a better choice. Thus, a more predictably behaved bitopic XB donor, *p*-DITFB, was used to investigate the construction of extended metal structures using $[Ru(bpy)(CO)_2X_2]$ as the XB acceptors and the formation of XBs with the zwitterionic XB donor, 1-(4-pyridyl)-4-thiopyridine (PTP).

Previous studies[105-109] have reported that the S coordinated thiocyanate was able to form XB while the thiocyanate N was mostly involved in either HB[103, 105] or coordinating to a metal[104, 105, 107]. Therefore, it was of great interests to investigate the XB preference from an energetic perspective in the system of $[Ru(bpy)(CO)_2(S\text{-}NCS)_2]$ (**Scheme 6b**) and I_2.

Multidentate XB acceptors are the key tectons for high dimensional structures. SCN^- is an excellent building block for such purpose: the sp^3-S is a bidentate XB acceptor and the N assures 1:1 interaction ratio to XB donor. However, using SCN^- as the XB acceptor can result in introduction of undesired cations into the system. Thus, PTP, a neutral zwitterionic compound (**Scheme 6c**), incorporating of both a sp^3-S and a sp^2-N, was synthesized to avoid such problem. Moreover, the location of S and N on each end of the PTP molecule enables a better study of the selectivity of XB between S and N without the influence of resonance effect which can happen on SCN^-.[38] To avoid strong XB donor "covering up" the difference in XB accepting ability of S and N, a series of XB donors with different strength (**Scheme 6d**) was used in this study.

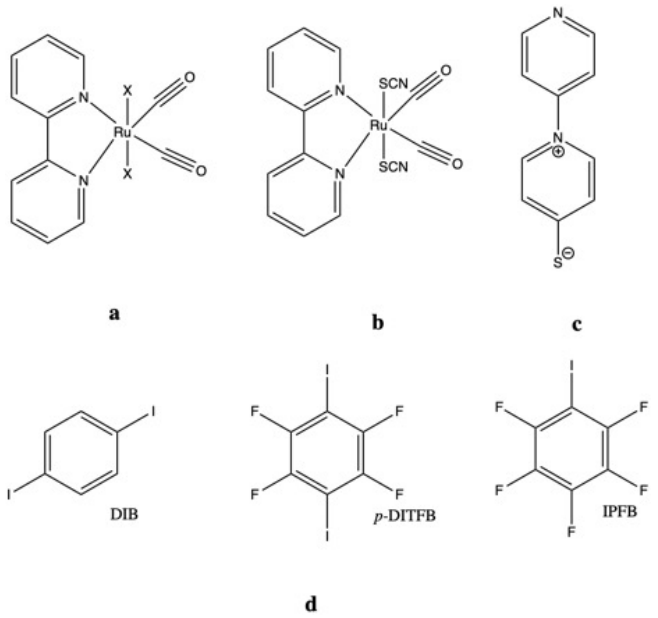

Scheme 6. Schematic structures of halogen bond donors and acceptors used in this study. **a:** [Ru(bpy)$(CO)_2X_2$] (X=Cl, Br, I); **b:** [Ru(bpy)$(CO)_2$(S-NCS)$_2$]; **c**: PTP, **d**: halogen bond donors.

2 EXPERIMENTAL

2.1 Synthesis

Both $[Ru(bpy)(CO)_2X_2]$ (X=Cl, Br, I) and $[Ru(bpy)(CO)_2(S\text{-}NCS)]$ were synthesized according to previous studies.[110-112] All the XB donors were commercially available and used as received. Slow evaporation at room temperature was used to harvest single X-ray suitable crystals.

1-(4-pyridyl)-4-thionpyridine (PTP) Zwitterion. 4-Mercaptopyridine of 100 mg was heated at 67°C for 16 hours with constant stirring. Then the orange-yellow powder was dissolved into boiling water of 5mL. The solution was adjusted to pH 10 with saturated NaOH aqua solution and was filtered. The filtrate was extracted with dichloromethane (6x10mL). The organic phase was reduced to 5mL by rotary evaporation. The reduced solution was purified through a chromatography column with acetonitrile as the eluent, and then was vacuumed dry. The obtained PTP is pale greenish yellow solid. The yield is 16.1%. mp: 155.3-157.1°C.

2.2 Characterization

Single X-ray diffraction was used to determine all the crystal structures. All the crystallization was not optimized to maximize the yield, as the main purpose was to investigate the primary products. Melting point of the newly synthesized PTP was measured and the differential scanning calorimetry (DSC) data was also obtained in the study of XB selectivity when PTP was the XB acceptor.

2.3 Computational Details

The interaction energy and the frontier molecular orbitals were calculated to gain insights into the S as the preferred XB acceptor over N in [Ru(bpy)$(CO)_2$(S-NCS)]. The geometry of the obtained [Ru(bpy)$(CO)_2$(S-NCS)]•I_2 was optimized. All the models were calculated with Gaussian 09 program package[113] at the density function level of theory (DFT) with a hybrid functional PBE0[114]. The DFT wavefunctions were used for the topological charge density analysis with the Quantum Theory of Atoms in Molecules (QTAIM)[115], which was performed with AIMALL program[116].

3 RESULTS AND DISCUSSION

The relative strength of XB is often presented using the halogen bonding interaction ratio, R_{XB}, defined as $R_{XB}=d_{XB}/(X_{vdW} + B_{vdW})$, where d_{XB} is the distance between XB donor X and XB acceptor B in Å (Bondi vdW radii are used to describe X_{vdW} and B_{vdW}).[119-121] A smaller value of R_{XB} indicates a stronger XB.

3.1 Assemblies of $Ru(bpy)(CO)_2X_2$ (X=Cl, Br, I) and DITFB (Paper II)

The key structural parameters of the XBs are listed in the three structures $[Ru(bpy)(CO)_2Cl_2]$•DITFB (**1**), $[Ru(bpy)(CO)_2Br_2]$•DITFB (**2**), and $[Ru(bpy)(CO)_2I_2]$•DITFB (**3**) in **Table 1**.

Table 1. Halogen bonds in **1-3** and in [Ru(bpy)$(CO)_2X_2$]•I_2 from **Reference 56**.

Compound	**Ru-X···I (Å)**	**C-I···X (°)**	**M-X···I (°)**	**R_{XB}**
1	3.1790(8)	170.60(9)	114.94(3)	0.85
2	3.3191(4)	171.34(10)	112.108(14)	0.87
3	3.5301(3)	177.66(13)	96.672(9)	0.89
Reference 56	Ru-X···I (Å)	I-I···X (°)	M-X···I (°)	R_{XB}
Cl···I_2	3.0421(3)	174.566(8)	115.76(1)	0.82
Br···I_2	3.2938(4)	170.28(1)	101.3(1)	0.86
Br···I_2	3.3627(3)	173.80(1)	102.27(1)	0.88
Br···I_2	3.2381(3)	175.405(9)	101.66(1)	0.85
Br···I_2	3.3001(3)	174.164(9)	102.57(1)	0.86
I···I_2	3.1984(3)	177.941(7)	97.91(1)	0.81
I···I_2	3.7984(3)	152.083(6)	104.26(1)	0.96
I···I_2	3.2553(13)	172.75(2)	97.81(2)	0.82
I···I_2	3.4108(15)	166.50(2)	98.90(2)	0.86

Cocrystals **1-3** demonstrate 1D chain structure *via* XB where *p*-DITFB is the symmetric XB donor linking the ruthenium complexes in all the three structures. **1** and **2** are isomorphs, showing zig-zag chains (**Figure 17)**, while **3** shows linear chains (**Figure 18**). In **1** and **2**, *p*-DITFB is located at an inversion center, and in **3** the XB donor is situated in a mirror plane. Similarly, the ruthenium atoms in **1** and **2** are placed in a two-fold rotation axis, but the metal center in **3** is in mirror plane. Such symmetry means that the distance between the two I atoms of *p*-DITFB to the halido ligand of the ruthenium complex are equal in all assemblies due to the unchanged behavior of the second I atom in *p*-DITFB when the first I atom forms XB.

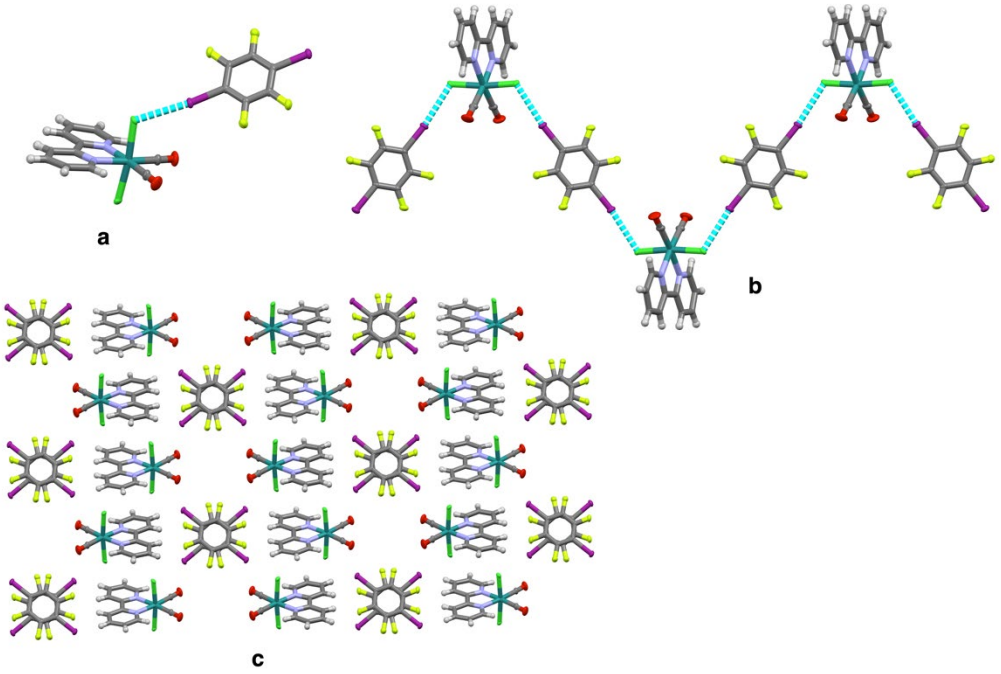

Figure 17. Crystal structure of [Ru(bpy)(CO)$_2$Cl$_2$]•*p*-DITFB (**1**). **a:** Cl···I interaction; **b**: zig-zag chain structure; **c:** packing along the crystallographic *c*-axis.

The halido ligands in both **1** and **2** are engaged in the XB formation, yielding M-Cl···I and M-Br···I, respectively ($d_{M\text{-}Cl\ldots I}$: 3.1790Å, $<_{Cl\ldots I\text{-}C}$: 170.60°, $<_{M\text{-}Cl\ldots I}$: 114.94°; $d_{M\text{-}Br\ldots I}$: 3.3191Å, $<_{Br\ldots I\text{-}C}$: 171.34°, $<_{M\text{-}Br\ldots I}$: 112.108°). Clearly, the angle of M-X···I in **1** and **2** deviates from 90°, indicating a relatively weak electron density redistribution towards the area perpendicular to the M-X. *p*-DITFB are stacked through π-π interaction between the aromatic rings. The shortest carbon-carbon distance between neighboring *p*-DITFB ranges from 3.178Å to 3.358Å in **1** and from 3.165Å to 3.685Å in **2**. Moreover, voids are formed in both **1** and **2** (259 Å^3 in **1**, 310 Å^3 in **2**), which are filled with disordered solvent molecules.

Different from **1** and **2**, **3** only has one of the two iodio ligand (I1) involves in the XB. The bidentate I1 bridges two *p*-DITFB molecules ($d_{M\text{-}I\ldots I}$: 3.5301Å, $<_{I\ldots I\text{-}C}$: 177.66°, $<_{M\text{-}I\ldots I}$: 96.672°). Clearly, the angle of M-X···I in **3** is significantly closer to 90° than that in **1** and **2**, due to the stronger polarizability of iodo ligand than bromo- and chloro ligand. The neighboring chains in **3** are further connected *via* F···O interaction without any significant voids formed.

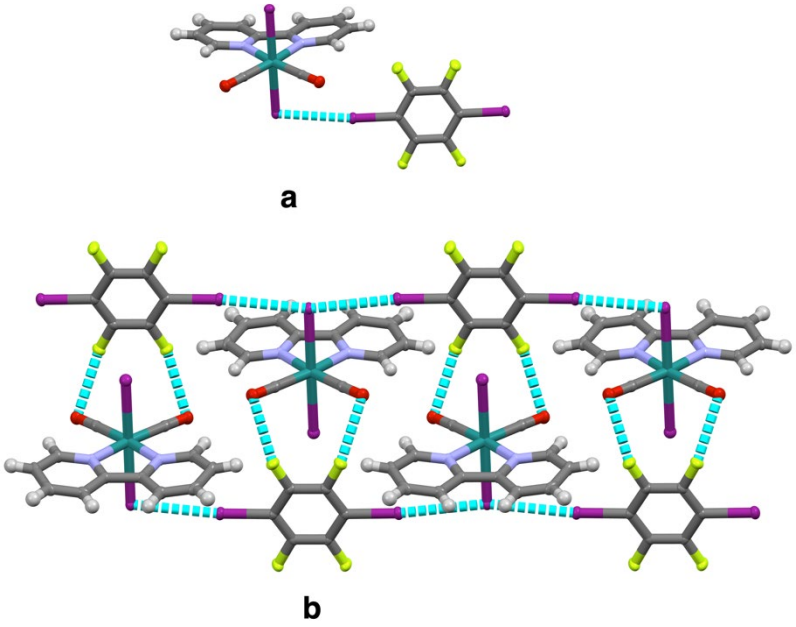

Figure 18. Crystal structure of [Ru(bpy)(CO)$_2$I$_2$]•*p*-DITFB (**3**). **a:** I···I interaction; **b:** Chain structure of **3** *via* I···I and O···F.

Compared with XBs in [Ru(bpy)(CO)$_2$X$_2$]•I$_2$, **1-3** illustrate geometric differences in XBs. Based on R$_{XB}$ values of **1-3**, a clear trend of the XB strength is observed: X=Cl>Br>I. Such order was also noticed in the system of halogen containing Pd pincer complexes with I$_2$.[121] However, in the [Ru(bpy)(CO)$_2$X$_2$]•I$_2$ system,[56] this trend is less obvious and is in the order of X=I>Cl>Br. That is probably caused by the increased charge transfer between iodo-ligand and I$_2$, resulting in more electron sharing between them, while in the cases of chloro- and bromo ligands electrostatic interaction is still dominant. Similarly, in [Ru(dcbpy)(CO)$_2$I$_2$]•I$_2$,[122] the R$_{XB}$ value is in the range from 0.79 to 0.82, smaller than that in **3**, indicating once again the increased electron sharing between the XB donor and acceptor. In system of [Ru(CNR)$_4$X$_2$]•I$_2$ (X=Cl, Br, I),[123-124] R$_{XB}$ of Ru-Cl···I is between 0.78 and 0.85, for Ru-Br···I is 0.84, and for Ru-I···I ranges from 0.79 to 0.84. Clearly, the trend of R$_{XB}$ in this system is not as obvious as in **1-3**. When other electrostatic dominant systems are inspected and compared with **1-3**, the R$_{XB}$ values are almost equal regardless of the metal center.[65, 121]

3.2 XB Preference for S over N in Thiocyanate Ligand (Paper I)

The asymmetric unit of cocrystal of [Ru(bpy)(CO)$_2$(S-NCS)]•I$_2$ (**4**) contains two Ru(bpy)(CO)$_2$(S-NCS)$_2$ molecules and two I$_2$ molecules. A dimeric structure (**Figure 19**) is formed *via* S1···I1 ($d_{S...I}$: 3.146Å, <$_{S...I-I}$: 172.87°, <$_{Ru-S...I}$: 107.62°). Different molar ratios of the ruthenium complex to I$_2$ were used for co-crystallization (1:1, 1:2, 1:5, 1:10); however, only one structure was observed with the ruthenium coordinated S as the XB acceptor, despite the fact that the

N-end of SCN is more sterically free, indicating the soft S is the preferred XB acceptor. Moreover, in the obtained structure only one -SCN ligand is engaged in XB, leaving the other one free, regardless of the amount of I_2 used. Therefore, the packing effects (other weak interactions) may play a major role in the crystalline product formation.

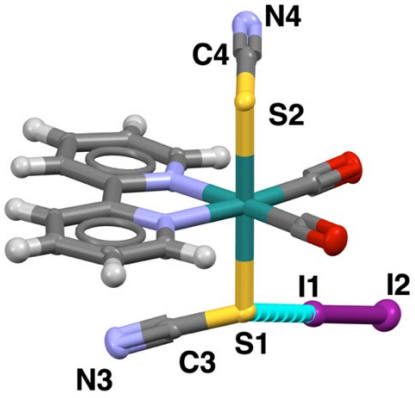

Figure 19. Crystal structure of $[Ru(bpy)(CO)_2(S\text{-}NCS)_2]\bullet I_2$ (**4**).

To further confirm that packing effect is the major contributor to the crystal structure formation, a computational analysis was performed. The geometry of $[Ru(bpy)(CO)_2(S\text{-}NCS)_2]$, the S···I adduct, and the N···I adduct were optimized using DFT technique. The selected bond distance and the AIM parameters are shown in **Figure 20**.

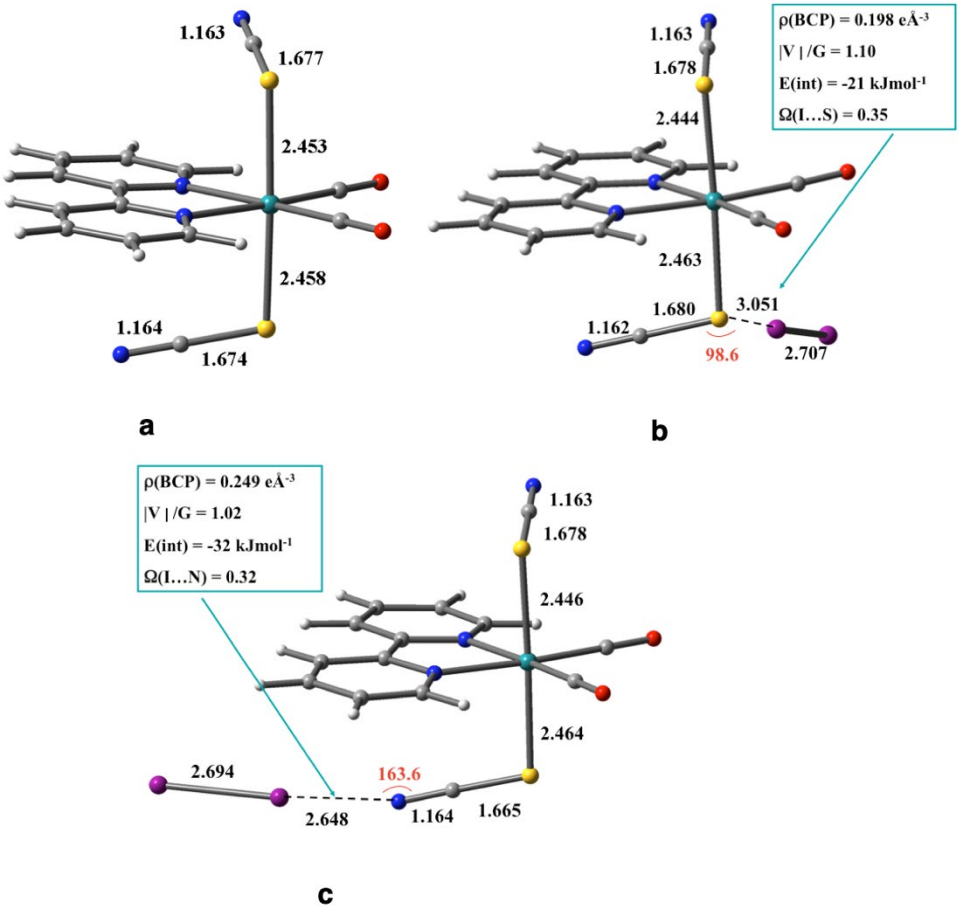

Figure 20. Optimized structure of models. **a:** [Ru(bpy)(CO)$_2$(S-NCS)$_2$]; **b:** structure with S···I contact; **c:** structure with N···I contact.

The geometric differences between the computational structures and the experimentally obtained ones are caused by the overestimation of charge transfer in gas-phase calculations, which in fact enables to reveal the differences in the I···S and I···N interaction energies and properties without the inference of any packing effects. The AIM defined atomic charges are listed in **Table 2**.

Table 2. Atomic charges according to the AIM analysis for Ru, I, N, and S atoms in the different configuration of the $[Ru(bpy)(CO)_2(S\text{-}NCS)_2]\bullet I_2$

Atom*	$[Ru(bpy)(CO)_2(S\text{-}NCS)_2$	I···N	I···S
q(Ru)	0.949	0.951	0.949
q(S1)	0.12	0.163	0.146
q(S2)	0.113	0.121	0.123
q(N3)	-1.198	-1.231	-0.166
q(N4)	-1.191	-1.184	-0.180
q(I1)	–	0.095	0.008
q(I2)	–	-0.156	-0.135

*: Numbering Scheme is the same as in **Figure 19**.

Clearly, the "hard" N induces more effective polarization of I_2 than the "soft" S does, generating larger charge difference between I1 and I2: 0.251 in N···I and 0.143 in S···I. The ratio of potential energy density and kinetic energy density, $|V|/G$, at the bond critical point indicates the nature of the interaction. If $|V|/G > 2$, the interaction is covalent; if $|V|/G < 1$, the interaction is electrostatic.[125-127] The value between 1 and 2 suggests both electrostatic and charge transfer take place. Moreover, the delocalization index Ω, another parameter defining the nature of contact, describes the extent to which electrons are shared. The value of Ω is 0 for electrostatic interaction and 1 for covalent bond. These two parameters of adduct S···I and N···I differ marginally, suggesting XB in both adducts are of the same nature: primarily electrostatic interaction with minor covalent character.

The difference in interaction energies, E(int), between the N···I adduct and S···I adduct is only 11 kJ/mol, which can be easily overcome by other noncovalent interactions in the crystal. Based on the value of E(int), N···I adduct is energetically more favorable. However, none of those computational results can negate the existence of the observed S···I adduct. On the other hand, both structures should be possible based on the computational analysis. Thus, the cause of the S···I adduct to be the only experimentally available product is the packing effect, i.e. other type of non-covalent intermolecular interactions.

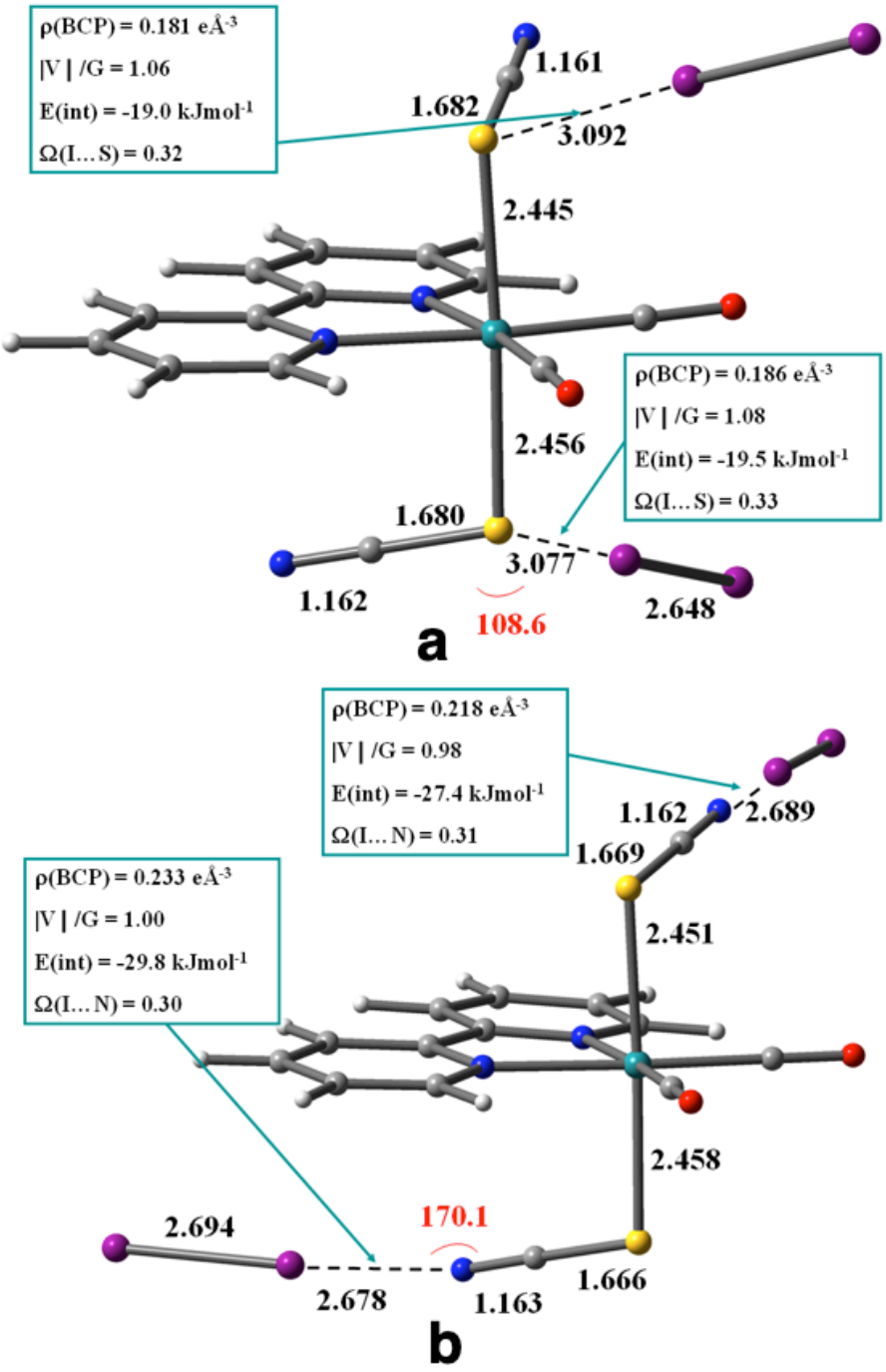

Figure 21. Optimized structure of crystals with both thiocyanate ligands involved in XB. **a:** doubly interacting crystals with S···I contacts; **b:** doubly interacting crystal with N···I contacts.

To investigate whether energy barrier is the cause of the absence of the second SCN ligand involved in XB, computational analysis was performed on [Ru(bpy)(CO)$_2$(S-SCN)]•2I$_2$ adducts (**Figure 21**). But the results indicate that to have both SCN ligand participating in XB is possible, regardless of the interaction site. The frontier molecular orbitals (FMOs) of [Ru(bpy)(CO)$_2$(S-SCN)]•I$_2$ and [Ru(bpy)(CO)$_2$(S-SCN)]•2I$_2$ (**Figure 22**) provide the explanation.

The HOMOs of the doubly interacting adduct are comparable to that of the singly interacting one. However, the LUMOs of the adduct with both SCN forming XB, regardless N or S, are stabilized, resulting in reduced overall stability.

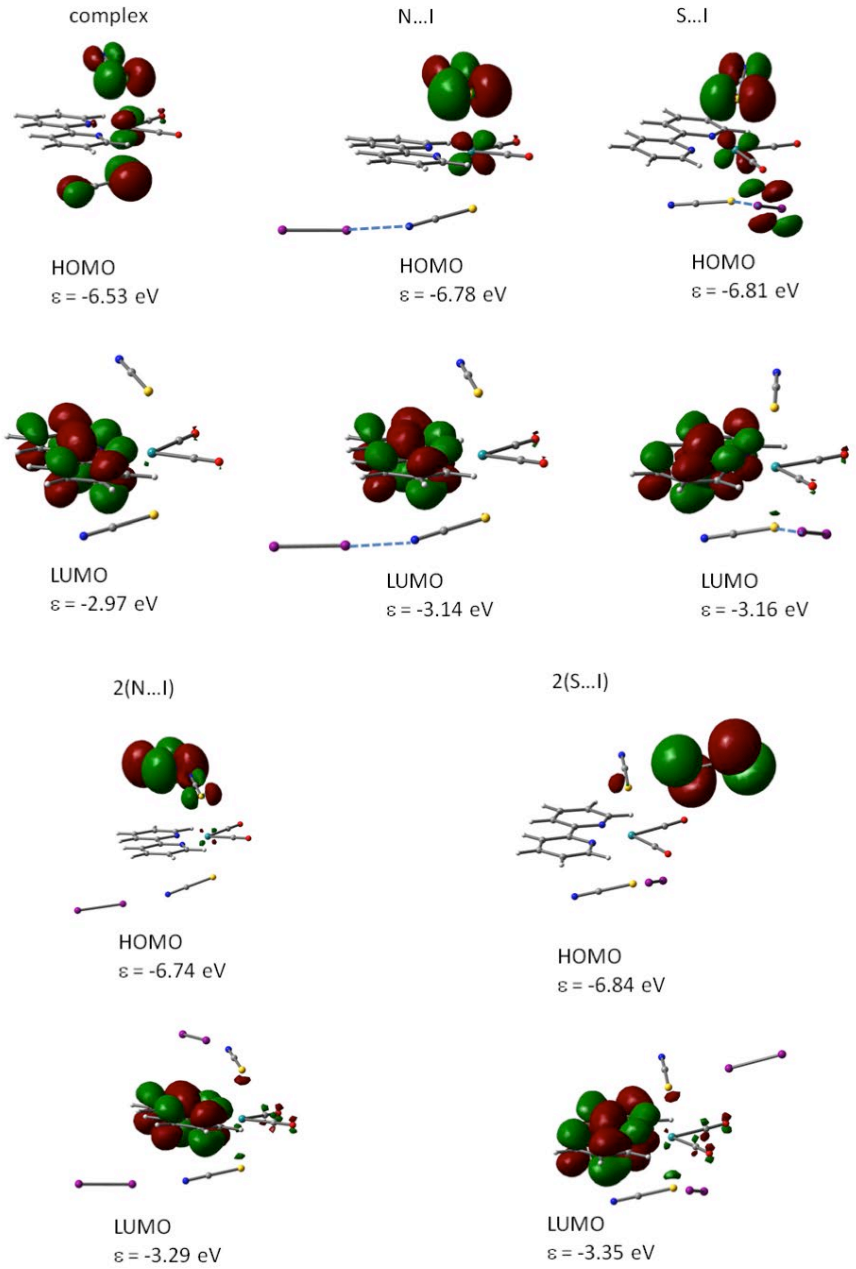

Figure 22. Frontier molecular orbitals (FMOs) of [Ru(bpy)$(CO)_2$(S-NCS)$_2$], the singly interacting adducts, and the doubly interacting adducts.

3.3 Zwitterion PTP as XB Acceptor (Paper III)

Three crystals were obtained from co-crystallization of PTP and three XB donors: PTP•DIB (**5**), PTP•*p*-DITFB (**6**), and PTP•IPFB (**7**). The key structural parameters of halogen bonds in **5-7** are listed in **Table 3**.

Table 3. Halogen bonds in **5-7**

Crystals	I···A	*d*(I…A) Å	<C-I…A °	R_{XB}
5	I···N	2.968(3)	177.01(9)	0.839
6	I1···N2	2.845(6)	171.4(2)	0.806
	I2···N4	2.915(6)	176.7(2)	0.826
	I3···S1	3.096(1)	174.6(1)	0.819
	I6···S1	3.215(1)	171.8(1)	0.851
	I4···S2	3.137(1)	172.6(1)	0.830
	I5···S2	3.300(1)	171.7(1)	0.873
7	I1···S1	3.1224(8)	175.47(7)	0.826
	I2···S1	3.1122(8)	176.9(1)	0.823

In **5** (**Figure 23**) the N atom of PTP forms XB with one I atom of DIB ($d_{N...I}$: 2.968 Å, $<_{C\text{-}I...N}$: 177.01°). The DIB acts as a symmetric XB donor, linking two PTP molecules on N. The S atom in PTP forms three weak HBs with two neighboring PTP molecules and an adjacent DIB molecule ($d_{S...C5}$: 3.808Å, $<_{C5\text{-}H...S}$: 155.3°; $d_{S...C7}$: 3.795Å, $<_{C7\text{-}H...S}$: 164.97°; $d_{S...C12}$: 3.712Å, $<_{C12\text{-}H...S}$: 136.09°).

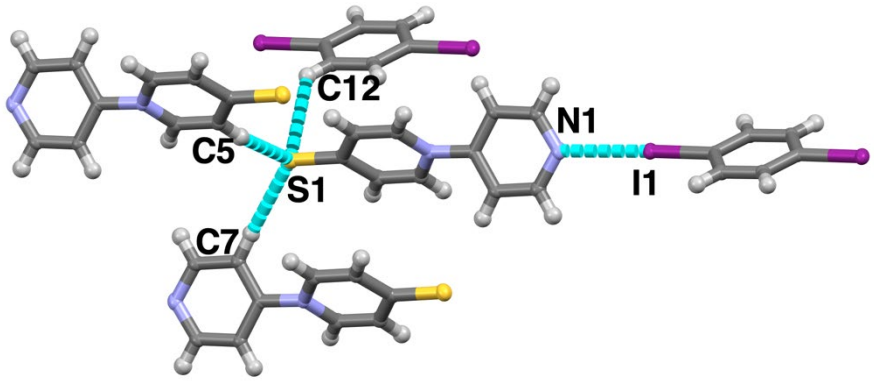

Figure 23. Crystal structure of PTP•DIB (**5**).

In **6** (**Figure 24a**) both N and S are involved in XB formation. One *p*-DITFB molecule bridges two PTP molecules *via* N···I ($d_{N2...I1}$: 2.845Å, $<_{C\text{-}I1...N2}$: 171.4°; $d_{N4...I2}$: 2.915Å, $<_{C\text{-}I2...N4}$: 176.7°). Meanwhile, S of PTP functions as a bidentate XB acceptor, binding two other *p*-DITFB molecules ($d_{S1...I3}$: 3.096Å, $<_{C\text{-}I3...S1}$: 174.6°; $d_{S1...I6}$: 3.215Å, $<_{C\text{-}I6...S1}$: 171.8°; $d_{S2...I4}$: 3.137Å, $<_{C\text{-}I4...S2}$: 172.6°; $d_{S2...I5}$: 3.300Å, $<_{C\text{-}I5...S2}$: 171.7°). Additionally, S1 forms S1···H-C ($d_{S1...C}$: 2.929Å, $<_{S1...H\text{-}C}$: 162.89°) with a neighboring PTP molecule and I4 is involved in HB formation with an adjacent PTP molecule ($d_{I4...C}$: 3.927Å, $<_{I...H\text{-}C}$: 136.98°). Furthermore, through the N···I and the bifurcated S···I halogen bonds twelve membered rings are formed, yielding a wavy 2D network with S as the node (**Figure 24b**). The 2D network is further expanded into five folded interpenetrated 3D network *via* F···H, F···C, and S···H with neighboring units. No solvent occupied channels are formed despite the presence of CH_2Cl_2 in the structure.

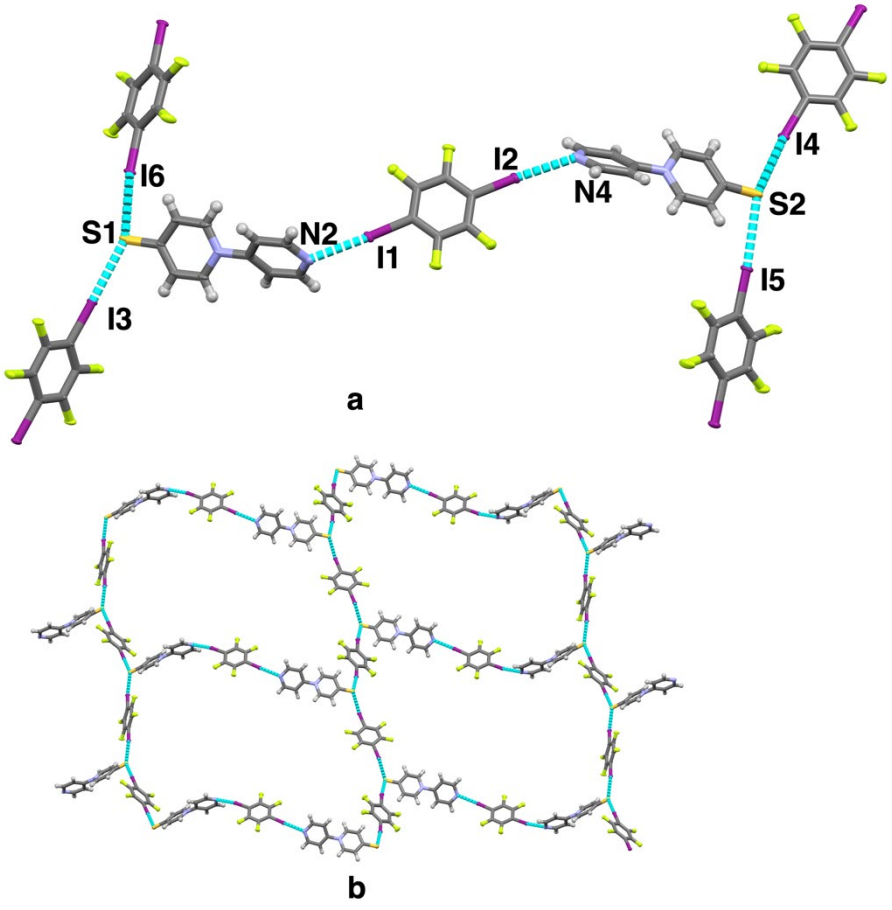

Figure 24. Crystal structure of PTP•*p*-DITFB (**6**). **a:** N···I and S···I; **b:** extended 2D network. Solvent molecules CH_2Cl_2 are omitted for clarity.

In **7** (**Figure 25**) the S atom of PTP forms a pair of bifurcated XBs ($d_{S1...I1}$: 3.1224Å, $<_{C\text{-}I1...S1}$: 175.47°; $d_{S2...I2}$: 3.1122Å, $<_{C\text{-}I2...S1}$: 176.9°). The N atom of PTP is involved in the formation of HB with two adjacent PTP atoms ($d_{N...C2}$: 3.423Å, $<_{N...H\text{-}C2}$: 132.55°; $d_{N...C9}$: 3.259Å, $<_{N...H\text{-}C9}$: 117.59°; $d_{N...C10}$: 3.250Å, $<_{N...H\text{-}C10}$: 117.38°). The

relatively large deviation of the three N···H from 180° is probably due to the dispersion interactions, which impacts the geometry of HB in bulky systems.[128]

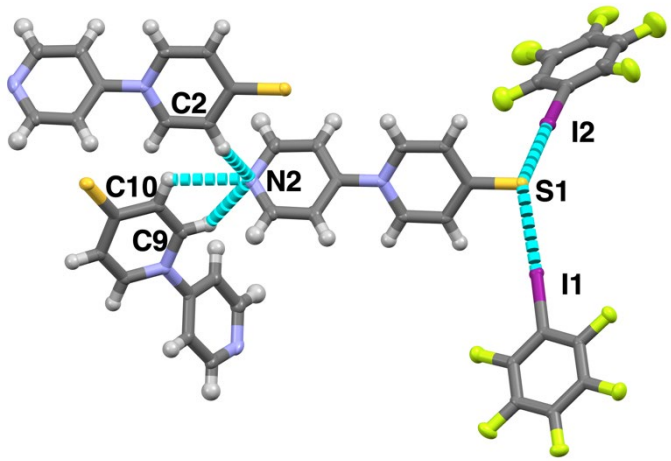

Figure 25. Crystal structure of PTP•IPFB (**7**).

The strength of XBs in **5-7** are compared with previously reported ones in similar synthons with a CCDC survey (C=N, sp^3-S-C, no organometallic complexes, $d_{N\cdots I}$<3.53Å, and $d_{S\cdots I}$<3.78Å, CSD version 5.41, Nov. 2019). The median of $d_{N\cdots I}$ from the survey is 3.050Å, longer than the length of N···I ranging from 2.845Å to 2.968Å in **5-7**. Similarly, the median of $d_{S\cdots I}$ from the survey is 3.668Å, much longer than the length of S···I in the range of 3.096 and 3.330 in **5-7**. Thus, both N···I and S···I in **5-7** are stronger than most reported ones, indicating that PTP is capable of forming robust XBs with its acceptor atoms.

The R_{XB} of N···I in **5** is 0.839, while the R_{XB} of the two N···I in **6** are 0.806 and 0.826, respectively, suggesting that DITFB is a stronger XB donor than DIB. Moreover, the average $d_{S1\cdots I}$ is 3.117Å and the average $d_{S2\cdots I}$ is 3.219 in **6**, while the average $d_{S1\cdots I}$ in **7** is 3.117Å. Clearly, the S···I in **7** is stronger than that in **6**, revealing IPFB is a stronger XB donor than *p*-DITFB. The strength of XB donors is ranked in the order: DIB<*p*-DITFB<IPFB. Such result is expected as the I atom is surrounded by the strongest electronegative environment in IPFB and by the weakest in DIB.

In **5** only N participates in XB formation, while in **7** only S does. Different from **5** and **7**, **6** has both N and S are involved in XB. A clear selectivity in XB formation is demonstrated. HSAB theory has successfully explained the selectivity in XB; however, it fails in this case as the hardest I in IPFB chooses the soft S instead of the hard N. In fact, the I is still soft in nature, especially compared with N, despite that the I is in a stronger electronegative environment in IPFB than in *p*-DITFB and DIB. Thus, the selectivity of XB is probably mainly under the influence of other noncovalent interactions. Hirschfeld surface analyses[129-130], a method to inspect the interactions in molecular packing and comparison of crystal structures, was used to estimate the contribution of XB to the total molecular interaction. CrystalExplorer 17.5[131]

was use to gain insight into the contribution of XB to the Hirshfeld surface, which is summarized in **Table 4**.

Table 4. Contribution of XBs to Hirshfeld surfaces in **5-7**

Cocrystals	XB	Contribution %
1	N···I	2.1
2	N···I	3.2
2	S···I	3.4
3	S···I	5.2

The XB contribution to the Hirschfeld surface is less than 10% in **5-7**, indicating that it is not the major crystal stabilizing force. The DSC measurements (**Table 5**) support the conclusions as well: DIB, the weakest XB donor, forms the most thermally stable crystal **5**, whereas IPFB, the strongest XB donor, yields the most thermally unstable **7**, suggesting that other types of noncovalent interactions are the prominent ones in these crystals.

Table 5. DSC measurements of 5-7

Crystals	5	6	7
T_c/°C	127.67	114.46	85.36

SUMMARY

This work aims at using XB in crystal engineering and investigating the selectivity of XB between the soft XB acceptor S and the hard N. A series of [Ru(bpy)(CO)$_2$X$_2$]•*p*-DITFB (X=Cl, Br, I) were crystallized and analyzed. Both [Ru(bpy)(CO)$_2$Cl$_2$]•*p*-DITF (**1**) and [Ru(bpy)(CO)$_2$Br$_2$]•*p*-DITFB (**2**) form isomorphic zig-zag chain structure, and further expand *via* π-π interaction between neighboring *p*-DITFB molecules into 3D network with solvent occupied voids. In **1** and **2** both halido ligands, as monodentate XB acceptors, are involved in the XB formation. Differently, in [Ru(bpy)(CO)$_2$I$_2$]•*p*-DITFB (**3**) only one of the two ruthenium coordinated iodine atoms are engaged in XB, connecting two *p*-DITFB molecules and forming linear chains, which are further linked *via* F···O contacts. Furthermore, when compare the series **1-3** with corresponding series with I_2 as the XB donor, differences due to the XB nature are surfaced in respect to the symmetry and XB bond strength. When I_2 as the bridging XB donor, the second XB bond is influenced by the first one, as charge transfer overtakes the electrostatic interactions as the major force. whereas When *p*-DITFB replaces I_2, electrostatic force is prominent, forming more symmetric XBs. Therefore, in the series of 1-3 the XB acceptor strength is in the order of Ru-Cl>Ru-Br>Ru-I.

The preference of XB for S atom over N atom in thiocyanate ligand in [Ru(bpy)(CO)$_2$(S-NCS)$_2$] was studied by crystalizing the ruthenium complex with I_2. Only one of the two sulfur coordinated SCN ligands participates in XB formation on the S atom, leaving the less steric hindered N free, yielding [Ru(bpy)(CO)$_2$(S-NCS)$_2$]•I_2 (**4**). However, the computational analysis indicates SCN···I_2 is slightly more energetically favorable than NCS···I, revealing that packing effect dictates the XB preference for S over N. The FMOs shed lights to the absence of [Ru(bpy)(CO)$_2$(S-NCS)$_2$]•2I_2, though energetically possible. The LUMO of the doubly interacting adduct is of lower energy than that of the singly interacting one, while the HOMO of both type of adducts are almost equal, and thus, the stability of the doubly interacting adduct is reduced.

To leverage the bidentate feature of sp^3-S and the controllability of sp^2-N as XB accepting atoms and to avoid the introduction of undesired cations when SCN^- as XB acceptor, a neutral zwitterionic XB acceptor, PTP, was synthesized for such purpose. Three crystals (**5-7**) were obtained with DIB, *p*-DITFB, and IPFB as XB donor, respectively. Strong XBs are formed in these three crystals, demonstrating PTP is a robust XB acceptor. A 2D wavy network structure of **6** was formed with the symmetric bitopic XB donor, *p*-DITFB. The selectivity of XBs in this series was investigated with Hirschfeld surface analyses and DSC measurements. The minor contribution of XB to the Hirschfeld surface and the reversed thermal stability with respect to the XB strength suggest that other noncovalent interactions are the major factors determining the final arrangement of the molecules.

All in all, this work demonstrates that both [Ru(bpy)$(CO)_2X_2$] (X=Cl, Br, I) and zwitterion PTP are able to form extended structures with *p*-DITFB. Moreover, the study on the selectivity of XB regarding S and N indicate that a holistic view must adopted in building a supramolecular architecture. However, the challenge lays in the prediction of the dominant noncovalent interaction, which hampers the controllability of supramolecular construction.

REFERENCES

1. Mukherjee, A.; Desiraju, R. G., *Cryst. Growth Des.* **2011**, 11, 3735-3739.
2. Rosokha, S. V.; Stern. C. L.; Vinakos, M. K., *CrystEngComm.* **2016**, 18, 488-495.
3. Christopherson, J.; Potts, K. P.; Bushuyev, O. S.; Topić, F.; Huskić, I.; Rissanen, K.; Barrett, C. J.; Friščić, T., *Faraday Discuss.* **2017**, 203, 441-457.
4. Nemec, V.; Fotović, L.; Friščić, T, Cinčić, D., *Cryst. Growth Des.* **2017**, 17, 6169-6173.
5. Su, M.; Yan X.; Guo, X.; Li, Q.; Zhang, Y.; L, C., *Chem. Eur. J.* **2020**, 26, 4505-4509.
6. Desiraju, G. R.; Ho, P. S.; Kloo, L.; Legon, A. C.; Marquardt, R.; Metrangolo, P.; Politzer, P.; Resnati, G.; Rissanen, K., *Pure Appl. Chem.* **2013**, 85, 8, 1711-1713.
7. Politzer, P.; Murray, J. S.; Clark, T., *Phys. Chem. Chem. Phys.* **2010, 12**, 7748-7757.
8. Priimagi, A.; Cavallo, G.; Metrangolo, P.; Resnati, G. *Acc. Chem. Res.* **2013**, 46, 11, 2686-2695
9. Clark, T. *Faraday Discuss*. **2017**, 203, 9-27.
10. Stilinović, V.; Horvat, G.; Hrenar, T.; Nemec, V.; Cinčić, D., *Chem. Eur. J.* **2017**, 23, 5244-5257.
11. Awwadi, F. F.; Willett, R. D.; Peterson, K. A.; Twamley, B. *Chem. Eur. J.* **2006**, 12, 8952-8960.
12. Voth, A.; Khuu, P.; Oishi, K.; Ho, P. S., *Nat. Chem.* **2009**, 1, 74-79.
13. Forni, A.; Franchini, D.; Daiaggi, F.; Pieraccini, S.; Sironi, M.; Scilabra, P.; Pilati, T.; Petko, K.; Resnati, G.; Yagupolkii, Y. L., *Cryst. Growth Des.* **2019**, 19, 1621-1631.
14. Awwadi, F. F.; Willett, R. D.; Peterson, K. A.; Twamley, B., *J. Phys. Chem. A* **2007**, 111, 2319-2328.
15. Awwadi, F. F.; Taher, D.; Haddad, S. F., *Cryst. Growth Des.* **2014**, 14, 1961-1971.
16. Metrangolo, P.; Meyer, F.; Pilati, T.; Resnati, G.; Terraneo, G., *Chem. Commun.* **2008**, 1635-1637.

17. Abate, A.; Marti-Rujias, J.; Metrangolo, P.; Pilati, T.; Resnati, G.; Terraneo, G., *Cryst. Growth Des.* **2011**, 11, 4220-4226.

18. Raffo, P. A.; Marcolongo, J. P.; Funes, A. V.; Slep, L. D.; Baggio, R. F.; Cukiernik, F. D., *J. Mol. Struct.* **2016**, 1108, 235-244.

19. Rosokha, S. V.; Stern, C. L.; Vinakost, M. K., *CrystEngComm*. **2016**, 18, 488-495.

20. Bosch, E.; Kruse, S. J.; Groeneman, R. H., *CrystEngComm.* **2019**, 21, 990-993.

21. Daub, K. S.; Habermann, B.; Hahn, T.; Teich, L.; Eger, K. *Eur. J. Org. Chem.* **2004**, 894-898.

22. Fujiwara, Y.; Domingo, V.; Seiple, I. B.; Gianatassio, R.; Bel, M. D.; Baran, P. S.*J. Am. Chem. Soc.* **2011**, 133, 3292-3295.

23. Cinčić, D.; Friščić, T.; Jones, W., *CrystEngComm.* **2011**, 13, 3224-3231.

24. Wu, W. X.; Wang, H.; Jin, W. J., *Cryst. Growth Des.* **2018**, 18, 11, 6742-6747.

25. Jay, J. I.; Padgett, C. W.; Walsh, R. D. B.; Hanks, T. W.; Pennington, W. T., *Cryst. Growth Des.* **2001**, 1, 6, 501-507.

26. Knight, F. R.; Fuller, A. L.; Bühl, Slawin, A. M. Z.; Woolins, J. D., *Chem. Eur. J.* **2010**, 16, 7605-7616.

27. Lieffrig, J.; Jeannin, O.; Frąckowiak, A.; Olejniczak, I.; świetlik, R.; Dahaoui, S.; Aubert, E.; Espinosa, E.; Auban-Senzier, P.; Fourmigué, M., *Chem. Eur. J.* **2013**, 19, 14804-14813.

28. Aakeröy, C. B.; Baldrighi, M.; Desper, J.; Metrangolo, P.; Resnati, G., *Chem. Eur. J.* **2013**, 19 16240-16247.

29. Hidalgo, P.; Leal, S.; Jiménez, C. A.; Vöhringer-Martinez, E.; Herrera, B.; Pasán, J.; Ruiz-Pérez, C.; Bruce, D. W., *CrystEngComm*. **2016**, 18, 42-47.

30. Lucenti, E.; Forni, A.; Botta, C.; Giannini, C.; Malpicci, D.; Marinotto, D.; Previtali, A.; Righetto, S.; Cariati, E., *Chem. Eur. J.* **2019**, 25, 2452-2456.

31. Wang, J-W.; Chen, C.; Li, Y-J.; Luo, Y-H.; Sun, B-W., *New J. Chem.* **2017**, 41, 9444-9452.

32. Xu, Y.; Huang, J.; Gabidullin, B.; Bryce, D. L., *Chem. Commun*. **2018**, 54, 11041-11043.

33. Holmesland, O.; Rømning, C., *Acta Chem. Scand.* **1966**, 20, 9, 2601-2610.

34. Aakeröy, C. B.; Spartz, C. L.; Dembowski, S.; Dwyre, S.; Desper, J., *IUCrJ.* **2015**, 2, 498-510.

35. Li, C.; Chai, Y.; Zhou, X.; Shen, Z.; Ma, B.; Chen, B.; Huang, R.; Chen, H.; Li, W.; He, Y., *CrystEngComm*. **2018**, 20, 3006-3010.

36. J. C.; Sinha, A. S.; Desper, J.; Đaković, M.; Aakeröy, C. B., *New J. Chem.* **2018**, 42, 10539-10547.

37. Nemec, V.; Fotović, L.; Vitasović, T.; Cinčić, D., *CrystEngComm.* **2019**, 21, 21, 3251-3255.

38. Cauliez, P.; Polo, V.; Roisnel, T.; Llusar, R.; Fourmigué, M., *CrystEngComm*. **2010**, 12, 558-566.

39. Clark, T.; Hennemann, M.; Murray, J. S.; Politzer, P., *J Mol Model.* **2007**, 13, 291-296.

40. Auffinger, P.; Hays, F. A.; Westchof, E.; Ho, P. S., *PNAS*. **2004**, 101, 48, 16789-16794.

41. Awwadi, F. F.; Willett, R. D.; Peterson, K. A.; Twamley, B., *Chem. Eur. J.* **2006**, 12, 8952-8960.

42. Riley, K. E.; Murray, J. S.; Fanfrlík, J.; Řezáč, J.; Solá, R. J.; Concha, M. C.; Ramos, F. M.; Politzer, P., *J Mol Model*. **2011**, 17, 3309-3318.

43. Aakeröy, C. B.; Wijethunga, T. K.; Desper, J., *J. Mol. Struct.* **2014**, 1072, 20-27.

44. Metrangolo, P.; Resnati, G., *IUCrJ*. **2014**, 1, 5-7.

45. Huber, S. M.; Jimenez-Izal, E.; Ugalde, J. M.; Infante, I., *Chem. Commun*. **2012**, 48, 7708-7710.

46. Rosokha, S. V.; Vinakos, M. K., *Crst.Growth Des.* **2012**, 12, 4149-4156.

47. Huber, S, M.; Scanlon, J. D.; Jimenez-Izal, E.; Ugalde, J. M.; Infante, I., *Phys. Chem. Chem. Phys.* **2013**, 15, 10350-10357.

48. Koskinen, L.; Hirva, P.; Kalenius, E.; Jääskeläinen, S.; Rissanen, K.; Haukka, M., *CrystEngComm*. **2015**, 17, 1231-1236.

49. Riley, K. E.; Hobza, P., *Phys. Chem. Chem. Phys.* **2013**, 15, 17742-17751.

50. Metrangolo, P.; Resnati, G., *IUCrJ.* **2014**, 1, 5-7.

51. Walsh, R. B.; Padgett, C. W.; Metrangolo, P.; Resnati, G.; Hanks, T. W., Pennington, W. T., *Cryst. Growth Des.* **2001**, 1, 165-175.

52. Rosokha, S. V.; Vinakos, M. K., *Cryst. Growth Des.* **2012**, 12, 4149-4156.

53. Huber, S. M.; Jimenez-Izal, E.; Ugalde, J. M.; Infante, I., *Chem. Comm.* **2012**, 48, 7708-7710.

54. Wang, C.; Danovich, D.; Mo, Y.; Shaik, S., *J. Chem. Theory Comput.* **2014**, 10, 3726-3737.

55. Mulliken, R. S. *J. Am. Chem. Soc.* **1950**, 72, 600-608.

56. Ding, X.; Tuikka, M.; Hirva, P.; Kukushkin, V. Y.; Novikov, A. S.; Haukka, M. *CrystEngComm*. **2016**, 18, 1987-1995.

57. Řezáč, J.; Riley, K. E.; Hobza, P. *J. Chem. Theory Comput.* **2012,** 8, 4285-4292.

58. Kozuch, S.; Martin, J. M. L., *J. Chem. Theory Comput.* **2013**, 9, 1918-1931.

59. Riley, K. E.; Hobza, P., *J. Chem. Theory Comput.* **2008**, 4, 232-242.

60. Politzer, P.; Lane, P.; Concha, M. C.; Ma, Y.; Murray, J. S. *J. Mol. Model.* **2007**, 13, 305-311.

61. Cavallo, G.; Metrangolo, P.; Milani, R.; Pilati, T.; Priimagi, A.; Resnati, G.; Terraneo, G. *Chem. Rev.* **2016**, 116, 2478-2601.

62. Kitagawa, S.; Kitaura, R.; Noro, S., *Angew. Chem. Int. Ed.* **2004**, 43, 2334-2375.

63. Duriska, M. B.; Neville, S. M.; Lu, J.; Iremonger, S. S.; Boas, J. F.; Kepert, C. J.; Batten, S. R., *Angew. Chem. Int. Ed.* **2009**, 48, 8919-8922.

64. Silva, P.; Vilela, S. M.; Tomé, J. P.; Paz, F. A. A., *Chem. Soc. Rev.* **2015**, 44, 6774-6803.

65. Sivchik, V. V.; Solomatina, A. I.; Chen, Y-T.; Karttunen, A. J.; Tunik, S. P.; Chou, P-T.; Koshevoy, I. O., *Angew. Chem. Int. Ed.* **2015**, 54, 14057-14060.

66. Sivchik, V.; Sarker, R. K.; Liu, Z-Y.; Chung, K-Y.; Grachova, E. V.; Karttunen, A. J.; Chou, P-T.; Koshevoy, I. O., *Chem. Eur. J.* **2018**, 24, 11475-11484.

67. Janczak, J.; Kubiak, R.; Hahn, F., *Inorg. Chim. Acta*. **1999**, 287, 101-104.

68. Janczak, J. *Acta Cryst. C.* **2004**, 60, 330-332.

69. Bolhuis, F. V.; Koster, B. P.; Migchelsen, T. *Acta Cryst.* **1967**. 23, 90-91.

70. Enders, M.; Ludwig, W.; Pritzkow, H. *Organometallics*. **2001**, 20, 5, 827-833.

71. Bigoli, F.; Deplano, P.; Mercuri, M. L.; Pellinghelli, M. A.; Pintus, G.; Serpe, A.; Trogu, E. F., *Chem. Commun.* **1998**, 2351-2352.

72. Zbačnik, M.; Vitković, M.; Vulić, V.; Nogalo, I.; Cinčić, D.,*Cryst. Growth Des.* **2016**, 16, 6381-6389.

73. Carletta, A.; Zbačnik, M.; Vulić, V.; Tumanov, N.; Stilinović, V.; Wouters, J. Cinčić, D.,*CrystEngComm.* **2018**, 20, 5332-5339.

74. Choquesillo-Lazarte, D.; Nemec, V.; Cinčić, D., *CrystEngComm.* **2017**, 19, 5293-5299.

75. Takemura, A.; Mcallister, L.; Karadakov, P. B.; Pridmore, N. E.; Whitwood, A. C.; Bruce, D. W., *CrystEngComm*. **2014**, 16, 4254-4264.

76. Gal, Y. L.; Colas, A.; Barrière, F.; Dorcet, V.; Roisnel, T.; Lorcy, D., *CrystEngComm*. **2019**, 21, 1934-1939.

77. Cloutier, J-P.; Vabre, B.; Moungang-Soumé, Zargarian, D.*Organometallics*. **2015**, 34, 133-145.

78. Schneider, D.; Schier, A.; Schidbaur, H. *Dalton Trans.* **2004**, 1995-2005.

79. Torubaev, Y. V.; Skabitskiy, I. V.; Rusina, P.; Pasynskii, A. A.; Rai, D. K.; Singh, A. *CrystEngComm.* **2018**, 20, 2258-2266.

80. Lisac, K.; Cinčić, D. *Crystals*. **2017**, 7, 363.

81. Sivchik, V.; Sarker, R. K.; Liu, Z-Y.; Chung, K-Y.; Grachova, E. V.; Karttunen, A. J.; Chou, P-T.; Koshevoy, I. O. *Chem. Eur. J.* **2018**, 24, 11475-11484.

82. Walbaum, C.; Pantenburg, I.; Meyer, G. *Cryst. Res. Technol.* **2008**, 43, 1183-1186.

83. Morita, Y.; Miyazaki, E.; Maki, S.; Toyoda, J.; Yamochi, H.; Saito, G.; Nakasuji, K. *Mol. Cryst. Liq. Cryst.* **2002**, 379, 77-82.

84. Walbaum, C.; Pantenburg, I.; Meyer, G. *Cryst. Res. Technol.* **2008**, 43, 1183-1186.

85. Fiolka, C.; Richter, M.; Pantenburg, I.; Mudring, A-V.; Meyer, G. *Crystals*. **2011**, 1, 220-228.

86. Mahmoudi, A.; Khalaj, M.; Gao, S.; Ng, S. W.; Mohammadgholiha, M. *Acta Cryst.* **2009**, E65, m555.

87. Puttreddy, R.; von Essen, C.; Peuronen, A.; Lahtinen, M.; Rissanen, K. *CrystEngComm*. **2018**, 20, 1954-1959.

88. Ding, X.; Tuikka, M.; Huakka, M. *Crystals*. **2020**, 10, 165.

89. Shankar, S.; Chovnik, O.; Shimon, L. J. W.; Lahav, M.; van der Boom, M. E. *Cryst. Growth Des.* **2018**, 18, 1967-1977.

90. Capucci, D.; Balestri, D.; Mazzeo, P. P.; Pelagatti, P.; Rubini, K.; Bacchi, A. *Cryst. Growth Des.* **2017**. 17. 4958-4964.

91. Choquesillo-Lazarte, D.; Nemec, V.; Cinčić, D. *CrystEngComm*. **2017**, 19, 5293-5299.

92. Cinčić, D.; Friščić, T.; Jones, W. *Chem. Eur. J.* **2008**, 14, 747-753.

93. Mills, A. M.; van Beek, J. A. M.; van Koten, G.; Spek, A. L. *Acta Cryst.* **2002**, C58, 304-306.

94. Schnelder, D.; Schier, A.; Schmidbaur, H. *Dalton Trans.* **2004**, 1995-2005.

95. Zordan, F.; Brammer, L. *Cryst. Growth Des.* **2006**, 6, 1374–1379.

96. Topić, F.; Puttreddy, R.; Rautiainen, J. M.; Tuononen, H. M.; Rissanen, K. *CrystEngComm*. **2017**, 19, 4960–4963.

97. Shankar, S.; Chovnik, O.; Shimon, J. W.; Lahav, M.; van der Boom, M. E. *Cryst. Growth Des.* **2018**, 1967-1977.

98. Cauliez, P.; Polo, V.; Roisnel, T.; Llusar, R.; Foumigué, M. *CrystEngComm*. **2010**, 12, 558–566.

99. Aakeröy, C. B.; Wijethunga, T. K.; Desper, J.D.; Đaković, M., *Cryst. Growth Des.* **2016**, 16, 2662-2670.

100. Aakeröy, C. B.; Chopade, P. D.; Desper, J., *Cryst. Growth Des.* **2011**, 11, 5333-5336.

101. Gunawardana, C. A.; Desper, J.; Sinha, A. S.; Đaković, M.; Aakeröy, C. B., *Faraday Discuss.* **2017**, 203, 371-388.

102. Nayak, A.; Pedireddi, V. R., *J. Mol. Struct.* **2017**, 1130, 251-263.

103. Aakeröy, C. B.; Wijethunga, T, K.; Desper, J. D.; Moore, C., *J. Chem. Crystallogr.* **2015**, 45, 267-276.

104. Riel, A. M. S.; Jessop, M. J.; Decato, D. A.; Massena, C. J.; Nascimento, V. R.; Berryman, O. B., *Acta Cryst.* **2017**, B73, 203-209.

105. Pramanik, A.; Das, G., *Polyhedron.* **2010**, 29, 2999-3007.

106. Goher, M. A. S.; Mautner, F. A.; Hafez, A. K.; Abu-Youssef, M. A.M.; Gspan, C.; Badr, A. M. -A., *Polyhedron*. **2003**, 22,-975-979.

107. Li, X.; Killarney, J. P.; Patterson, H. H., *Inorg. Chem.* **2011**, 50, 7239-7249.

108. Guo, B.; Zhang, X.; Yu, J-H; Xu, J-Q., *Dalton Trans.* **2015**, 44, 11470-11481.

109. Fourmigué, M.; Auban-Senzier, P., *Inorg. Chem.* **2008**, 47, 21, 9979-9986.

110. Haukka, M.; Kiviaho, J.; Ahlgrén, M.; Pakkanen, T. A., *Organometallics.* **1995**, 14, 2, 825-833.

111. Haukka, M.; Ahlgrén, M.; Pakkanen, T. A., *Dalton Trans.* **1996**, 1, 1927-1933.

112. Homanen, P.; Haukka, M.; Pakkanen, T. A.; Pursianinen, J.; Laitinen, R. H., *Organometallics.* **1996**, 15, 19, 4081-4084.

113. Frisch, M. J.; Trucks, G. W.; Schlegel, H. B.; Scuseria, G. E.; Robb, M. A.; Cheeseman, J. R.; Scalmani, G.; Barone, V.; Mennucci, B.; Petersson, G. A.; Nakatsuji, H.; Caricto, M.; Li, X.; Hratchian, H. P.; Izmaylov, A. F.; Bloino, J.; Zheng, G.; Sonnenberg, J. L.; Hada, M.; Ehara, M.; Toyota, K.; Fukuda, R.; Hasegawa, J.; Ishida, M.; Nakajima, T.; Honda, Y.; Kitao, O.; Nakai, H.; Vreven, T.; Montgomery Jr., J. A.;Pralta, J. E.; Ogliaro, F.; Bearpark, M.; Heyd, J. J.; Brothers, E.; Kudin, K. N.; Staroverov, V. N.; Kobyashi, R.; Normand, J.; Rahavachari, K.; Rendell, A.; Burant, J, C.; Iyengar, S. S.; Tomasi, J.; Cossi, M.; Rega, N.; Millam, J. M.; Klene, M.; Knox, J. E.; Cross, J. B.; Bakken, V.; Adamo, C.; Jaramillo, J.; Gompers, R.; Stratmann, R. E.; Yazyev, O.; Austin, A. J.; Cammi, R.; Pomelli, C.; Ochterski, J. W.; Martin, R. I.; Morokuma, K.; Zakrzewski, V. G.; Voth, G. A.; Salvador, P.; Dannenberg, J. J.; Dapprich, S.; Daniels, A. D.; Farkas, Ö:; Foresman, J. B.; Ortiz, J. V.; Cioslowski, J.; Fox, D. J.; Gaussian 09, Revision C.01, Gaussian, Inc., Wallingford CT, 2009.

114. Perdew, J. P.; Ernzerhof, M.; Burke, K. *J. Chem. Phys.* **1996**, 105, 9982-9985.

115. Bader, R. F. W. In Atoms in molecules: a Quantum Theory, Clarendon Press, Oxford, 1990.

116. Todd, A. K. AIMALL (Version 12. 06. 03), TK Gristmill Software, Overland Park KS, USA, 2012. aim.tkgristmill.com.

117. Bondi, A. *J. Phys. Chem.* **1964,** 68, 441-451.

118. Lommerse, P. M.; Stone, A. J.; Taylor, R.; Allen, F. H. *J. Am. Chem. Soc.* **1996**, 118, 3108-3116.

119. Brammer, L.; Bruton, E. A.; Sherwood, P. *Cryst. Growth Des.* **2001**, 1, 227-290.

120. Zordan, F.; Brammer, L.; Sherwood, P. *J. Am. Chem. Soc.* **2005**, 127, 5879-5989.

121. Johnson, M. T.; Džolić, Z.; Cetina, M.; Wendt, O. F.; Öhrström, L.; Rissanen, K. *Cryst. Growth Des.* **2012**, 12, 362-368.

122. Tuikka, M.; Niskanen, M.; Hirva, P.; Rissanen, K.; Valkonen, A.; Haukka, M., *ChemComm*. **2011**, 47, 3427-3429.

123. Mosquera, M. E. G.; Gómez-Sal, P.; Diaz, I.; Aguirre, L. M.; Ienco, A.; Manca, G.; Mealli, C., *Inorg. Chem.* **2016**, 55, 283-291.

124. Mosqera, M. E. G.; Egido, I.; Hortelano, C.; López-López, M.; Gómez-Sal, P., *Faraday Discuss.* **2017**, 203, 2257-283.

125. Espinosa, E.; Molins, E.; Lecomte, C.; *Chem. Phys. Lett.* **1998**, 285, 170-173.

126. Gatti, C., *Z. Kristallogr.* **2005**, 220, 399-457.

127. Espinosa, E.; Alkorta, I.; Elguero, J.; Molins, E. *J. Chem. Phys.* **2002**, 117, 5529-5542.

128. Van Der Lubbe, S. C. C.; Guerra, C. F. *Chem. Asian J.* **2019**, 14, 2760-2769.

129. Spackman, M. A.; Jayatilaka, D. *CrystEngComm*. **2009**, 11, 19-32.

130. Yang, P.; Qin, C.; Du, S.; Jia, L.; Qin, Y.; Gong, J.; Wu, S. *Crystals.* **2019**, 9, 367.

131. Turner, M. J.; McKinnon, J. J.; Wolff, S. K.; Grimwood, D. J.; Spackman, M. A. *ICUrJ.* **2017**, 4, 547-587.

132. Schneider, D.; Schier, A.; Schmidbaur, H., *Dalton Trans.* **2004**, 1995-2005.

133. Topić, F.; Rissanen, K., *J. Am. Chem. Soc.* **2016**, 138, 20, 6610-6616.

134. Pfrunder, M.; Brock, A. J.; Brown, J. J.; Grosjean, A.; Ward, J.; McMurtrie, J. C.; Clegg, J. K., *Chem. Commun.* **2018**, 54, 3974-3976.

135. Cavallo, G.; Biella, S.; Lü, J.; Metrangolo, P.; Pilati, T.; Resnati, G.; Terraneo, G., *J. Fluor. Chem.* **2010**, 131, 1165-1172.

136. Lindeman, S. V.; Hecht, J.; Kochi, J. K., *J. Am. Chem. Soc.* **2003**, 125, 38, 11597-11606.

ORIGINAL PAPERS

I

HALOGEN BOND PREFERENCES OF THIOCYANATE LIGAND COORDINATED TO RU(II) VIA SULPHUR ATOM

by

Xin Ding, Matti Tuikka, Pipsa Hirva & Matti Haukka, 2017

Journal of *Solid State Sci.* vol 71, 8-13

Solid State Sciences 71 (2017) 8–13

Contents lists available at ScienceDirect

Solid State Sciences

journal homepage: www.elsevier.com/locate/ssscie

Halogen bond preferences of thiocyanate ligand coordinated to Ru(II) via sulphur atom

Xin Ding [a], Matti Tuikka [a], Pipsa Hirva [b], Matti Haukka [a, *]

[a] University of Jyvaskyla, Department of Chemistry, P. O. Box 35, FI-40014, Finland
[b] University of Eastern Finland, Department of Chemistry, P.O. Box 111, FI-80101 Joensuu, Finland

ARTICLE INFO

Article history:
Received 17 March 2017
Received in revised form
21 June 2017
Accepted 29 June 2017
Available online 30 June 2017

Keywords:
Halogen bond
Ru
Iodine
Thiocyanate

ABSTRACT

Halogen bonding between [Ru(bpy)(CO)$_2$(*S*-SCN)$_2$] (bpy = 2,2'-bipyridine), I_2 was studied by co-crystallising the metal compound and diiodine from dichloromethane. The only observed crystalline product was found to be [Ru(bpy)(CO)$_2$(*S*-SCN)$_2$]·I_2 with only one NCS···I_2 halogen bond between I_2 and the metal coordinated S atom of one of the thiocyanate ligand. The dangling nitrogen atoms were not involved in halogen bonding. However, computational analysis suggests that there are no major energetic differences between the NCS···I_2 and SCN···I_2 bonding modes. The reason for the observed NCS···I_2 mode lies most probably in the more favourable packing effects rather than energetic preferences between NCS···I_2 and SCN···I_2 contacts.

1. Introduction

Halogen bond (XB) refers to non-covalent interactions between a polarised halogen atom with its electron-poor region (Lewis acid) and an entity (molecule, atom, or anion) with an electron-rich region (Lewis base) [1]. In this context the Lewis acid is called XB donor and the Lewis base as XB acceptor. Halogen bond as a tool for crystal engineering has attracted increasing interests since 1990s, due to its comparable bond strength to hydrogen bond, strong directionality, and more hydrophobic nature compared with hydrogen bond [2–11]. Most commonly used XB donors are organic halogen compounds but entities such as dihalogens or halonium ions can also act as donors [1]. Typically, XB donors follow a general rule that the more easier polarizable halogen atoms tend to form stronger the XB bonds.

In principle, any Lewis acid can act as XB acceptor. A variety of molecules with different electron donor atoms including oxygen, sulphur, nitrogen, and selenium as well as organic molecules with π-system have been reported as useful XB acceptors. In addition, metal complexes with suitable ligands, such as halogen atoms [12–14] or pseudohalogen groups [14–16], can also serve as XB acceptors. Thiocyanate ion is basically ambivalent ligand that can coordinate both through its nitrogen and sulphur atoms. Therefore, SCN^- ion as well as metal coordinated SCN–ligand can be involved as acceptor in halogen bonds that can be rationalized by σ-hole theory [6]. Thiocyanate can also participate in halogen interactions in which the donor-acceptor nature of the participating components is less obvious [17–29]. In principle both N, S ends of the thiocyanate can serve as halogen bond acceptor [17]. It has been suggested that the soft-hard nature of the two terminal atoms may play a significant role in formation of halogen bonds. It means that the soft sulphur end favours soft halogen bond donors such as iodine [17].

It is obvious that nitrogen-coordinated thiocyanate can only form halogen bonds through its sulphur atom since in this case the nitrogen atom is no longer available for further interactions. Adduct between [Ru(dcbpy)$_2$(*N*-NCS)$_2$] and I_2 is a good example of such a case [16]. It also shows that sulphur can be involved in more than one XB simultaneously. There are some previous examples where S-coordinated thiocyanate forms a halogen bond or halogen interactions with soft halogen bond donor through its softer sulphur atom despite the sulphur is coordinated to a metal [28,29]. However, in most of these cases the thiocyanate nitrogen is either coordinated to another metal centre [28] or involved in hydrogen bonding [29].

In the current paper we investigated halogen bonding preferences of S-coordinated thiocyanate by co-crystallising [Ru(bpy)(CO)$_2$ (*S*-NCS)$_2$] with very soft halogen bond donor I_2. Energetics

* Corresponding author.
E-mail address: matti.o.haukka@jyu.fi (M. Haukka).

http://dx.doi.org/10.1016/j.solidstatesciences.2017.06.016
1293-2558/

and both possible halogen bond contacts, NCS···I_2 and SCN···I_2, were compared by computational QTAIM method [30].

2. Results, discussion

2.1. Crystals of $[Ru(bpy)(CO)_2(S\text{-}SCN)_2]\cdot I_2$ (S···I)

Co-crystallisations of $[Ru(bpy)(CO)_2(S\text{-}SCN)_2]$ with I_2 from CH_2Cl_2 were carried out by using different molar ratios of the metal complex and I_2 (1:1, 1:2, 1:5, 1:10). In all cases the only observed crystalline product was an adduct where iodine formed halogen bond through sulphur (Fig. 1). This happened even if the *N*-end of SCN had more sterical freedom for halogen bonding than the Ru coordinated S atom. Such results indicate a clear preference for soft-soft I···S contacts over soft-hard I···N interaction. On the other hand, the fact that only one of the thiocyanates was halogen bonded even if the amount of I_2 was increased 10-fold, may indicate that packing effects (i.e. other weak interactions) actually play a pivotal role in formation of the primary crystalline product.

In the structure shown in Fig. 1, the iodine atom I1, acts as XB donor and the sulphur atom, S1, as XB acceptor. As mentioned above, the other thiocyanate sulphur S2 is not involved in halogen bonds. Similarly, only one end of I_2 participates in XB contacts. The S1···I1 distance is 3.146(2) Å, which is about 83% of the sum of Bondi's van der Waals radii of I and S [30]. The angle I2-I1···S1 is nearly linear (172.87(4)°) as expected in a XB system with I_2 donor. The Ru1-S1···I1 and Ru1-S1-C3 angles of 107.62(6)° and 103.5(2)° are in line with bonds and contact angles found in compounds that contain ruthenium coordinated SCN ligands [32–36].

2.2. Topological QTAIM charge density analysis

The goal was to study if the soft-soft I···S halogen bond is energetically favoured over soft-hard I···N interaction by comparing $[Ru(bpy)(CO)_2(S\text{-}SCN)_2]$ molecule and $[Ru(bpy)(CO)_2(S\text{-}SCN)_2]\cdot I_2$ adducts with I···S and I···N halogen bonds. Computationally established models of $[Ru(bpy)(CO)_2(S\text{-}SCN)_2]$ molecule as well as its I···S and I···N halogen bonded I_2 adducts were optimized to the energetically most favourable geometries using DFT tech-

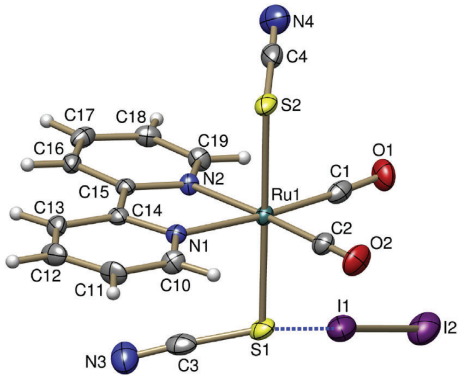

Fig. 1. Crystal structure of $[Ru(bpy)(CO)_2(S\text{-}SCN)_2]\cdot I_2$ (**1**). The anisotropic displacement ellipsoids are drawn at 50% probability level. Selected bond lengths (Å) and angles (°): Ru1-S1: 2.445(2) Å, S1-C3: 1.658(8), C3-N3: 1.166(10), Ru1-S2: 2.422(2), S2-C4: 1.668(8), C4-N4: 1.148(10), S1···I1: 3.146(2), I1-I2: 2.7143(8), Ru1-S1-C3: 103.5(2), S1-C3-N3: 177.1(7), Ru1-S2-C4: 102.0(3), S2-C4-N4: 176.8(7), Ru1-S1···I1: 107.62(6), I2-I1···S1: 172.87(4), C3-S1···I1: 113.3(3).

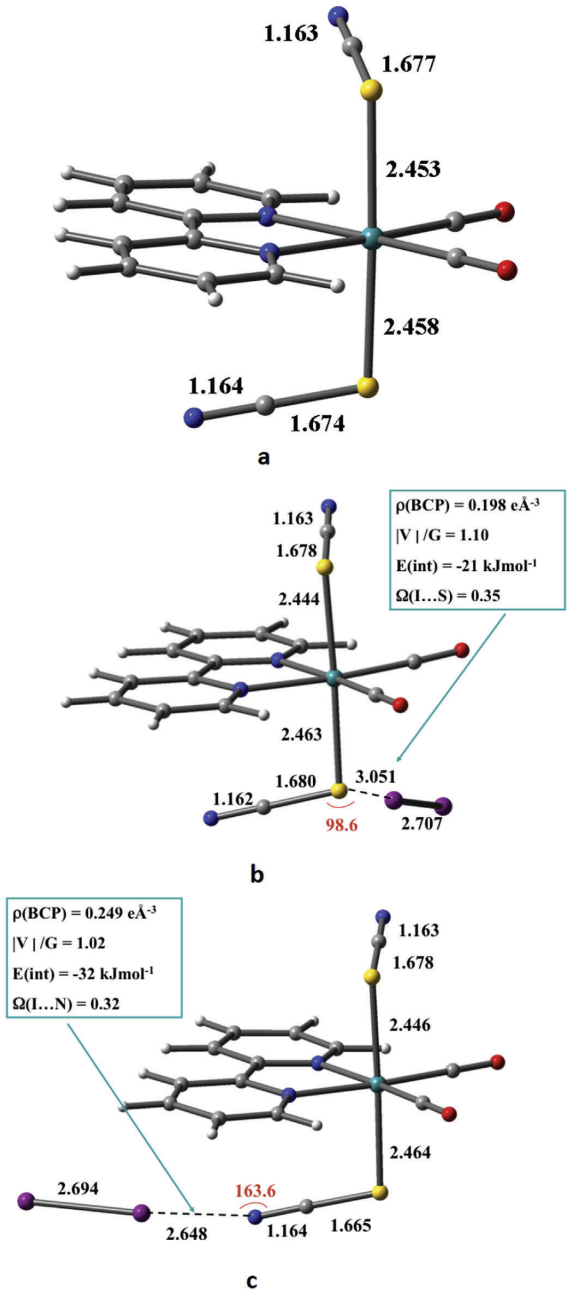

Fig. 2. Optimized structures of the models for a) an isolated $[Ru(bpy)(CO)_2(S\text{-}SCN)_2]$ complex, b) molecular complex in the co-crystal structure with S···I contact, c) molecular complex in the co-crystal structure with N···I contact. Colour scheme is the same as that of Fig. 1. Legends include selected properties of the electron density at the (I, N) or (I, S) bond critical points: ρ(BCP) = electron density at the bond critical point; |V|/G = ratio between potential energy density, kinetic energy density; E(int) = interaction energy at the BCP, Ω = delocalization index between I atom and N or S atoms. (For interpretation of the references to colour in this figure legend, the reader is referred to the web version of this article.)

nique. The obtained geometries with selected bond distances, angles are presented in Fig. 2.

The variations in selected bond lengths, XB bond angles between the computational and experimentally obtained structures are due to the gas-phase calculations that tend to overestimate charge transfer effect and interactions between the ruthenium molecule, I_2. This can be seen in shorter computational XB distance compared to the experimental results [17]. On the other hand, omitting the crystal environment should reveal possible differences in the actual I···S and I···N interaction energies and properties without interference of any packing effects. In addition to AIM parameters shown in Fig. 2, also the AIM defined atomic charges were calculated (Table 1).

It is known that strong XB contact with charge transfer or electron sharing will polarize the I_2 molecule [13,37]. The negative charge tends to accumulate on the iodine, which is not involved in halogen bonding (I2 in Fig. 1). Similarly, the XB-bonded iodine (I1) is getting more positive charge. According to the AIM results, interaction of I_2 with the "hard" nitrogen atom induces more effective polarization on diiodine molecule than when I_2 is interacting with the "soft" sulphur atom. This generates larger charge difference between the two ends of I_2. The ratio of potential energy density and kinetic energy density, $|V|/G$, at the bond critical point is indicative of the nature of the contact. If $|V|/G > 2$ the contact is a shared shell interaction (covalent) and if $|V|/G < 1$ the interaction is electrostatic [38–40]. Values between one and two indicate intermediate between the two type of interactions. Another parameter defining the nature of the contact is delocalisation index Ω [38–40]. In an ideal pure electrostatic system the value of Ω should be close to zero and in a single covalent bond close to 1. In the case of I···N and I···S systems, there are no major differences in these two parameters (Fig. 2). In both systems the interaction is essentially electrostatic with some minor covalent character. It has been suggested that increase in charge transfer or electron sharing from the XB acceptor to donor will also elongate the I-I distance [13–37,41]. However, the longer I-I distance in I···S adduct, where the charge difference between iodine atoms is smaller, does not support effect of charge transfer as the main reason for slight difference in I-I distance. It may be that small increase in electron sharing could be the reason for the longer I-I bond in this case.

Table 1
Atomic charges according to the AIM analysis for Ru, I, N, and S atoms in different configurations of the adducts $[Ru(bpy)(CO)_2(S\text{-}SCN)_2]\cdot I_2$.

Atom[a]	$[Ru(bpy)(CO)_2(S\text{-}SCN)_2]$	I···N	I···S
q(Ru)	0.949	0.951	0.949
q(S1)	0.120	0.163	0.146
q(S2)	0.113	0.121	0.123
q(N3)	−1.198	−1.231	−0.166
q(N4)	−1.191	−1.184	−0.180
q(I1)	–	0.095	0.008
q(I2)	–	−0.156	−0.135

[a] Numbering scheme the same as in Fig. 1.

The difference in interaction energies, E(int), between the I···N and I···S systems quite small, 11 kJ/mol, and can be overcome via other stabilising interactions in the crystal structure. According to the interaction energies the I···N adduct should actually be the slightly more favourable one when these systems are compared. Obviously, none of the computational results rule out the existence of the observed sulphur-iodine interaction. Based on the over all similarity of the computational results of the two configurations, both structures should be fully possible and one should be able to isolate both of them. The fact that only I···S crystals could be found suggests that the main factor, which determines the preferred primary crystalline form is due to the packing effects i.e. other weak intermolecular interactions. In other words, the overall packing of adduct with I···S is simply more favourable.

In order to investigate the weak interactions in the crystal structure in more detail, we performed QTAIM analysis on the extended model comprising one I_2 molecule surrounded by five $[Ru(bpy)(CO)_2(SCN)_2]$ complexes. The resulting bond paths and BCPs can be seen in Fig. 3. In addition to the main I···S interactions, there are much weaker intermolecular I···N and several CO···I interactions from the neighbouring carbonyl complexes.

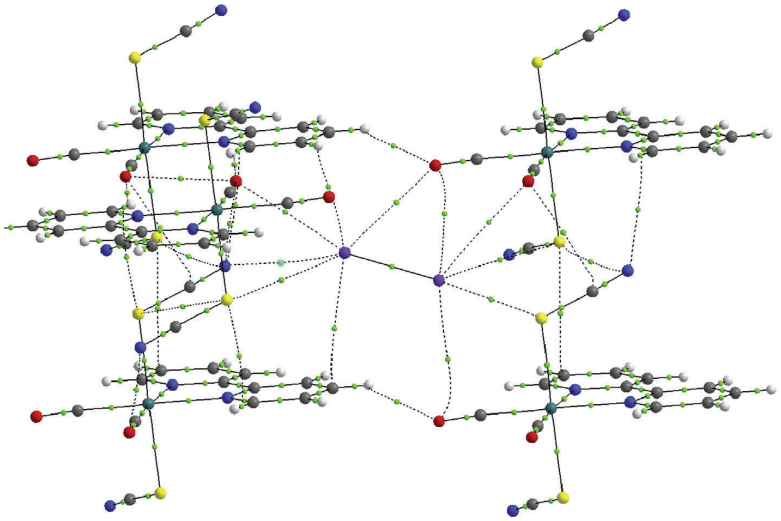

Fig. 3. Bond paths and bond critical points (green dots) in the extended $[Ru(bpy)(CO)_2(S\text{-}SCN)_2]_5\cdot I_2$ model of the crystal structure. (For interpretation of the references to colour in this figure legend, the reader is referred to the web version of this article.)

Although the interaction energies are small, varying between −2 and −5 kJ/mol, and the nature of the CO···I interaction is clearly electrostatic (|V|/G ~0.8), they are able to provide extra support for the sulphur coordination and explain the preference found in the crystal structure of the adduct. It should be noted, that in the extended model, a weak I···N interaction is also found, supporting the computationally found similarity of the two halogen bond sites.

Since experimental results showed that only one of the SCN ligands is involved in halogen bonding, we decided to analyse computationally if there are energetic reasons preventing formation of $[Ru(bpy)(CO)_2(S\text{-}SCN)_2]\cdot 2I_2$ adducts (Fig. 4). The results indicate that there is a little more electron sharing involved in I···S adducts and energetically the I···N mode should be slightly more favourable. However, despite the small differences both modes of $[Ru(bpy)(CO)_2(S\text{-}SCN)_2]\cdot 2I_2$ should be fully possible.

The nature of the frontier molecular orbitals was calculated to compare the doubly interacting compounds with adducts of only one diiodine. The appearance of the FMOs can be seen in Fig. 5. Regardless of the interaction site, whether it is the nitrogen or the sulphur end, the energies of HOMOs were found comparable with the systems having only one interacting SCN ligand. It means that the second XB contact is not contributing considerable additional stabilization to the system. On the other hand, the LUMOs are stabilized in the doubly interacting system, which indicates reduced stability, when both SCN ligands are involved in halogen bonding.

3. Experimental

3.1. Synthesis

All starting materials are from Sigma-Aldrich or from Johnson & Matthey and were used as received. The synthesis of $[Ru(bpy)(CO)_2(S\text{-}SCN)_2]$ was carried out following the previously reported procedure [36]. The adducts were obtained by dissolving $[Ru(bpy)(CO)_2(S\text{-}SCN)_2]$ and I_2 in CH_2Cl_2 and mixing the solutions at room temperature. A series of reactions were carried out varying the molar ratio of $[Ru(bpy)(CO)_2(S\text{-}SCN)_2]$ and I_2 (1:1, 1:2, 1:5, 1:10). After careful mixing the combined $[Ru(bpy)(CO)_2(S\text{-}SCN)_2]/I_2$ solution was placed in a vial covered with parafilm. Crystals were obtained by using slow evaporation technique at room temperature. X-Ray quality crystals were collected after three days and the yield of crystalline $[Ru(bpy)(CO)_2(S\text{-}SCN)_2]\cdot I_2$ adduct range from 33% to 45%. When collecting the product the solution was not allowed to evaporate to dryness. Among the collected crystalline material the dark red $[Ru(bpy)(CO)_2(S\text{-}SCN)_2]\cdot I_2$ was the only crystalline reaction product. The residual material consisted of staring compounds $[Ru(bpy)(CO)_2(S\text{-}SCN)_2]$ and I_2. No other products were observed. The synthesis was not optimized for maximum yield. The goal was to collect the initial crystalline material to analyse the preferred primary product.

3.2. Crystal structure determinations

The crystal of $[Ru(bpy)(CO)_2(S\text{-}SCN)_2]\cdot I_2$ was immersed in cryo-oil, mounted in a MiTeGen loop, and measured at 170 K on a Rigaku Oxford Diffraction Supernova diffractometer using Mo Kα (λ = 0.71073) radiation. The *CrysAlisPro* [42] program package was used for cell refinement and data reduction. Multi-scan absorption correction (*CrysAlisPro*) was applied to the intensities before the structure solution. The structure was solved by charge flipping method using the *SUPERFLIP* [43] software. Structural refinements were carried out using *SHELXL-2016* [44]. Hydrogen atoms were positioned geometrically and constrained to ride on their parent atoms, with C-H = 0.95 Å, U_{iso} = 1.2•U_{eq} (parent atom). The crystallographic details are summarized in Table 2.

3.3. Computational details

All single molecule models were fully optimized with the Gaussian 09 programme package [45] at the DFT level of theory with a hybrid functional PBE0 [46]. The selected basis set included the standard all-electron basis 6-311++G(d, p) for C, H, S, N atoms, and relativistic effective core potential basis sets LANL2DZspdf for I atoms [47] and LANL2TZ (f) for Ru [48]. The DFT wave function was used in the topological charge density analysis with QTAIM [30], which was performed with AIMALL program [49].

The geometry of the extended model $[Ru(bpy)(CO)_2(SCN)_2]_5\cdot I_2$ was taken directly from the experimental crystal structure, and the charge density analysis of the weak interactions was done without further optimization using the wavefunction obtained at the same DFT level than the smaller models.

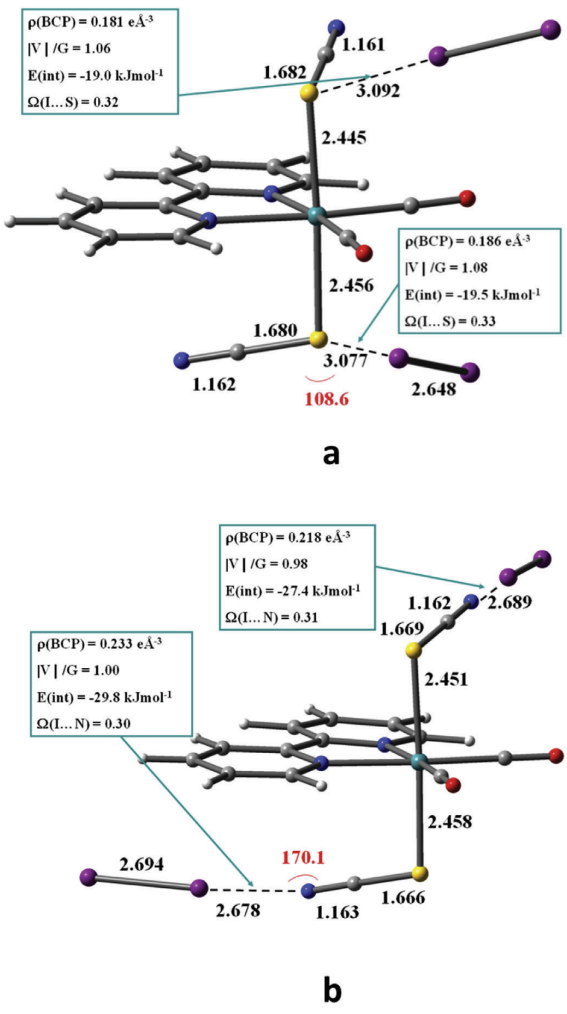

Fig. 4. Optimized structures for interaction of $[Ru(bpy)(CO)_2(S\text{-}SCN)_2]$ with two I_2 molecules.

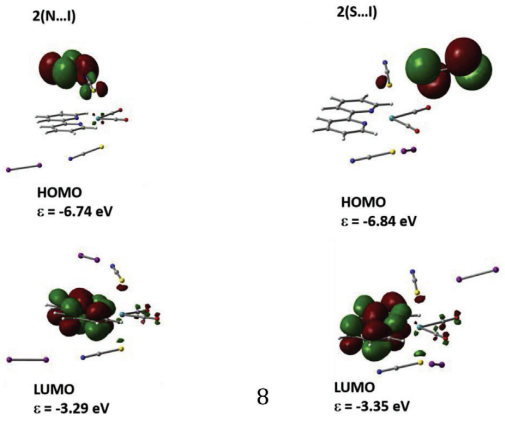

Fig. 5. Frontier molecular orbitals of $[Ru(bpy)(CO)_2(S\text{-}SCN)_2]\cdot 2I_2$.

Table 2
Crystal data.[†]

Empirical formula	$C_{14}H_8I_2N_4O_2RuS_2$
fw	683.23
Temp (K)	170(2)
λ (Å)	0.71073
cryst. syst.	Triclinic
Space group	$P\bar{1}$
a (Å)	7.2729(3)
b (Å)	10.9807(4)
c (Å)	12.5479(4)
α (deg)	79.278(3)
β (deg)	74.862(4)
γ (deg)	82.918(4)
V (Å^3)	947.49(7)
Z	2
ρ_{calc}(Mg/m^3)	2.395
μ(Mo Kα) (mm^{-1})	4.322
No. reflns.	7362
Unique reflns.	4642
GOOF (F^2)	1.032
R_{int}	0.0165
R1[a]($I \geq 2\sigma$)	0.0469
wR2[b]($I \geq 2\sigma$)	0.1297

[a] $R1 = \Sigma||F_o| - |F_c||/\Sigma|F_o|$.
[b] $wR2 = [\Sigma[w(F_o^2 - F_c^2)^2]/\Sigma[w(F_o^2)^2]]^{1/2}$.

4. Conclusions

Halogen bond preferences of the S-coordinated thiocyanate in $[Ru(bpy)(CO)_2(S\text{-}SCN)_2]\cdot I_2$ adduct were studied by using computational methods. Experimentally, soft XB-donor I_2 was found to favour soft sulphur atom as the primary XB acceptor. However, DFT and QTAIM analysis indicate that the XB contact between the dangling nitrogen of Ru-SCN and the I_2 donor should also be stable. In fact, energetically this should even be slightly more favourable option compared to the observed XB-system. Also, computational results indicate that both SCN-ligands should be able to act as XB acceptors simultaneously. The fact that only one of the thiocyanates was found to be involved in halogen bonding in experimental structure is most probably due to the highly favourable packing of the experimentally observed $[Ru(bpy)(CO)_2(S\text{-}SCN)_2]\cdot I_2$ adduct. It has been suggested that soft XB acceptors favour soft XB donors such as I_2. This could explain that the only observed crystalline product was $[Ru(bpy)(CO)_2(S\text{-}SCN)_2]\cdot I_2$ with I···S contact. However, computational analysis did not reveal any strong evidence that I···S interaction is energetically superior to I···N contact. The reason for I···S contact as the primary halogen bond mode can be found from the packing effects, especially from supporting weak CO···I contacts, which further stabilize the preferred crystal structure.

Acknowledgements

Financial support provided by the Academy of Finland (project 139571 M. H., M. T., X. D., 295581 M. H.) and the COST Action 1302 “Smart Inorganic Polymers” are gratefully acknowledged. We acknowledge grants of computer capacity from the Finnish Grid and Cloud Infrastructure (persistent identifier urn:nbn:fi:research-infras-2016072533).

Supporting data. Supporting information

[†]CCDC 1524888 contains the supplementary crystallographic data for compound $[Ru(bpy)(CO)_2(SCN)_2]\cdot I_2$. These data can be obtained free of charge via http://www.ccdc.cam.ac.uk/conts/retrieving.html, or from the Cambridge Crystallographic Data Centre, 12 Union Road, Cambridge CB2 1EZ, UK; fax: (+44) 1223-336- 033; or e-mail: deposit@ccdc.cam.ac.uk.

References

[1] G.R. Desiraju, P.S. Ho, L. Kloo, A.C. Legon, R. Marqard, P. Metrangolo, P. Politzer, G. Resnati, K. Rissanen, Pure Appl. Chem. 85 (2013) 1711–1713.
[2] G. Cavallo, P. Metrangolo, R. Milani, T. Pilati, A. Priimagi, G. Resnati, G. Terraneo, Chem. Rev. 116 (2016) 2478–2601.
[3] S.H. Jungbauer, D. Bulfield, F. Kniep, C.W. Lehmann, E. Herdtweck, S.M. Huber, J. Am. Chem. Soc. 136 (2014) 16740–16743.
[4] P. Polizer, J.S. Murray, ChemPhysChem 14 (2013) 278–294.
[5] A.C. Legon, Angew. Chem. Int. Ed. 38 (1999) 2686–2714.
[6] T. Clark, M. Hennemann, J.S. Murray, P. Polizer, J. Mol. Model. 13 (2007) 291–296.
[7] P. Metrangolo, G. Resnati, IUCrJ 1 (2014) 5–7.
[8] L.P. Wolters, F.M. Bickelhaupt, Chem. Open 1 (2012) 96–105.
[9] A.C. Legon, PCCP 12 (2010) 7736–7747.
[10] P. Polizer, J.S. Murray, T. Clark, PCCP 12 (2010) 7748–7757.
[11] C.B. Aakeröy, T.K. Wijethunga, J. Desper, C. Moore, J. Chem. Crystallogr. 45 (2015) 267–276.
[12] M. Tuikka, M. Niskanen, P. Hirva, K. Rissanen, A. Valkonen, M. Haukka, Chem. Commun. 47 (2011) 3427–3429.
[13] X. Ding, M.J. Tuikka, P. Hirva, V. Yu Kukushkin, A.S. Novikov, M. Haukka, CrystEngComm 18 (2016) 1987–1995.
[14] M.T. Johnson, Z. Džolić, M. Cetina, O.F. Wendt, L. Öhrström, K. Rissanen, Cryst. Growth & Des. 12 (2012) 362–368.
[15] J.E. Ormond-Prout, P. Smart, L. Brammer, Cryst. Growth & Des. 12 (2012) 205–216.
[16] M. Tuikka, P. Hirva, K. Rissanen, J. Korppi-Tommola, M. Haukka, Chem. Commun. 47 (2011) 4499–4501.
[17] P. Cauliez, V. Polo, T. Roisnel, R. Llusarb, M. Fourmigué, CrystEngComm 12 (2010) 558–566.
[18] A. Pramanik, S. Majumdara, G. Das, CrystEngComm 12 (2010) 250–259.
[19] H. Bock, S. Holl, Z. Naturforsch, B Chem. Sci. 57 (2002) 713–725.
[20] J. Viger-Gravel, I. Korobkov, D.L. Bryce, Cryst. Growth & Des. 11 (2011) 4984–4995.
[21] S.V. Rosokha, C.L. Stern, A. Swartza, R. Stewart, PCCP 16 (2014) 12968–12979.
[22] W. Phonsri, D.J. Harding, P. Harding, K.S. Murray, B. Moubaraki, I.A. Gass, J.D. Cashion, G.N.L. Jamesone, H. Adams, Dalton Trans. 43 (2014) 17509–17518.
[23] S.V. Rosokha, I.S. Neretin, T.Y. Rosokha, J. Hecht, J.K. Kochi, Heteroat. Chem. 17 (2006) 449–459.
[24] J.-X. Chen, W.-H. Zhang, X.-Y. Tang, Z.-G. Ren, Y. Zhang, J.-P. Lang, Inorg. Chem. 45 (2006) 2568–2580.
[25] H. Bock, S. Holl, Z. Naturforsch, B Chem. Sci. 57 (2002) 843–858.
[26] Y.B. Martínez, L.S.R. Pirani, M.F. Erben, R. Boese, C.G. Reuter, Yu V. Vishnevskiy, N.W. Mitzel, C.O.D. Véedova, J. Mol. Struct. 1132 (2017) 175–180.
[27] J. Seeman, W. Preetz, Z. Anorg, Allg. Chem. 624 (1998) 179–184.
[28] R.E. Marsh, Acta Cryst. B55 (1999) 931–936.
[29] A. Pramanik, G. Das, Polyhedron 29 (2010) 2999–3007.
[30] R.F.W. Bader, In Atoms in Molecules: a Quantum Theory, Clarendon Press, Oxford, 1990.
[31] A. Bondi, J. Phys. Chem. 68 (1964) 441–451.
[32] L. Vandenburgh, M.R. Buck, D.A. Freedman, Inorg. Chem. 47 (2008) 9134–9136.
[33] P. Homanen, M. Haukka, S. Luukkanen, M. Ahlgren, T.A. Pakkanen, Eur. J. Inorg.

Chem. (1999) 101–106.
[34] T.P. Brewster, W. Ding, N.D. Schley, N. Hazari, V.S. Batista, Inorg. Chem. 50 (2011) 11938–11946.
[35] K. Tabatabaeian, P. Downing, H. Adams, B.E. Mann, C. White, J. Organomet. Chem. 688 (2003) 75–81.
[36] P. Homanen, M. Haukka, T.A. Pakkanen, J. Pursiainen, R.H. Laitinen, Organometallics 15 (1996) 4081–4084.
[37] L. Koskinen, S. Jääskeläinen, P. Hirva, M. Haukka, Cryst. Growth & Des. 15 (2015) 1160–1167.
[38] E. Espinosa, E. Molins, C. Lecomte, Chem. Phys. Lett. 285 (1998) 170–173.
[39] C. Gatti, Z. Kristallogr., 220 (2005) 399–457.
[40] E. Espinosa, I. Alkorta, J. Elguero, E. Molins, J. Chem. Phys. 117 (2002) 5529–5542.
[41] M. Tuikka, M. Haukka, Acta Cryst. E71 (2015) o463.
[42] Rikagu Oxford Diffraction, CrysAlisPro, Agilent Technologies inc., Yarnton, Oxfordshire, England, 2013.
[43] L. Palatinus, G. Chapuis, J. Appl. Cryst. 40 (2007) 786–790.
[44] G.M. Shedrick, Acta Cryst. C71 (2015) 3–8.
[45] M.J. Frisch, G.W. Trucks, H.B. Schlegel, G.E. Scuseria, M.A. Robb, J.R. Cheeseman, G. Scalmani, V. Barone, B. Mennucci, G.A. Petersson, H. Nakatsuji, M. Caricto, X. Li, H.P. Hratchian, A.F. Izmaylov, J. Bloino, G. Zheng, J.L. Sonnenberg, M. Hada, M. Ehara, K. Toyota, R. Fukuda, J. Hasegawa, M. Ishida, T. Nakajima, Y. Honda, O. Kitao, H. Nakai, T. Vreven, J.A. Montgomery Jr., J.E. Pralta, F. Ogliaro, M. Bearpark, J.J. Heyd, E. Brothers, K.N. Kudin, V.N. Staroverov, R. Kobyashi, J. Normand, K. Rahavachari, A. Rendell, J.C. Burant, S.S. Iyengar, J. Tomasi, M. Cossi, N. Rega, J.M. Millam, M. Klene, J.E. Knox, J.B. Cross, V. Bakken, C. Adamo, J. Jaramillo, R. Gompers, R.E. Stratmann, O. Yazyev, A.J. Austin, R. Cammi, C. Pomelli, J.W. Ochterski, R.L. Martin, K. Morokuma, V.G. Zakrzewski, G.A. Voth, P. Salvador, J.J. Dannenberg, S. Dapprich, A.D. Daniels, Ö. Farkas, J.B. Foresman, J.V. Ortiz, J. Cioslowski, D.J. Fox, Gaussian 09, Revision C.01, Gaussian, Inc., Wallingford CT, 2009.
[46] J.P. Perdew, M. Ernzerhof, K. Burke, J. Chem. Phys. 105 (1996) 9982–9985.
[47] N. Begovic, Z. Markovic, S. Anic, L. Kolar-Anic, J. Phys. Chem. A 108 (2004) 651–657.
[48] (a) P.J. Hay, W.R. Wadt, J. Chem. Phys. 82 (1985) 299–310;
(b) L.E. Roy, P.J. Hay, R.L. Martin, J. Chem. Theory Comput. 4 (2008) 1029–1031;
(c) A.W. Ehlers, M. Bohme, S. Dapprich, A. Gobbi, A. Hollwarth, V. Jonas, K.F. Kohler, R. Stegmann, A. Veldkamp, G. Frenking, Chem. Phys. Lett. 208 (1993) 111–114.
[49] A.K. Todd, AIMALL (Version 12. 06. 03), TK Gristmill Software, Overland Park KS, USA, 2012. aim.tkgristmill.com.

II

EXTENDED ASSEMBLIES OF RU(BPY)(CO)$_2$X$_2$ (X=CL, BR, I) MOLECULES LINKED BY 1,4-DIIODOTETRAFLUORO-BENZENE (DITFB) HALOGEN BOND DONORS

by

Xin Ding, Matti Tuikka, Kari Rissanen & Matti Haukka, 2019

Journal of *Crystals*. vol 9, 319

crystals

MDPI

Article

Extended Assemblies of Ru(bpy)$(CO)_2X_2$ (X = Cl, Br, I) Molecules Linked by 1,4-Diiodotetrafluoro-Benzene (DITFB) Halogen Bond Donors

Xin Ding, Matti Tuikka, Kari Rissanen and Matti Haukka *

Department of Chemistry, University of Jyväskylä, P.O. Box 35, FI-40014 Jyväskylä, Finland; xin.dingharas@gmail.com (X.D.); MTU@dinex.fi (M.T.); kari.t.rissanen@jyu.fi (K.R.)

* Correspondence: matti.o.haukka@jyu.fi; Tel.: +358-40-8054666

Received: 20 May 2019; Accepted: 19 June 2019; Published: 24 June 2019

Abstract: The ruthenium carbonyl compounds, Ru(bpy)$(CO)_2X_2$ (X = Cl, Br or I) act as neutral halogen bond (XB) acceptors when co-crystallized with 1,4-diiodotetrafluoro-benzene (DITFB). The halogen bonding strength of the Ru-X···I halogen bonds follow the nucleophilic character of the halido ligand. The strongest halogen bond occurs between the chlorido ligand and the iodide atoms of the DITFB. All three halogen bonded complexes form polymeric assemblies in the solid state. In Ru(bpy)$(CO)_2Cl_2$·DITFB (1) and in Ru(bpy)$(CO)_2Br_2$·DITFB (2) both halido ligands are halogen bonded to only one DITFB donor. In Ru(bpy)$(CO)_2I_2$·DITFB (3) only one of the halido ligands is involved in halogen bonding acting as ditopic center for two DITFB donors. The polymeric structures of 1 and 2 are isomorphic wave-like single chain systems, while the iodine complexes form pairs of linear chains attached together with weak F···O≡C interactions between the closest neighbors. The stronger polarization of the iodide ligand compared to the Cl or Br ligands favors nearly linear C-I···I angles between the XB donor and the metal complex supporting the linear arrangement of the halogen bonded chain.

Keywords: halogen bond; ruthenium; crystal structure; bipyridine; carbonyl

1. Introduction

Halogen bond (XB) has found to be a useful tool in crystal engineering in recent years due to its strength and directional preferences [1–6]. A molecular entity with electrophilic region on a halogen atom is defined as XB donor, while an entity with nucleophilic region, i.e., Lewis base, is defined as an XB acceptor [7]. The strength and the directionality of halogen bond are well explained by σ-hole theory and by the nature of the elements attached to the halogen atoms [8–20]. Typical XB acceptors include covalently bonded nitrogen or sulfur atoms but also electron donors such as oxygen, selenium, and silicon are known to act as XB acceptors [21–24]. Even metal centers in square planar and linear metal compounds have shown XB acceptor properties [25–27]. Metal coordinated electron donor ligands provide another group of potential XB acceptors [28–36]. Especially metal halides are quite commonly used as XB acceptors. Even if coordination to a metal center is not usually enough to generate strong σ-hole on a halido ligand, the electron density around a coordinated halogen atom, X, is polarized [28,31]. This means that the M-X···X angle in a halogen bonded M-X···X-R system is typically ranging between 90° and 150°, depending on the nature of the metal center [13,30,31]. By using bidentate halogen bond donors, such as I_2, it is possible to link metal complexes together to form non-covalent metallopolymers [14,30,31,37–47]. However, I_2 is not necessarily the most desirable linking unit due to its redox behavior and its impact on the metal complex [45,47]. When the interaction between the metal coordinated halogen atom and the I_2 donor remains mainly electrostatic,

symmetrical bridges between the metal centers can be obtained. However, when the charge transfer and electron sharing, i.e., covalency, between the halogen atoms are increased, the electron distribution in the linking I_2 may change. This, in turn, may hamper the formation of symmetrical bridges and nature of the contacts between the linking unit and the metal complexes [31]. From this point of view, other XB donors, such as fluorinated iodobenzenes, behave more predictably as linkers in XB complexes and are, therefore, more reliable bridging units. In general, the motivation in building halogen bonded extended metal complex systems arises from the possibilities to modify the redox, magnetic, photophysical and optical properties of the complexes extended by halogen bonds [4,6,29,48].

Previously, we studied crystal structures and the nature of XBs in I_2 linked assemblies of $[Ru(bpy)(CO)_2X_2]$ (X = Cl, Br, I) compounds (Figure 1) [31]. Since the I_2 linkers XB properties are dependent on the nature of the halogen bond contacts, here, we used another potentially bridging XB donor, i.e., tetrafluorodiiodobenzene (DITFB, Figure 1) as the linker for $[Ru(bpy)(CO)_2X_2]$ molecules (X = Cl, Br, I). The goal was to further investigate the extended assemblies that can be obtained through XB by using organometallic $[Ru(bpy)(CO)_2X_2]$ molecules as XB acceptors.

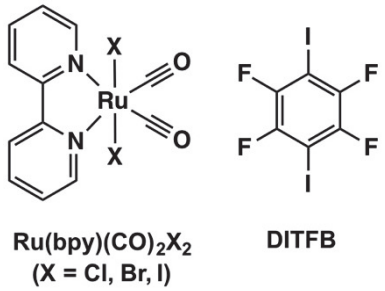

Figure 1. The schematic structures of $Ru(bpy)(CO)_2X_2$ (X = Cl, Br, I) and 1,4-diiodotetrafluorobenzene (DITFB).

2. Materials and Methods

2.1. Materials

All reagents and solvents were obtained from commercial sources and were used as received. The syntheses and crystal structures of the parent metal compounds $[Ru(bpy)(CO)_2X_2]$ (X = Cl, Br, I) have been reported in the literature [49,50]. All co-crystallizations were optimized only for obtaining high-quality single crystals, not for obtaining maximum yields.

2.2. Syntheses of co-crystals 1–3

$[Ru(bpy)(CO)_2Cl_2]$·DITFB (1). The light-yellow crystals were obtained by dissolving 5 mg of the metal complex and 10.5 mg of DITFB in CH_2Cl_2 solvent. The crystallization was carried out at room temperature by slow evaporation of the solvent. The X-ray quality crystals were harvested in two days.

$[Ru(bpy)(CO)_2Br_2]$·DITFB (2). The yellowish green crystals were obtained by dissolving 5 mg of the metal complex and 8.5 mg of DITFB in CH_2Cl_2 solvent. The crystallization was carried out at room temperature by slow evaporation of the solvent. The X-ray quality crystals were harvested in a week.

$[Ru(bpy)(CO)_2I_2]$·DITFB (3). The bright orange crystals were obtained by dissolving 5 mg of the metal complex and 7.1 mg of DITFB in CH_2Cl_2 solvent. The crystallization was carried out at room temperature by slow evaporation of the solvent. The X-ray quality crystals were harvested in a week.

2.3. X-ray Structure Determination

The crystals of 1–3 were measured at 120 K on a Rigaku Oxford Diffraction Supernova diffractometer (Oxford Diffraction, Woodlands, Tex, USA) (1), or on a Bruker Kappa Apex II diffractometer (Bruker Nonius, Delft, The Netherlands) (2,3) using Mo Kα (λ = 0.71073 Å) radiation. The CrysAlisPro [51] or Apex2 [52] program packages were used for cell refinements and data reductions. Multi-scan

absorption corrections based on equivalent reflections (CrysAlisPro, Apex2, Yarnton, Oxfordshire, England) were applied to the intensities before structure solutions. The structures were solved by the charge flipping method using the SUPERFLIP [53] software or by the intrinsic phasing method using SHELXT (v. 2014/5) [54]. All structures were refined by using SHELXL program [54]. Both structures 1 and 2 contained voids with heavily disordered and partially lost solvent of crystallization. A series of crystals were analyzed, and the residual electron density was found to vary from crystal to crystal indicating a variable amount of solvent in different crystals. Therefore, the final structural models of 1 and 2 were refined without the solvent molecules, and the contribution of the missing solvent to the calculated structure factors were taken into account by using the SQUEEZE routine of PLATON(v. 141217) [55]. Since the amount of solvent could not be determined accurately, the missing solvent molecules were not taken into account in the unit cell content. The hydrogen atoms were positioned geometrically and constrained to ride on their parent atoms, with C-H = 0.95 Å and $U_{iso} = 1.2 \cdot U_{eq}$ (parent atom). The crystallographic details are summarized in Table 1.

CCDC 1820788–1820790 contain the crystallographic data for 1–3, respectively. These data can be obtained free of charge via http://www.ccdc.cam.ac.uk/cgi-bin/catreq.cgi, or from the Cambridge Crystallographic Data Centre, 12 Union Road, Cambridge CB2 1EZ, UK; fax: (+44) 1223 336 033; or e-mail: deposit@ccdc.cam.ac.uk.

Table 1. Crystal Data.

	1	**2**	**3**
Formulas	$C_{18}H_8Cl_2F_4I_2N_2O_2Ru$ [+ solvent] [+ solvent]	$C_{18}H_8Br_2F_4I_2N_2O_2Ru$ [+ solvent]	$C_{18}H_8F_4I_4N_2O_2Ru$
Fw	786.03 *	874.95 *	968.93
temp (K)	120(2)	120(2)	120(2)
λ(Å)	0.71073	0.71073	0.71073
Crystal system	Monoclinic	Monoclinic	Orthorhombic
space group	C2/c	C2/c	Pnma
a (Å)	11.9736(7)	12.2824(4)	8.3320(3)
b (Å)	29.8725(13)	30.3634(11)	14.0070(5)
c (Å)	6.7654(3)	6.8630(2)	20.6378(7)
β (°)	96.925(5)	100.444(2)	90
V (Å^3)	2402.2(2)	2517.05(14)	2408.56(15)
Z	4	4	4
ρ_{calc} (Mg/m^3)	2.173	2.309	2.672
μ(Kα) (mm^{-1})	3.493	6.297	5.826
No. reflns.	18821	12583	26750
θ Range (°)	3.326–32.783	2.626–29.145	2.636–29.258
Unique reflns.	4175	3387	3384
GOOF (F^2)	1.064	1.147	1.152
R_{int}	0.0498	0.0292	0.0505
R1 [a] ($I \geq 2\sigma$)	0.0359	0.0281	0.0360
wR2 [b] ($I \geq 2\sigma$)	0.0761	0.0586	0.0795

[a] $R1 = \Sigma||F_o| - |F_c||/\Sigma|F_o|$. [b] $wR2 = [\Sigma[w(F_o^2 - F_c^2)^2]/\Sigma[w(F_o^2)^2]]^{1/2}$. * Fw without solvent of crystallization.

3. Results and Discussion

3.1. Strength of the Halogen Bonds

The relative strength of halogen bonds can be estimated by the commonly used concept of the halogen bond interaction ratio, R_{XB}, (sometimes also called as normalized interaction distance). It is defined as $R_{XB} = d_{XB}/(X_{vdw} + B_{vdw})$, where d_{XB} [Å] is the distance between the donor atom (X) and the acceptor atoms (B), divided by the sum of vdW radii [Å] of X and B, and the XB donor···acceptor (XB···A) [56–58]. Smaller values indicate stronger XB interactions. Small differences in R_{XB} values do

not reflect differences in the overall structures. For example, structure 1 and 2 are isomorphous even if there is a small difference (2%) in the R_{XB} values. Although the correlation between the crystal/overall structure and the XBs and their strength is not always straightforward, structural analysis provides a fast way to compare halogen bonds 116–125. The key structural parameters of the halogen bonds between the ruthenium coordinated halido ligand and the iodine of the DITFB XB donor in the three structures [Ru(bpy)$(CO)_2Cl_2$]·DITFB (**1**), [Ru(bpy)$(CO)_2Br_2$]·DITFB (2) and [Ru(bpy)$(CO)_2I_2$]·DITFB (3) are summarized in Table 2.

Table 2. Halogen bonds in 1–3 and in the [Ru(bpy)$(CO)_2X_2$]·I_2 XB complexes from Reference [31].

Compound	**Ru-X···I (Å)**	**C-I···X (°)**	**M-X···I (°)**	**R_{XB}**
1	3.1790(8)	170.60(9)	114.94(3)	0.85
2	3.3191(4)	171.34(10)	112.108(14)	0.87
3	3.5301(3)	177.66(13)	96.672(9)	0.89
Ref. [31]	Ru-X···I (Å)	I-I···X (°)	M-X···I (°)	R_{XB}
Cl···I_2	3.0421(3)	174.566(8)	115.76(1)	0.82
Br···I_2	3.2938(4)	170.28(1)	101.3(1)	0.86
Br···I_2	3.3627(3)	173.80(1)	102.27(1)	0.88
Br···I_2	3.2381(3)	175.405(9)	101.66(1)	0.85
Br···I_2	3.3001(3)	174.164(9)	102.57(1)	0.86
I···I_2	3.1984(2)	177.941(7)	97.91(1)	0.81
I···I_2	3.7984(3)	152.083(6)	104.26(1)	0.96
I···I_2	3.2553(13)	172.75(2)	97.81(2)	0.82
I···I_2	3.4108(15)	166.50(2)	98.90(2)	0.86

3.2. Crystal Structures

Unlike in the case of I_2 XB donor reported earlier [31], the diiodotetrafluorobenze acts as a symmetrical XB donor bridging the Ru complexes in all three structures 1–3. In 1 and 2 the DITFB molecules are located on an inversion center, while in 3 it is located on a mirror plane. Similarly, the Ru atoms in 1 and 2 are located on a two-fold rotation axis, while in 3 the ruthenium atom is on a mirror plane. Due to the symmetry, the distances from both iodines of DITFB to the halido ligand of the metal complex are equal in all cases. This is due to the fact that when one end of the DITFB molecule forms a halogen bond, it does not change the behavior of the second iodine, which is possible in the case of I_2 linker [31].

The extended structures of Ru(bpy)$(CO)_2Cl_2$]·DITFB (1) and Ru(bpy)$(CO)_2Br_2$]·DITFB (2) are isomorphous zig-zag chains (Figure 2).

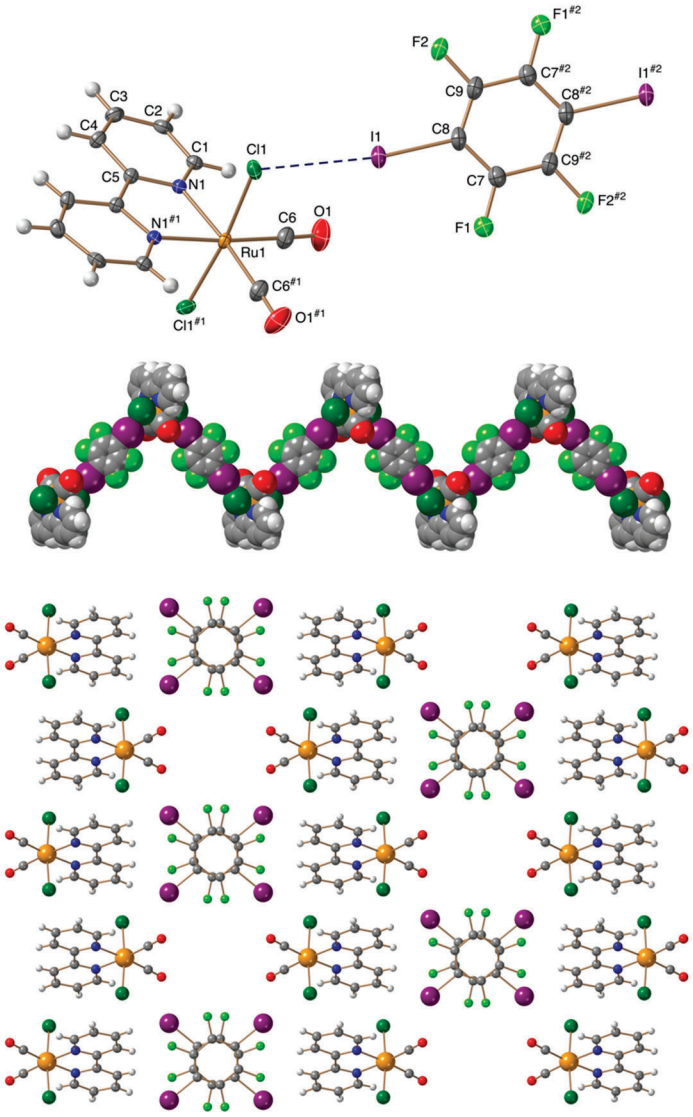

Figure 2. Top: TELP drawing of 1. Thermal ellipsoids have been drawn at 50% probability level. **Middle**: the polymeric zig-zag chain of 1. **Bottom**: Packing of 1 along the crystallographic c-axis. The corresponding figures of the isomorphous structure 2 are given in the Supplementary Materials. Symmetry transformations used to generate equivalent atoms: #1: −x + 1, y, −z + 3/2, #2: −x, −y + 1, −z + 1.

The TELP and packing images of 2 are given in the supplementeray material. In both 1 and 2 the halido ligands of the metal complexes are involved in halogen bonding and the halogen-halogen distances in both of these contacts are equal, as mentioned above. The M-Cl···I and M-Br···I contacts are 3.1790(8) Å and 3.3191(4) Å, respectively. The C-I···X angles are reasonably close to the linear contacts in both structures being 170.60(9)° for 1 and 171.34(10)° for 2. Both Ru-Cl···I and Ru-Br···I angles deviate quite clearly from the ideal 90° being 114.94(3)° and 112.108(14)° for 1 and 2, respectively. Such a deviation indicates that the electron density around the halido ligands is redistributed, increasing the electron density perpendicular to the Ru-X bond, but the effect is not particularly strong. In both 1 and 2, the aromatic DITFB donors are stacked with weak π–π interactions between the aromatic rings. The shortest carbon–carbon distances between the neighboring DITFB molecules range from 3.178(5) Å to 3.358(5) Å for 1 and from 3.165(5) Å to 3.685(5) Å for 2. In both 1 and 2 there are apparent voids in the structure (259 $Å^3$ and 310 $Å^3$, respectively). However, these voids are actually filled with disordered

solvent molecules, which were omitted from the crystal structure via SQUEEZE procedure (see X-Ray Structure Determination section).

The structure of 3 differs clearly from 1 and 2. Only one of the iodido ligands (I1) is involved in halogen bonding. The I1 of the Ru-complex acts as a ditopic XB acceptor linking simultaneously two DITFB donors (Figure 3).

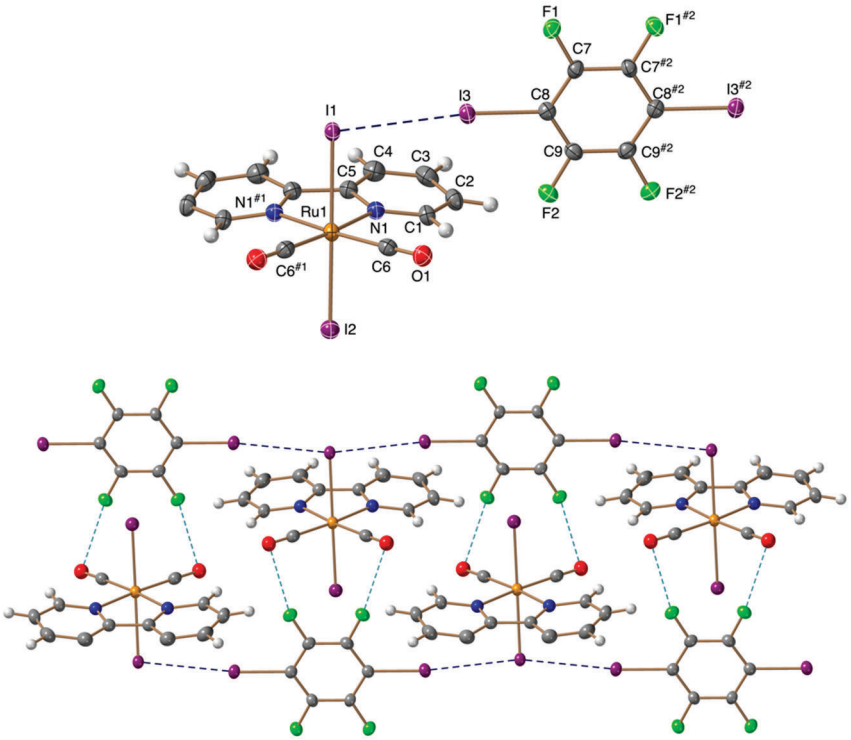

Figure 3. Top: TELP drawing of 3. **Bottom**: The chain of 3 with I···I halogen bonds and F···O contacts (2.833(5) Å). Symmetry transformations used to generate equivalent atoms: #1: x, −y + 1/2, z, #2: x, −y + 3/2, z.

The C-I···I angle of 177.66(13)° in 3 is closer to 180° and Ru-I···I angle of 96.672(9)° closer to 90° than the corresponding angles in 1 and 2. The Ru-I···I angle close to 90° is expected since the polarization of the iodido ligand is likely to be more efficient than the polarization of chlorido or bromido ligands. Just like in 1 and 2, all Ru-I···I halogen bond distances are also equal [3.5301(3) Å] in the structure 3. When the geometric parameters of 1–3 are compared to the values found in iodine linked $[Ru(bpy)(CO)_2X_2]\cdot I_2$ system some differences can be observed. First of all, based on the interaction ratios (R_{XB}) the order of the XB strength in 1–3 is increased systematically, i.e., X = Cl > Br > I (Table 2). In all cases, the R_{XB} values were calculated by using Bondi van der Waals' radii [59]. Johnson et al. have reported the same order for the halogen-containing Pd pincer complexes with I_2 donors [14]. However, in $[Ru(bpy)(CO)_2X_2]\cdot I_2$ systems the order is less obvious. In these co-crystals the strength of the first halogen–halogen interaction between the halido ligand and I_2 have an impact on the XB donor strength of the second I atom [31]. The order of the strongest interactions in the $[Ru(bpy)(CO)_2X_2]\cdot I_2$ series is X = I > Cl > Br (see the Table 1). This is due to the increased electron sharing, i.e., covalency and charge transfer in the case of $[Ru(bpy)(CO)_2I_2]\cdot I_2$. In the case of Cl and Br complexes, the halogen bonds are more clearly electrostatic, and therefore the XB strength follows the same order as 2 and 3. In general, the R_{XB} values found in structures 1–3 are slightly greater than the values found in other systems with halogen-containing ruthenium complexes and I_2 donors. Mosquera et al. have studied a series of $[Ru(CNR)_4X_2]\cdot I_2$ (X = Cl, Br, I) acceptors and their interactions with I_2 [45,47]. In these structures the M-X···I R_{XB} value for X = Cl systems range between 0.78 and 0.85, for X = Br, R_{XB} is 0.84 and for X = I the R_{XB} value range between 0.79 and 0.84. Again, the order of the XB strength in these systems

is not so straightforward as in the case of 1–3. The R_{XB} values in $[Ru(dcbpy)(CO)_2I_2]\cdot I_2$ complexes are also somewhat smaller than in 3 with R_{XB} = 0.79–0.82 [30] indicating again increased electron sharing and covalency between the XB donor and acceptor in I_2 donor systems. When structures 1–3 are compared with other, mainly electrostatic XB systems, such as trimethylplatinum(IV) iodide with iodopentafluoro-benzene XB donor, the observed R_{XB} values match well [60]. This can also be seen if structures 1–3 are compared with the other metal complex adducts having DITFB as a halogen bond donor. The R_{XB} values are nearly equal even if the metal and other ligands around the metal are different. For example, in PCPdX pincer complexes with DITFB donor the R_{XB} values are 0.87 (X = Cl) and 0.88 (X = Br), respectively [14]. The slightly larger values found in these systems may be due to the steric hindrance reflected by the relatively wide M-X···I angle (131–143°). In the sterically more relaxed square planar cyclometallated $[Pt(btpy)(PPh_3)Cl]\cdot$DITFB complex the R_{XB} value for the Pt-Cl···I is 0.86, which is nearly the same value that can be found in structure 1 as well [29].

4. Conclusions

A series of $[Ru(bpy)(CO)_2X_2]\cdot$DITFB (X = Cl, Br or I) halogen-bonded complexes were crystallized and analyzed. The $[Ru(bpy)(CO)_2Cl_2]\cdot$DITFB and $[Ru(bpy)(CO)_2Br_2]\cdot$DITFB complexes form isomorphous polymeric zig-zag chains where the 1,4-diiodotetrafluoro-benzenes (DITFB) act as symmetrical halogen bonding bridges linking metal complexes together. Although halogen bonds are relatively weak intermolecular interactions, they have a similar directional/directing role in crystallization as hydrogen bonds. Both halido ligands of the metal complex are involved in halogen bonding forming a single X···I contacts. The structure of $[Ru(bpy)(CO)_2I_2]\cdot$DITFB differs from the other two systems. Only one of the iodido ligands is involved in XB interactions as a ditopic acceptor leading to a nearly linear polymeric chain of metal complexes. Furthermore, the neighboring chains are linked together via weak F···O contacts. The strength of the halogen bonds M-X···I, estimated by the halogen bond interaction ratio, R_{XB}, follows the order of nucleophilicity of the halido ligands being 0.85, 0.87, and 0.89 for X = Cl, X = Br, and X = I, respectively. When the $[Ru(bpy)(CO)_2X_2]\cdot$DITFB series is compared with the corresponding series containing I_2 as the bridging halogen bond donors, the main differences arise from the behavior and nature of the XB donor. In the case of $[Ru(bpy)(CO)_2X_2]\cdot$DITFB the halogen bonds, formed by the two iodines of DITFB, are equal in all structures. This differs from the behavior of the two ends of the I_2 linker, where the second contact depend on the strength and nature of the initial halogen bond. Almost solely electrostatically behaving DITFB provide thus a more predictably behaving linker for XB-bonded assemblies of metal halides.

Supplementary Materials: The following materials are available online at http://www.mdpi.com/2073-4352/9/6/319/s1, Figure S1: TELP drawing of structure 2; Figure S2: The polymeric zig-zag chains of 2; Figure S3: Packing of 2 along the crystallographic c-axis.

Author Contributions: Syntheses, initial X-ray structure characterization and original draft preparation X.D.; final structure analysis M.T.; manuscript review and editing: K.R.; conceptualization, supervision, funding acquisition and project administration, manuscript review and editing: M.H.

Funding: This research was funded by Academy of Finland, grant numbers 130571 and 295881.

Conflicts of Interest: The funders had no role in the design of the study; in the collection, analyses, or interpretation of data; in the writing of the manuscript, or in the decision to publish the results.

References

1. Metrangolo, P.; Resnati, G.; Pilati, T.; Liantonio, R.; Meyer, F. Engineering functional materials by halogen bonding. *J. Polym. Sci. Part A Polym. Chem.* **2007**, *45*, 1–15. [CrossRef]
2. Cinčić, D.; Friščić, T.; Jones, W. Isostructural Materials Achieved by Using Structurally Equivalent Donors and Acceptors in Halogen-Bonded Cocrystals. *Chem. A Eur. J.* **2008**, *14*, 747–753. [CrossRef] [PubMed]
3. Nemec, V.; Fotović, L.; Friščić, T.; Cinčić, D. A large family of halogen-bonded cocrystals involving metal-organic building blocks with open coordination sites. *Cryst. Growth Des.* **2017**, *17*, 6169–6173. [CrossRef]

4. Ovens, J.S.; Geisheimer, A.R.; Bokov, A.A.; Ye, Z.G.; Leznoff, D.B. The Use of Polarizable $[AuX_2(CN)_2]^-$ (X = Br, I) Building Blocks Toward the Formation of Birefringent Coordination Polymers. *Inorg. Chem.* **2010**, *49*, 9609–9616. [CrossRef] [PubMed]
5. Rosokha, S.V.; Vinakos, M.K. Hybrid Network Formation via Halogen Bonding of the Neutral Bromo-Substituted Organic Molecules with Anionic Metal–Bromide Complexes. *Cryst. Growth Des.* **2012**, *12*, 4149–4156. [CrossRef]
6. Bertani, R.; Sgarbossa, P.; Venzo, A.; Lelj, F.; Amati, M.; Resnati, G.; Pilati, T.; Metrangolo, P.; Terraneo, G. Halogen bonding in metal-organic-supramolecular networks. *Coord. Chem. Rev.* **2010**, *254*, 677–695. [CrossRef]
7. Desiraju, G.R.; Ho, P.S.; Kloo, L.; Legon, A.C.; Marquardt, R.; Metrangolo, P.; Politzer, P.; Resnati, G.; Rissanen, K. Definition of the halogen bond (IUPAC Recommendations 2013). *Pure Appl. Chem.* **2013**, *85*, 1711–1713. [CrossRef]
8. Clark, T.; Hennemann, M.; Murray, J.S.; Politzer, P. Halogen bonding: The σ-hole. *J. Mol. Model.* **2007**, *13*, 291–296. [CrossRef] [PubMed]
9. Politzer, P.; Murray, J.S. σ-Holes and π-holes: Similarities and Differences. *J. Comput. Chem.* **2018**, *39*, 464–471. [CrossRef]
10. Politzer, P.; Murray, J.; Clark, T.; Resnati, G. The σ-Hole revisited. *Phys. Chem. Chem. Phys.* **2017**, *19*, 32166–32178. [CrossRef]
11. Esrafili, M.D.; Mousavian, P. The strengthening effect of a halogen, chalcogen or pnicogen bonding on halogen–π interaction: A comparative ab initio study. *Mol. Phys.* **2017**, *116*, 526–535. [CrossRef]
12. Cavallo, G.; Metrangolo, P.; Milani, R.; Pilati, T.; Priimagi, A.; Resnati, G.; Terraneo, G. The Halogen Bond. *Chem. Rev.* **2016**, *116*, 2478–2601. [CrossRef] [PubMed]
13. Cheng, N.; Liu, Y.; Zhang, C.; Liu, C. A theoretical study on the halogen bonding interactions of C_6F_5I with a series of group 10 metal monohalides. *J. Mol. Model.* **2013**, *19*, 3821–3829. [CrossRef] [PubMed]
14. Johnson, M.T.; Džolić, Z.; Cetina, M.; Wendt, O.F.; Öhrström, L.; Rissanen, K. Neutral Organometallic Halogen Bond Acceptors: Halogen Bonding in Complexes of PCPPdX (X = Cl, Br, I) with Iodine (I_2), 1,4-Diiodotetrafluorobenzene (F4DIBz), and 1,4-Diiodooctafluorobutane (F8DIBu). *Cryst. Growth Des.* **2012**, *12*, 362–368. [CrossRef] [PubMed]
15. Tsuzuki, S.; Wakisaka, A.; Ono, T.; Sonoda, T. Magnitude and origin of the attraction and directionality of the halogen bonds of the complexes of C_6F_5X and C_6H_5X (X = I, Br, Cl and F) with pyridine. *Chem. Eur. J.* **2012**, *18*, 951–960. [CrossRef] [PubMed]
16. Politzer, P.; Murray, J.S.; Clark, T. Halogen bonding: An electrostatically-driven highly directional noncovalent interaction. *Phys. Chem. Chem. Phys.* **2010**, *12*, 7748–7757. [CrossRef] [PubMed]
17. Legon, A.C. The halogen bond: An interim perspective. *Phys. Chem. Chem. Phys.* **2010**, *12*, 7736–7747. [CrossRef]
18. Politzer, P.; Lane, P.; Concha, M.C.; Ma, Y.; Murray, J.S. An overview of halogen bonding. *J. Mol. Model.* **2007**, *13*, 305–311. [CrossRef]
19. Alkorta, I.; Sanchez-Sanz, G.; Elguero, J.; Del Bene, J.E. FCl:PCX complexes: Old and new types of halogen bonds. *J. Phys. Chem. A* **2012**, *116*, 2300–2308. [CrossRef]
20. Murray, J.S.; Macaveiu, L.; Politzer, P. Factors affecting the strengths of σ-hole electrostatic potentials. *J. Comput. Sci.* **2014**, *5*, 590–596. [CrossRef]
21. Zbačnik, M.; Pajski, M.; Stilinović, V.; Vitković, M.; Cinčić, D. The halogen bonding proclivity of the ortho-methoxy–hydroxy group in cocrystals of o-vanillin imines and diiodotetrafluoro-benzenes. *CrystEngComm* **2017**, *19*, 5576–5582.
22. Jeske, J.; du Mont, W.-W.; Jones, P.G. Iodophosphane Selenides: Building Blocks for Supramolecular Soft ± Soft. *Chem. Eur. J.* **1999**, *5*, 385–389. [CrossRef]
23. Madzhidov, T.I.; Chmutova, G.A.; Martín Pendás, Á. The nature of the interaction of organoselenium molecules with diiodine. *J. Phys. Chem. A* **2011**, *115*, 10069–10077. [CrossRef] [PubMed]
24. Politzer, P.; Murray, J.S. Halogen bonding and beyond: Factors influencing the nature of CN-R and SiN-R complexes with F-Cl and Cl_2. *Theor. Chem. Acc.* **2012**, *131*, 1–10. [CrossRef]
25. Ivanov, D.M.; Novikov, A.S.; Ananyev, I.V.; Kirina, Y.V.; Kukushkin, V.Y. Halogen bonding between metal centers and halocarbons. *Chem. Commun.* **2016**, *52*, 5565–5568. [CrossRef] [PubMed]

26. Groenewald, F.; Dillen, J.; Esterhuysen, C. Ligand-driven formation of halogen bonds involving Au(I) complexes. *New J. Chem.* **2018**, *42*, 10529–10538. [CrossRef]
27. Novikov, A.S. Theoretical confirmation of existence of X···Au non-covalent contacts. *Inorg. Chim. Acta* **2018**, *471*, 126–129. [CrossRef]
28. Brammer, L.; Mínguez Espallargas, G.; Libri, S. Combining metals with halogen bonds. *CrystEngComm* **2008**, *10*, 1712–1727. [CrossRef]
29. Sivchik, V.V.; Solomatina, A.I.; Chen, Y.T.; Karttunen, A.J.; Tunik, S.P.; Chou, P.T.; Koshevoy, I.O. Halogen Bonding to Amplify Luminescence: A Case Study Using a Platinum Cyclometalated Complex. *Angew. Chem. Int. Ed.* **2015**, *54*, 14057–14060. [CrossRef]
30. Tuikka, M.; Niskanen, M.; Hirva, P.; Rissanen, K.; Valkonen, A.; Haukka, M. Concerted halogen and hydrogen bonding in $[RuI_2(H_2dcbpy)(CO)_2]\cdots I_2\cdots(CH_3OH)\cdots I_2\cdots[RuI_2(H_2dcbpy)(CO)_2]$. *ChemComm* **2011**, *47*, 3427–3429. [CrossRef]
31. Ding, X.; Tuikka, M.J.; Hirva, P.; Kukushkin, V.Y.; Novikov, A.S.; Haukka, M. Fine-tuning halogen bonding properties of diiodine through halogen–halogen charge transfer—Extended [Ru(2,2′-bipyridine)$(CO)_2X_2]\cdot I_2$ systems (X = Cl, Br, I). *CrystEngComm* **2016**, *18*, 1987–1995. [CrossRef]
32. Ding, X.; Tuikka, M.; Hirva, P.; Haukka, M. Halogen bond preferences of thiocyanate ligand coordinated to Ru(II)via sulphur atom. *Solid State Sci.* **2017**, *71*, 8–13. [CrossRef]
33. Lisac, K.; Cinčić, D. Simple design for metal-based halogen-bonded cocrystals utilizing the M–Cl···I motif. *CrystEngComm* **2018**, *20*, 5955–5963. [CrossRef]
34. Kia, R.; Mahmoudi, S.; Raithby, P.R. New rhenium-tricarbonyl complexes bearinghalogen-substituted bidentate ligands: Structural, computational and Hirshfeld surfaces studies. *CrystEngComm* **2019**, *21*, 77–93. [CrossRef]
35. Torubaev, Y.V.; Skabitskiy, I.V.; Rusina, P.; Pasynskii, A.A.; Raic, D.K.; Singhd, A. Organometallic halogen bond acceptors: Directionality, hybrid cocrystal precipitation, and blueshifted CO ligand vibrational band. *CrystEngComm* **2018**, *20*, 2258–2266. [CrossRef]
36. Scheiner, S. On the capability of metal–halogen groups to participate in halogen bonds. *CrystEngComm* **2019**, *21*, 2875–2883. [CrossRef]
37. Mills, A.M.; Van Beek, J.A.M.; Van Koten, G.; Spek, A.L. {2, 6-bis[(dimethylamino-κN)methyl]phenyl-κc}iodopalladium(ii) bis(diiodine). *Acta Cryst. Sect. C Cryst. Struct. Commun.* **2002**, *58*, m304–m306. [CrossRef]
38. Slugovc, C.; Kirchner, K.; Mereiter, K. (Hydridotripyrazolylborato)iodo{(1,2,5,6-η)-1-[(Z)-1-iodo-2-phenylethenyl]cycloocta-1,5-diene} ruthenium(II)–diiodine (2/1). *Acta Cryst. Sect. E Struct. Rep. Online* **2005**, *E61*, m1646–m1648. [CrossRef]
39. Palmer, S.M.; Stanton, J.L.; Jaggi, N.K.; Hoffman, B.M.; Ibers, J.A.; Schwartz, L.H. Preparation, Structures, and Physical Properties of Two Products from the Iodination of (Phthalocyaninato)iron(II). *Inorg. Chem.* **1985**, *24*, 2040–2046. [CrossRef]
40. Enders, M.; Ludwig, G.; Pritzkow, H. Nitrogen-functionalized cyclopentadienyl ligands with a rigid framework: Complexation behavior and properties of Cobalt(I), -(II), and -(III) half-sandwich complexes. *Organometallics* **2001**, *20*, 827–833. [CrossRef]
41. Zhao, S.-B.; Wang, R.-Y.; Wang, S. Reactivity of $SiMe_3$-and SnR_3-Functionalized Bis (7-azaindol-1-yl) methane with $[PtR_2(\mu\text{-}SMe_2)]_n$ (R)=Me, Ph) and the Resulting Pt(II) and Pt(IV) Complexes. *Organometallics* **2009**, *28*, 2572–2582. [CrossRef]
42. Buse, K.D.; Keller, H.J.; Pritzkow, H. Reaction of Molecular Iodine with cis-Dihalo (2,2′-bipyridyl) platinum(II) and cis-Dihalo (1,lQ-phenanthroline) platinum(II). Oxidative Addition and Inclusion Compounds. *Inorg. Chem.* **1977**, *16*, 1072–1076. [CrossRef]
43. Fanizzi, F.P.; Natile, G.; Lanfranchi, M.; Tiripicchio, A.; Laschi, F.; Zanello, P. Steric Crowding and Redox Reactivity in Platinum(II) and Platinum(IV) Complexes Containing Substituted 1,10-Phenanthrolines. *Inorg. Chem.* **1996**, *35*, 3173–3182. [CrossRef]
44. Safa, M.; Puddephatt, R.J. Organoplatinum complexes with an ester substituted bipyridine ligand: Oxidative addition and supramolecular chemistry. *J. Organomet. Chem.* **2013**, *724*, 7–16. [CrossRef]
45. Mosquera, M.E.G.; Egido, I.; Hortelano, C.; López-López, M.; Gómez-Sal, P. Comparison of Halogen Bonding networks with Ru(II) complexes and analysis of the influence of the XB interaction on their reactivity. *Faraday Discuss.* **2017**, *203*, 257–283. [CrossRef]

46. Hewison, L.; Crook, S.H.; Mann, B.E.; Meijer, A.J.H.M.; Adams, H.; Sawle, P.; Motterlini, R.A. New types of CO-releasing molecules (CO-RMs), based on iron dithiocarbamate complexes and $[Fe(CO)_3I(S_2COEt)]$. *Organometallics* **2012**, *31*, 5823–5834. [CrossRef]
47. Mosquera, M.E.G.; Gomez-Sal, P.; Diaz, I.; Aguirre, L.M.; Ienco, A.; Manca, G.; Mealli, C. Intriguing I_2 Reduction in the Iodide for Chloride Ligand Substitution at a Ru(II) Complex: Role of Mixed Trihalides in the Redox Mechanism. *Inorg. Chem.* **2016**, *55*, 283–291. [CrossRef] [PubMed]
48. Coronado, E.; Day, P. Magnetic Molecular Conductors. *Chem. Rev.* **2004**, *104*, 5419–5448. [CrossRef] [PubMed]
49. Haukka, M.; Kiviaho, J.; Ahlgrén, M.; Pakkanen, T.A. Studies on Catalytically Active Ruthenium Carbonyl Bipyridine Systems. Synthesis and Structural Characterization of $[Ru(bpy)(CO)_2Cl_2]$, $[Ru(bpy)(CO)_2Cl(C(O)OCH_3)]$, $[Ru(bpy)(CO)_2Cl]_2$, and $[Ru(bpy)(CO)_2ClH]$ (bpy = 2,2′-Bipyridine). *Organometallics* **1995**, *14*, 825–833. [CrossRef]
50. Haukka, M.; Ahlgrén, M.; Pakkanen, T.A. Reactions of $[Ru(bipy)(CO)_2Cl_2]$ in aqueous HX and HX–HNO_3 solutions (X = F, Br or I; bipy = 2,2′-bipyridine). *J. Chem. Soc. Dalton Trans.* **1996**, 1927–1933. [CrossRef]
51. Rikagu Oxford Diffraction. *CrysAlisPro V. 1.171.37.35*; Rikagu Oxford Diffraction: Yarnton, Oxfordshire, UK, 2015.
52. Bruker AXS. *APEX2-Software Suite for Crystallographic Programs*; Bruker AXS, Inc.: Madison, WI, USA, 2009.
53. Palatinus, L.; Chapuis, G. Superflip—A computer program for the solution of crystal structures by charge flipping in arbitrary dimensions. *J. Appl. Cryst.* **2007**, *40*, 786–790. [CrossRef]
54. Sheldrick, G.M. Crystal structure refinement with *SHELXL*. *Acta Cryst.* **2015**, *C71*, 3–8.
55. Spek, A.L. Structure validation in chemical crystallography. *Acta Cryst.* **2009**, *D65*, 148–155. [CrossRef] [PubMed]
56. Lommerse, P.M.; Stone, A.J.; Taylor, R.; Allen, F.H. The nature and geometry of intermolecular interactions between halogens and oxygen or nitrogen. *J. Am. Chem. Soc.* **1996**, *118*, 3108–3116. [CrossRef]
57. Brammer, L.; Bruton, E.A.; Sherwood, P. Understanding the Behavior of Halogens as Hydrogen Bond Acceptors. *Cryst. Growth Des.* **2001**, *1*, 277–290. [CrossRef]
58. Zordan, F.; Brammer, L.; Sherwood, P. Supramolecular Chemistry of Halogens: Complementary Features of Inorganic (M−X) and Organic (C−X′) Halogens Applied to M−X···X′−C Halogen Bond Formation. *J. Am. Chem. Soc.* **2005**, *127*, 5979–5989. [CrossRef] [PubMed]
59. Bondi, A. van der Waals Volumes and Radii. *J. Phys. Chem.* **1964**, *68*, 441–451. [CrossRef]
60. Ghosh, B.N.; Lahtinen, M.; Kalenius, E.; Mal, P.; Rissanen, K. 2,2′:6′,2″-Terpyridine trimethylplatinum(IV) iodide complexes as bifunctional halogen bond acceptors. *Cryst. Growth Des.* **2016**, *16*, 2527–2534. [CrossRef]

Supporting information for:

Extended assemblies of $Ru(bpy)(CO)_2X_2$ (X = Cl, Br, I) molecules linked by 1,4-diiodotetrafluoro-benzene (DITFB) halogen bond donors

Xin Ding, Matti Tuikka, Kari Rissanen and Matti Haukka*

University of Jyväskylä, Department of Chemistry, P.O. Box 35, FI-40014 Jyväskylä, Finland, e-mail: matti.o.haukka@jyu.fi.

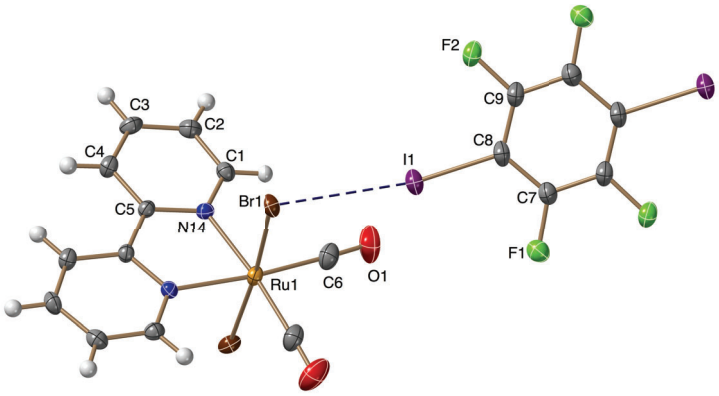

Figure S1. TELP drawing of structure **2**.

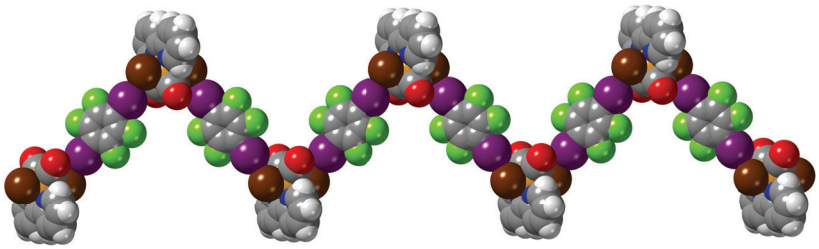

Figure S2. The polymeric zig-zag chain of **2**.

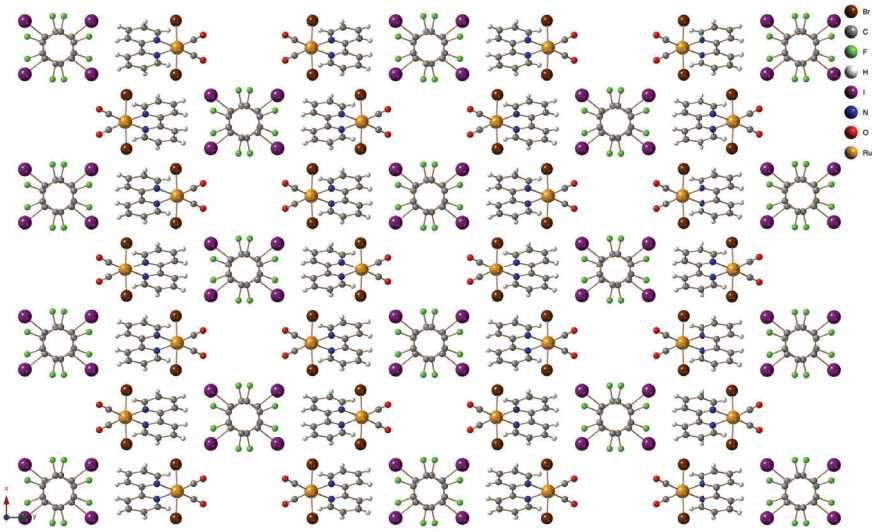

Figure S3. Packing of **2** along the crystallographic c-axis.

III

A NOVEL HALOGEN BOND ACCETOR: 1-(4-PYRIDYL)-4-THIOPYRIDINE (PTP) ZWITTERION

by

Xin Ding, Matti Tuikka & Matti Haukka, 2020

Journal of *Crystals* vol 10, 165

crystals

MDPI

Article

A Novel Halogen Bond Acceptor: 1-(4-Pyridyl)-4-Thiopyridine (PTP) Zwitterion

Xin Ding, Matti Tuikka and Matti Haukka *

Department of Chemistry, University of Jyväskylä, P.O. Box 35, FI-40014 Jyväskylä, Finland; xin.x.ding@jyu.fi (X.D.); MTU@dinex.fi (M.T.)

* Correspondence: matti.o.haukka@jyu.fi ; Tel.: +358-40-8054666

Received: 7 February 2020; Accepted: 29 February 2020; Published: 3 March 2020

Abstract: Sulfur is a widely used halogen bond (XB) acceptor, but only a limited number of neutral XB acceptors with bifurcated sp^3-S sites have been reported. In this work a new bidentate XB acceptor, 1-(4-pyridyl)-4-thiopyridine (PTP), which combines sp^3-S and sp^2-N acceptor sites, is introduced. Three halogen bonded cocrystals were obtained by using 1,4-diiodobenzene (DIB), 1,4-diiodotetrafluorobenzene (DIFB), and iodopentafluorobenzene (IPFB) as XB donors and PTP as acceptor. The structures of the cocrystals showed some XB selectivity between the S and N donors in PTP. However, the limited contribution of XB to the overall molecular packing in these three cocrystals and the results from DSC measurements clearly point out the synergetic influence and interplay of all noncovalent interactions in crystal packing of these compounds.

Keywords: Halogen bonds (XB); acceptor; cocrystals; selectivity

1. Introduction

Halogen bond (XB) is a noncovalent interaction occurring between an electrophilic region (σ-hole) of a halogen atom (XB donor) in a molecular moiety and a nucleophilic atom (XB acceptor) in the same or another moiety [1]. The major force in XB is electrostatic by nature [2], but charge transfer, polarization, and dispersion forces all play important roles in XB contacts [3,4]. The strength of a typical XB is comparable with the hydrogen bonds (HB) and in some cases is even stronger than HB [5]. Just like the hydrogen bond, XB is also highly directional [6–8]. Due to these characteristics, XB has emerged as a prominent tool in crystal engineering [9–13], organic synthesis [14,15], and biochemistry [16,17], etc.

Commonly used XB acceptors include sp^2 oxygen atoms (sp^2-O) [18,19], sp^3 oxygen atoms (sp^3-O) [20–22], sp^2 sulfur atoms (sp^2-S) [23–26], sp^3 sulfur atoms (sp^3-S) [27–29], and sp^2 nitrogen atoms (sp^2-N) [30–34]. Unlike the sp^2-N, both sp^2-S and sp^3-S can act as bifurcated XB acceptors in three-centered halogen bonds, due to the two available lone pairs on sulfur [9]. Similarly, both sp^2-O and sp^3-O can function as multidentate XB acceptors. However, a CCDC survey (C-X···S, C-X···O, X=Br, I; no organometallic complexes; CSD version 5.41, November 2019) gave 539 structures with C-X···S, of which 403 have sp^3-S as the XB acceptor, but only 20 structures include bifurcated sp^3-S. Eight of these structures involve SCN^- and 10 C-S-C synthon as the XB acceptor. Altogether 4799 structures with C-X···O were found in the CCDC survey with 1249 sp^3-O as the XB acceptor. However, only 39 structures have multidentate sp^3-O, of which 24 are N-O synthons and 12 are C-O synthons. Clearly, compared with the oxygen atom as XB acceptor, the sulfur atom is less commonly studied.

Thus, our aim was to develop a new neutral bidentate S-N-type XB acceptor capable of forming three-centered XBs via S and two-centered XBs through N. PTP, in Figure 1, was synthesized for such purpose. Unlike in the C-S-C synthon, the sp^3-S pendant in PTP is not sterically hindered and the sp^2-N at the other end of the PTP molecule assures the 1:1 ratio interaction with XB donors. Since

the PTP is a neutral zwitterionic molecule, it is possible to avoid introducing any undesirable cations into the system. I_2 is the simplest bidentate XB donor, which can be used to link organic molecules together via XB [35–40]. However, I_2 is not always the most ideal linker due to its redox properties, which easily lead to unwanted side reactions. Therefore, we chose less redox active organic iodides—1,4-diiodobenzene (DIB) and 1,4-diiodotetrafluorobenzene (DITFB) as the bidentate and iodopentafluorobenzene (IPFB) as monodentate XB donors—in this work (Figure 1).

The ultimate goal of this study was to investigate the ability of PTP to form robust supramolecular structures via XB interactions. Furthermore, the possible preferences between the S and N acceptors in XB formation were also investigated.

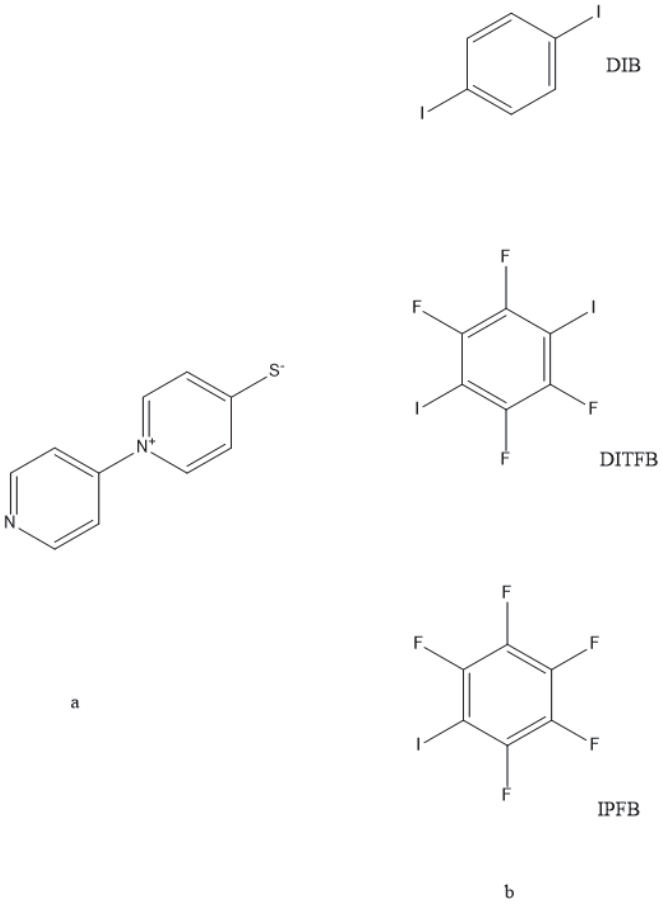

Figure 1. Schematic structure of XB acceptor and donors. **(a)** The schematic structure of PTP; **(b)** the schematic structure of 1,4-diiodobenzene (DIB), of 1,4-diiodotetrafluorobenzene (DITFB), and of iodopentafluorobenzene (IPFB).

2. Materials and Methods

Materials. 4-Mercaptopyridine (95%), sodium hydroxide (98%), DIB (99%), DITFB (98%), and IPFB (99%) were from Sigma-Aldrich. Dichloromethane (99%) and acetonitrile (99.8%) were obtained from VWR Chemicals. Silica-gel 60 (0.04–0.06 mm) was received from Merck. All reagents were used as received.

Solution Crystallization. Crystals of PTP were obtained by slowly evaporating the solution of 5 mg PTP + XB donor dissolved in 6 mL DCM at room temperature. The impact of the PTP/XB donor ratio on the cocrystal formation was studied using solutions with molar ratios of 1:1, 1:2, and 1:4 (PTP:XB donor). The X-ray quality crystals were typically obtained in 3 to 7 days when the solution was evaporated until crystals formed, but not completely dry. Analysis of all crystals obtained showed that the 1:1 ratio only yielded crystals of the starting materials, whereas the 1:2 and 1:4 ratios both gave similar assemblies of the same cocrystal structures.

Physical Properties Measurements. Melting point was measured with a Stuart Scientific Melting Point Apparatus SMP 3. Differential scanning calorimetry (DSC) data were obtained using Perkin Elmer STA600 (40 μL platinum pans, 20–600 °C, heating rate at 10.0 °C/min, Pyris Series software for data processing). Elemental analyzes were carried out by analytical services at the Department of Chemistry, University of Jyväskylä.

Single Crystal X-Ray Measurements. Crystals were measured at 120 K on a Rigaku Oxford Diffraction Supernova diffractometer (Oxford Diffraction, Woodlands, Tex, USA), using Cu Kα (λ = 1.54184 Å) radiation. The CrysAlisPro (Version 1. 171. 39. 43C) package was used for cell refinements and data reductions. Multi-scan (**1**, **2**) or analytical (**3**) absorption corrections (CrystAlisPro, Yarnton, Oxfordshire, England) were applied to the intensities before structure solutions. The structures were solved by the intrinsic phasing method using SHELXT [41]. All structures were refined by using SHELXL program. Crystal data of cocrystal **1**-**3** are listed in Table 1.

Table 1. Crystal data 1–3.

	1	**2**	**3**
Formula moiety	$(C_{10}H_8N_2S)$, $0.5(C_6H_4I_2)$	$2(C_{10}H_8N_2S)$, $3(C_6F_4I_2)$, (CH_2Cl_2)	$(C_{10}H_8N_2S)$, $2(C_6F_5I)$
Empirical formula	$C_{13}H_{10}IN_2S$	$C_{39}H_{18}Cl_2F_{12}I_6N_4S_2$	$C_{22}H_8F_{10}I_2N_2S$
Molecular weight	353.19	1666.99	776.16
Crystal system	Triclinic	Triclinic	Monoclinic
Space group	P-1	P-1	$P2_1/c$
a, Å	7.0677(3)	11.1401(3)	22.6204(3)
b, Å	8.6967(4)	15.9270(4)	8.53950(10)
c, Å	11.1576(5)	16.2566(4)	13.00460(10)
α, °	100.990(4)	63.216(3)	90
β,°	100.380(4)	76.370(2)	103.5430(10)
γ, °	104.057(4)	71.299(2)	90
Volume, Å	634.33(5)	2424.76(13)	2442.21(5)
Z	2	2	4
Density, g/cm^3	1.849	2.283	2.111
T, K	120(2)	120(2)	123(2)
μ (K_α) (mm^{-1})	21.185	32.729	21.895
No. relns.	6446	58,192	16,460
θ Range (°)	4.155-76.751	3.063-76.976	4.02-76.948
Unique reflns.	2649	10,175	5149
GOOF (F^2)	1.056	1.048	1.040
R_{int}	0.0345	0.0488	0.0387
R1($I \geq 2\sigma$)	0.0274	0.0311	0.0262
wR2 ($I \geq 2\sigma$)	0.0744	0.0827	0.0629

Synthesis of 1-(4-bipyridyl)-4-thionpyridine (PTP) Zwitterion. 4-Mercaptopyridine (100 mg) was heated at 67 °C for 16 hours with constant stirring until the color turned to orange-yellow. It was then dissolved in 5 mL of boiling water. Saturated NaOH aqueous solution was added in the solution dropwise until pH 10 was reached. The solution was filtered to remove any particulate matter. The filtrate was extracted with dichloromethane (DCM) (6 × 10 mL). The organic phase from the extraction was reduced to 5 mL in rotary evaporation. The reduced solution was further purified through a chromatography column with acetonitrile as the eluent, followed by drying in vacuum.

The solid, pale greenish yellow PTP was obtained with yield of 16.1%. mp 155.3–157.1 °C. Anal. Calcd for $C_{10}H_8N_2S$: C, 63.82; H, 4.29; N, 14.89. Found: C, 63.62; H, 4.29; N, 14.81. ^{1}H NMR ($CDCl_3$, 300MHz): δ- 8.83 (dd, 2H, J = 4.6), 7.53 (d, 2H, J = 7.4), 7.43 (d, 2H, J = 7.4), 7.34 (dd, 2H, J = 4.6). ^{13}C NMR ($CDCl_3$, 300 MHz): δ- 152.52, 132.21, 131.31, 116.05.

PTP/DIB (1). PTP (5 mg) and 16.5 mg DIB were dissolved in 6 mL DCM in a vial covered with a layer of parafilm and let stand at room temperature. After 3 days, light yellow crystals suitable for single X-ray diffraction were harvested. Anal. Calcd for $C_{13}H_{10}IN_2S$: C, 44.21; H, 2.85; N, 7.93. Found: C, 44.19; H, 2.84; N, 7,91.

PTP/DITFB (2). PTP (5 mg) and 21.5 mg DITFB were dissolved in 6 mL DCM in a vial covered with a layer of parafilm and allowed to stand at room temperature for 5 days. Yellow crystals suitable for single X-ray diffraction were obtained. Anal. Calcd for $C_{39}H_{18}Cl_2F_{12}I_6N_4S_2$: C, 28.08; H, 1.09; N, 3.36. Found: C, 28.08, H, 1.08; N, 3.34.

PTP/IPFB (3). PTP (5 mg) and 15.5 mg IPFB were dissolved in 6 mL DCM in a vial sealed with a layer of parafilm and evaporated at room temperature for a week to obtain greenish yellow crystals suitable for single X-ray diffraction. Anal. Calcd for $C_{28}H_8F_{15}I_3N_2S$: C, 34.04; H, 1.04; N, 3.61. Found: C, 34.09; H, 1.02; N, 3.64.

3. Results

The PTP molecule formed halogen bonded cocrystals with all three XB donors: PTP/DIB (1), PTP/DITFB (2), and PTP/IPFB (3).

The asymmetric unit of **1** contains one complete PTP molecule and half of the DIB molecule. The N-atom in PTP is engaged with one I-atom from DIB forming halogen bond [$d_{N\cdots I}$ 2.968(3)Å and $<_{C\text{-}I\cdots N}$ 177.01°]. In this structure the DIB molecule act as a symmetric ditopic XB donor bridging two PTP molecules through N-atoms. The S-atom of PTP is not involved in XB bonds. Instead it interacts with two neighboring PTP and one nearby DIB via weak C-H···S hydrogen bonds [$d_{S\cdots C5}$ 3.808Å, $<_{C5\text{-}H\cdots S}$ 155.3°; $d_{S\cdots C7}$ 3.795Å, $<_{C7\text{-}H\cdots S}$ 164.97°; $d_{S\cdots C12}$ 3.712Å, $<_{C12\text{-}H\cdots S}$ 136.09°] (Figure 2). Such an arrangement could indicate that the N atom of PTP is favored over S in XB formation.

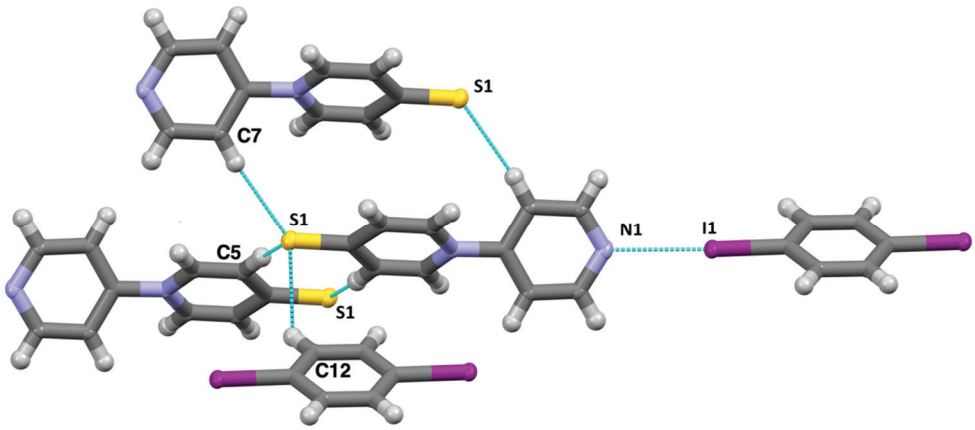

Figure 2. N···I XB and S···H contacts in **1**.

The asymmetric unit of **2** is comprised of two complete PTP molecules, one complete DITFB molecule, four halves of DITFB molecules, and a complete CH_2Cl_2 solvent molecule. In this structure both the S-atom and the N-atom of PTP interact with DITFB molecules by XBs. One DITFB molecule bridges two PTP molecules by N···I halogen bonds [$d_{N2\cdots I1}$ 2.845(6)Å and $<_{C\text{-}I1\cdots N2}$ 171.4(2) °; $d_{N4\cdots I2}$ 2.915(6) and $<_{C\text{-}I2\cdots N4}$ 176.7(2) °]. At the same time the S-atom of PTP also acts as a bifurcated bridging point binding two other DITFB molecules [$d_{S1\cdots I3}$ 3.096(1) and $<_{C\text{-}I3\cdots S1}$ 174.6(1)Å; $d_{S1\cdots I6}$ 3.215 and $<_{C\text{-}I6\cdots S1}$ 171.8(1) °; $d_{S2\cdots I4}$ 3.137(1) and $<_{C\text{-}I4\cdots S2}$ 172.6(1); $d_{S2\cdots I5}$ 3.300(1) and $<_{C\text{-}I5\cdots S2}$ 171.7(1) °], as shown in

Figure 3a. Noticeably, two PTP molecules are connected via S1···H-C [$d_{S1\ldots C}$ 2.929Å, $<_{S1\ldots H\text{-}C}$ 162.89°] and I4 simultaneously connects a neighboring PTP molecule via I4···H3-C3 [$d_{I4\ldots C3}$ 3.927Å, $<_{I4\ldots H3\text{-}C3}$ 136.98°]. The key feature of this structure is that through the I···N and the bifurcated I···S XBs twelve membered rings are formed, giving an expanded wavy 2D network structure with S as the node (Figure 3). Furthermore, 2D networks are connected with adjacent units via F···H, F···C and S···H intermolecular contacts to form a five-folded interpenetrated 3D network. No solvent occupied channels edged by PTP/DITFB are formed.

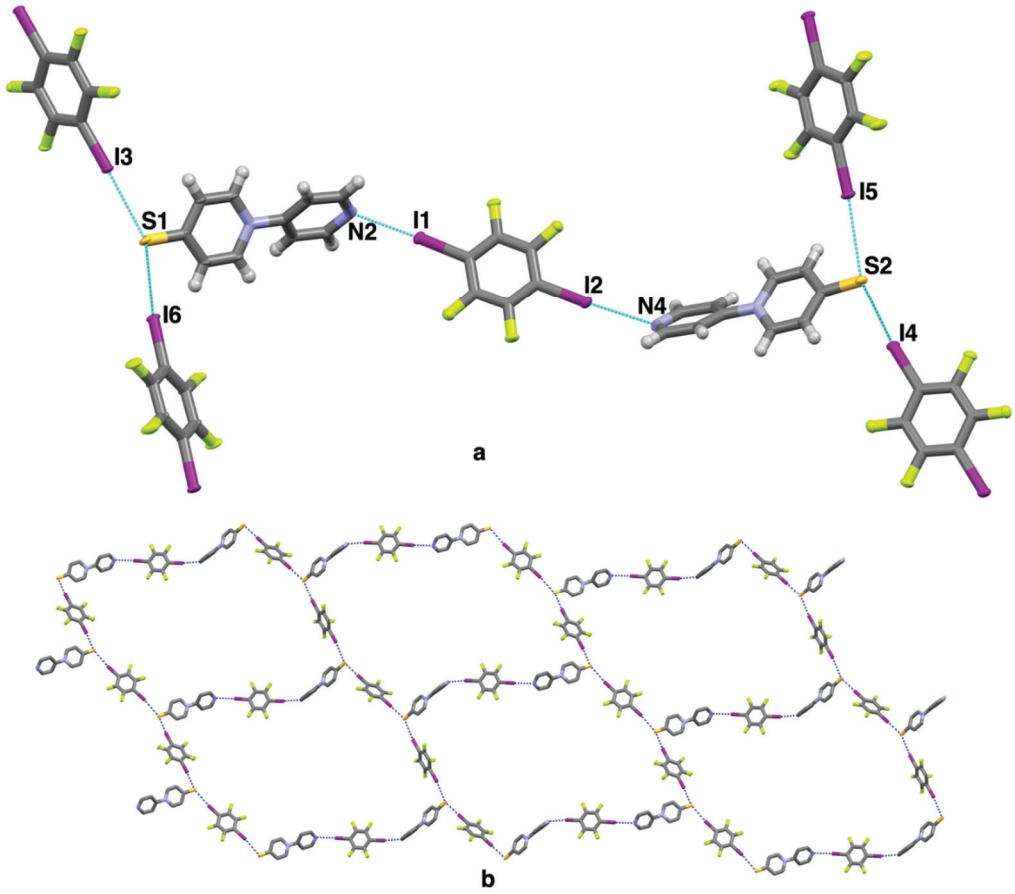

Figure 3. XBs and extended structure of **2**. (**a**) XBs on S and N; (**b**) extended 2D structure of **2**. Solvent CH_2Cl_2 and hydrogen atoms are omitted for clarity.

The asymmetric unit of **3** has one PTP molecule and two IPFB units. XB interactions only take place through the S-atom of PTP, which forms a pair of bifurcated XBs [$d_{S1\ldots I1}$ 3.1224(8)Å and $<_{C\text{-}I1\ldots S1}$ 175.47(7)°; $d_{S2\ldots I2}$ 3.1122(8) and $<_{C\text{-}I2\ldots S1}$ 176.9(1)°]. In this structure the N-atom interacts with two adjacent PTP molecules via weak C-H···N contacts [$d_{N\ldots C}$ 3.423Å, $<_{N\ldots H\text{-}C2}$ 132.55°; $d_{N\ldots C9}$ 3.259Å, $<_{N\ldots H\text{-}C9}$ 117.59°; $d_{N\ldots C10}$ 3.250Å, $<_{N\ldots H\text{-}C10}$ 117.38°] (Figure 4). The relatively large deviation from 180° of all three $<_{N\ldots H\text{-}C}$ is may be affected by the dispersion interactions, which can have an impact on the geometry of HBs in bulky systems [42]. Unlike in **1**, in **3** the XB formation favors I···S interactions. It could indicate that the stronger XB donor IPFB forms XBs with S-atom more easily than iodine in the DIB donor. The structure is further expanded through F···H and S···H contacts.

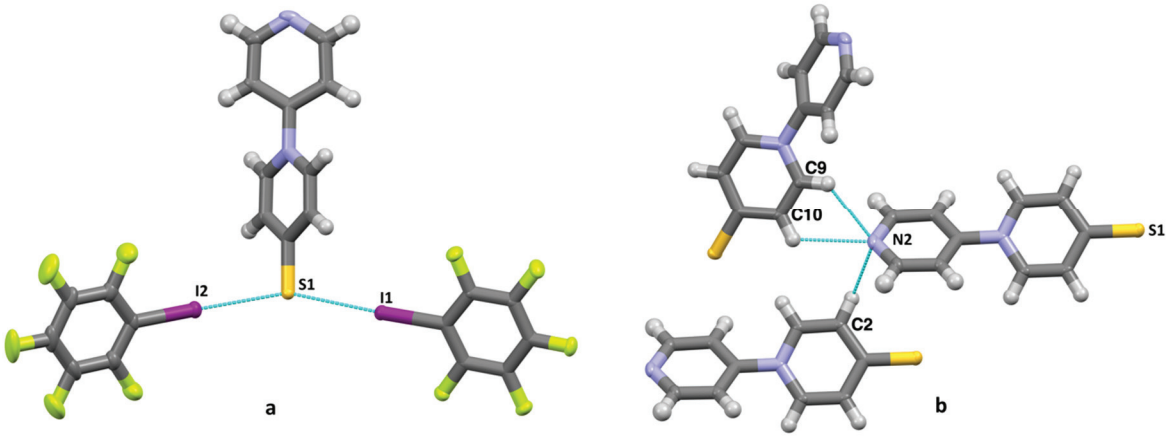

Figure 4. Nonvalent interactions in **3** involving S and N acceptors. (**a**) XBs on S; (**b**) H···N contacts.

Based on the DSC measurements, shown in Table 2, the order of the thermal stability of cocrystals **1–3** are **1** > **2** > **3**. Both **1** and **2** contain I···N halogen bonds. In **3** there are only bifurcated I···S interactions. This could indicate that formation of I···N interactions are stabilizing the structure of the cocrystals. However, it is likely that HBs between XB donor and the S-atom of the acceptor in **1** also play an important role in the overall packing. The results suggest that other type of intermolecular interactions than XBs could be the dominating factors behind the thermal stability in cocrystals 1-3.

Table 2. DSC measurements.

Crystals	T_c /°C
1	127.67
2	114.46
3	85.36

4. Discussion

The relative strength of XB is often described using the halogen bonding interaction ratio, R_{XB}, which is defined as $R_{XB} = d_{XB}/(X_{vdW} + B_{vdW})$ (d_{XB} is the distance between a halogen atom X and the acceptor atom B in Å). Typically, Bondi vdW radii are used for both X_{vdW} and B_{vdW}) [43–48]. A smaller value of R_{XB} indicates stronger XB strength. The key structure parameters of XBs in cocrystal **1–3** are listed in Table 3.

Table 3. Halogen bonds in 1–3.

Crystal*	I···A	d (I···A) Å	<C-I···A °	Symmetry Operations	R_{XB}
1	I···N	2.968(3)	177.01(9)	x, y, z	0.839
2	I1···N2	2.845(6)	171.4(2)	x, y, z	0.806
	I2···N4	2.915(6)	176.7(2)	x, y, z	0.826
	I3···S1	3.096(1)	174.6(1)	1−x, 1−y, 2−z	0.819
	I6···S1	3.215(1)	171.8(1)	1+x, y, z	0.851
	I4···S2	3.137(1)	172.6(1)	−1+x, y, −1+z	0.830
	I5···S2	3.300(1)	171.7(1)	−x, 1−y, 1−z	0.873
3	I1···S1	3.1224(8)	175.47(7)	2−x, 2−y, 1−z	0.826
	I2···S1	3.1122(8)	176.9(1)	1−x, −1/2+y, 1/2−z	0.823

According to this qualitative R_{XB} values, the strongest XB is an I···N contact found in **2**. On the other hand, the weakest contact is an I···S interaction. This time it is found in the second thermally most stable **2**. All in all, the variations in R_{XB} values are quite small and obviously they cannot alone

explain the favored packing patterns. The roles of the other non-covalent interactions, especially hydrogen bonds, are also important forces in determination of the final packing pattern.

The N···I length ranges from 2.845 Å to 2.968 Å in cocrystals **1–3**. To compare these values with other reported N···I distances, a CCDC survey was carried out (C=N, I-C, no organometallic complexes, N and I contact distance <3.53 Å, CSD version 5.41, November 2019). The survey gave a median value of $d_{N\cdots I}$ of 3.050 Å. Thus, the I···N in crystals **1–3** are shorter than most reported ones, indicating a stronger I···N halogen bond. Moreover, R_{XB} of **1** is 0.839, while the R_{XB} of the two I···N in **2** are 0.806 and 0.826, respectively, indicating that both I···N in **2** are stronger than the one found in **1**. Such a result is expected, as the iodine atom in DITFB is more electronegative compared to the corresponding value in DIB due to the fluorine substituents.

To compare the I···S found in cocrystals **2** and **3** with the previously reported sp^3-S contacts, another CCDC survey was performed (C-S and S is in sp^3 hybridization, I-C, no organometallic complexes, S and I contact distance <3.78 Å, CSD version 5.41, November 2019). $d_{I\cdots S}$ in **2** and **3** were in the range of 3.096–3.300 Å, which was shorter than the median of 3.668 Å found from the CCDC survey, indicating again stronger XBs in **2** and **3**. In **2** the average $d_{I\cdots S1}$ was 3.155 Å and the average $d_{I\cdots S2}$ was 3.219 Å, while in **3** the average $d_{I\cdots S1}$ was 3.117 Å. This suggested that I···S interactions in **3** were stronger than in **2**. Such difference in I···S strength is probably due to the fact that iodine is in a stronger electron withdraw environment in IPFB than in DITFB.

Clearly, PTP demonstrates its ability as an acceptor to form strong XBs through both its acceptor atoms. However, both N and S acceptors were not involved in XB interactions in all structures. In **1**, only the N-atom of PTP was acting as a XB acceptor interacting with the DIB, the weakest XB donor used in this study. Whereas in **2** both S-atom and N-atom interact with DITFB, a stronger XB donor than DIB, to form XBs. On the contrary to **1**, in **3** only the S-atom was involved in XB with IPFB, the strongest XB donor in this study. Such a trend could indicate some selectivity in the XB formation. The hard-soft acid-base (HSAB) theory, which gives a plausible explanation for the competition between XB and HB regarding S and N [49], fails to explain the XB selectivity in **1–3**, because the I-atom in IPFB, the hardest I-atom compared with that in DIB and DITFB due to the strongest polarization caused by F substitutions, chooses the soft S instead of the hard N. However, though I-atom in IPFB is the hardest among the three XB donors, it is still soft in nature, especially when compared to N. Thus, the apparent selectivity can be influenced by other noncovalent interactions. To estimate the contribution of XB to the total molecular interactions in **1–3**, Hirshfeld surface analyses was used, which is a method to analyze the interactions in molecular packing and comparison of crystal structures [50,51]. CrystalExplorer 17.5 [52] was used to create Hirshfeld surfaces around PTP in **1–3** in Figure 5. The contribution of XB to the Hirshfeld surface of each crystal structure is summarized in Table 4.

Table 4. Contributions of XBs to Hirshfeld surfaces in **1–3.**

Cocrystal	XB	Contribution/%
1	N···I	2.1
2	N···I	3.2
2	S···I	3.4
3	S···I	5.2

The difference in intensity in these fingerprints reveals the difference in XB bond length in the obtained cocrystals; the increase in intensity around $di/de \approx 1.2$ Å/1.65 Å in N···I of **2** compared to that of **1** shows that N···I in **2** is shorter than in **1**. Similarly, the increased intensity around $di/de \approx 1.5$ Å/1.7 Å in I···S of **3** compared to that of **2** arises from the much shorter S···I in **3**. Moreover, the different fingerprint patterns also reveal that the PTP molecule is in different immediate polymorph environment in **1–3** [51]. Fingerprints plot with HB contacts highlighted (supplementary material Figure S6.) illustrate each type of HB contacts with distinctive patterns. The strongest intensities can be found around $di/de \approx 1.0$-1.2 Å/1.4-2.4 Å region. S···H in **1** has strong intensity around $di/de \approx 1.1$ Å/1.8 Å, while in **2** the strongest region is $di/de \approx 1.2$ Å/1.9 Å. The F···H in **2**, compared with that in 3, reaches a shorter *di* region and has weaker intensity around $di/de \approx 1.2$ Å/1.4 Å. Moreover, the I···H in

2 demonstrates the strongest interactions around *di*/*de*≈1.2 Å/2.1 Å. Noticeably, the same type of HB contact in different cocrystals has different fingerprints patterns, due to the sensitivity of fingerprints plot to the environment surrounding PTP molecules [51]. Based on the analysis, the XB contribution to the Hirshfeld surface is small, less than 10% in all three cocrystals, indicating that XB is not the prominent crystal stabilizing force. The DSC results yield similar conclusions as well; the weakest XB donor forms the most thermally stable crystal, while the strongest XB donor yields the most thermally unstable one, suggesting other types of intermolecular interactions play more pivotal roles in these crystal structures.

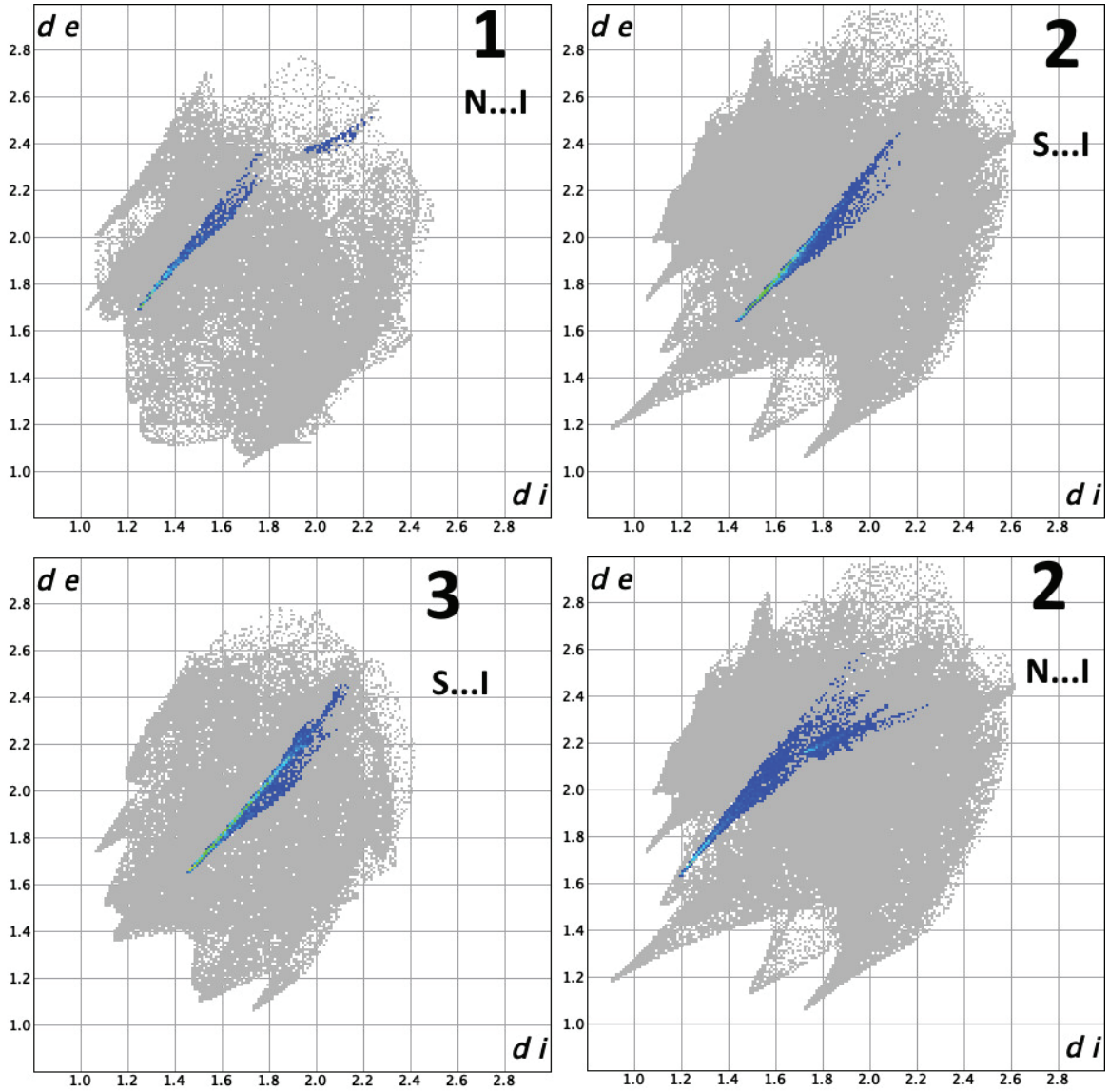

Figure 5. 2D fingerprint plots resolved into N···I in 1, S···I and N···I in 2, and S···I in 3. The full fingerprints appear in each plot as grey.

5. Conclusions

Bidentate, neutral 1-(4-pyridyl)-4-thiopryine (PTP), was synthesized and used as a XB acceptor in this study. Three cocrystals were obtained with comparatively strong XBs, showing that PTP is capable of forming robust XBs. Moreover, with DITFB as the XB donor, PTP demonstrated its ability to form bifurcated XBs on S and single XBs on N simultaneously, generating wavy continuous network structures. The analysis of XBs, together with the Hirshfeld surface analyses and DSC measurements, indicates that the formation of halogen bonds is not necessarily the dominating driving force in the formation of cocrystals. Other non-covalent interactions play key roles in the

final arrangement of molecules. In order to build systematic supramolecular constructions, all intermolecular interactions must always be considered. It is challenging to predict what types of intermolecular interactions will be the dominate ones and this hampers the prediction of non-covalent assemblies.

Supplementary Materials: The following are available online at www.mdpi.com/xxx/s1, Table S1: Descriptive statistics of CCDC survey of sp^2-N, Table S2: Descriptive statistics of CCDC survey of sp^3-S, Figure S1: TGA/DSC spectrum of cocrystal 1, Figure S2: TGA/DSC measurements of cocrystal 2, Figure S3: TGA/DSC spectrum of cocrystal 3, Figure S4: ^{1}H NMR of PTP, Figure S5: ^{13}C NMR of PTP, Figure S6: 2D fingerprints plot resolved in S···H in 1, F···H, S···H and I···H in 2, F···H and N···H in 3. The crystallographic data can also be obtained free of charge in *cif* format by request from the Cambridge Crystallographic Data Centre at www.ccdc.cam.ac.uk/data_request/cif. The CCDC numbers of compounds 1-3 are 982538, 1982539, and 1982540 respectively.

Author Contributions: Synthesis, initial X-ray structure characterization and draft preparation: X.D.; X-structure characterization: M.T.; project planning, supervision, funding acquisition and project administration, manuscript review and editing: M.H. All authors have read and agreed to the published version of the manuscript.

Funding: This research was funded by Academy of Finland, grant number 130571 and 295881.

Conflicts of Interest: The authors declare no conflict of interest.

References

1. Desiraju, G. R.; Ho, P. S.; Kloo, L.; Legon, A. C.; Marquard, R.; Metrangolo, P.; Politzer, P.; Resnati, G.; Rissanen, K. Definition of the Halogen Bond (IUPAC Recommendations 2013). *Pure Appl. Chem*., **2013**, *85*, 1711–1713.
2. Forni, A.; Franchini, D.; Dapiaggi, F.; Pieraccini, S.; Sironi, M.; Scilabra, P.; Pilati, T.; Petko, K.; Resnati, G.; Yagupolkii, Y. L. Featuring I…N Halogen Bond and Weaker Interactions in Iodoperfluoroalkylimidazoles: An Experimental and Theoretical Charge Density Study. *Cryst. Growth Des*. **2019**, *19*, 1621–1631.
3. Awwadi, F. F.; Willett, R. D.; Peterson, K. A.; Twamley, B. The Nature of Halogen···Halides Synthons: Theoretical and Crystallographic Studies. *J. Phys. Chem. A* **2007**, *111*, 2319–2328.
4. Awwadi, F. F.; Taher, D.; Haddad, S. F. Turnbull, M. M. Competition between Hydrogen and Halogen Bonding Interactions: Theoretical and Crystallographic Studies. *Cryst. Growth Des.* **2014**, *14*, 1961–1971.
5. Stilinovi ć, V.; Horvat, G.; Hrenar, T.; Nemec, V.; Cinčić, D. Halogen and Hydrogen Bonding between (N-Halogeno-)-succinimides and Pyridine Derivatives in Solution, the Solid State and In Silico. *Chem. Eur. J.* **2017**, 23, 5244–5257.
6. Politzer, P.; Murray, J. S.; Clark, T. Halogen Bonding: An Electrostatcially-Driven Highly Directional Noncovalent Interaction. *Phys. Chem. Chem. Phys.* **2010**, 12, 7748-7757.
7. Priimagi, A.; Cavallo, G.; Metrangolo, P.; Resntai, G. The Halogen Bond in the Design of Functional Supramolecular Materials: Recent Advances. *Acc. Chem. Res.* **2013**, 46, 11, 2686-2695.
8. Clark, T. Halogen bonds and σ-holes. *Faraday Discuss.*, 2017, *203*, 9–27.
9. Rowe, R. K.; Ho, P. S. Relationships between Hydrogen Bonds and Halogen Bonds in Biological Systems. *Acta Cryst.* **2017**, *B73*, 255–264.
10. Gunawardana, C. A.; Desper, J.; Sinha, A. S.; Đaković, M.; Aakeröy, C. B. Competition and Selectivity in Supramolecular Synthesis: Structural Landscape around 1-(Pyridylmethyl)-2,2′-biimidazoles. *Faraday Discuss.* **2017**, *203*, 371–388.
11. Pfrunder, M. C.; Brock, A. J.; Brown, J. J.; Grosjean, A.; Ward, J.; McMurtrie, J. C.; Clegg, J. J. A Three-dimensional Cubic Halogen-bonded Network. *Chem. Commun.*, **2018**, *54*, 3874–3976.
12. Ding, X.; Tuikka, M. J.; Hirva, P.; Kukushkin, V. Y.; Novikov, A. S.; Haukka, M. Fine-tuning Halogen Bonding Properties of Diiodine through Halogen-halogen Charge Transfer-Extended [Ru(2,2′-bipyridine)$(CO)_2X_2$]•I_2 Systems (X=Cl, Br, I). *Cryst. Eng. Comm*. **2016**, *18*, 1987–1995.
13. Pfrunder, M. C.; Micallef, A. S.; Rintoul, L.; Arnold, D. P.; McMurtrie, J. Interplay between the Supramolecular Motifs of Polypyridyl Metal Complexes and Halogen Bond Networks in Cocrystals. *Cryst. Growth Des.* **2016**, *16*, 681–695.
14. Chan, Y-C.; Yeung, Y-Y. Halogen Bond Catalyzed Bromocarbocyclization. *Angew. Chem. Int. Ed.* **2018**, 57, 3483-3487.

15. Carreras, L.; Serrano-Torné, M.; van Leeuwen, P. W. N. M.; Vidal-Ferran, A. XBpos-Rh: A Halogen-bond Assembled Supramolecular Catalyst. *Chem. Sci.*, **2018**, *9*, 3644–3648.
16. Lim, J. Y. C.; Marques, I.; Félix, V.; Beer, P. D. Enantioselective Anion Recognition by Chiral Halogen-Bonding [2]Rotaxanes. *J. Am. Chem. Soc.* **2017**, *139*, 12228–12239.
17. Cavallo, G.; Metrangolo, P.; Milani, R.; Pilati, T.; Priimagi, A.; Resnati, G.; Terraneo. The Halogen Bond. *Chem.Rev.* **2016**, 116, 2478–2601.
18. Riel, A. M. S.; Decato, D. A.; Sun, J.; Massena, C. J.; Jessop, M. J.; Berryman, O. B. The Intramolecular Hydrogen Bonded-halogen Bond: A New Strategy for Preorganization and Enhanced Binding. *Chem. Sci.*, **2018**, *9*, 5828–5836.
19. Dichiarante, V.; Kaiho, T.; Metrangolo, P.; Pilati, T.; Resnati, G.; Terraneo, G.; Ursini, M. The Diiodomethyl-sulfonyl Moiety: An Unexplored Halogen Bond-donor Motif. *Chem. Commun.* **2019**, *55*, 4234–4237.
20. Carletta, A.; Zbačnik, M.; Vitković, M.; Tumanov, N.; Stilinović, V.; Wouters, J.; Cinčić, D. Halogen-bonded Cocrystals of N-salicylidene Schiff Bases and Iodoperfluorinated Benzenes: Hydroxyl Oxgen as A Halogen Bond Acceptor. *Cryst. Eng. Comm*. **2018**, *20*, 5332–5339.
21. Zbačnik, M.; Vitković, M.; Vulić, V.; Nogalo, I.; Cinčić, D. Competiton between Halogen Bonds in Cocrystals of Imines Derived from *o*-Vanillin. *Cryst. Growth Des.* **2016**, *16*, 6381–6389.
22. Carletta, A.; Zbačnik, M.; Gysel. M. V.; Vitković, M.; Tumanov, N.; Stilinović, Wouters, J.; Cinčić. Playing with Isomerism: Cocrystallization of Isomeric N-Salicylideneaminopyridines with Perfluorinated Compounds as Halogen Bond Donors and Its Impact on Photochromism. *Cryst. Growth Des.* **2018**, *18*, 6833–6842.
23. Koskinen, L.; Jääskeläiinen, S.; Hirva, P.; Haukka; M. Tunnable Interaction Strength and Nature of the S···Br Halogen Bonds in [(Thione)Br_2] Systems. *Cryst. Growth Des.* **2015,** 15, 1160-1167.
24. Koskinen, L.; Hirva, P.; Hasu, A.; Jääskeläinen, S.; Koivistoinen, J.; Petterson, M.; Haukka, M. Modification of the Supramolecular Structure of [(Thione)IY] (Y=Cl, Br) Systems by Cooperation of Strong Halogen Bonds and Hydrogen Bonds. *Cryst. Eng. Comm*. **2015**, *17*, 2718–2727.
25. Eccles, K. S.; Morrison, R. E.; Sinha, A. S.; Maguire, A. R.; Lawrence, S. E. Investigating C=S···I Halogen Bonding for Cocrystallization with Primary Thionamides. *Cryst. Growth Des*. **2015**, *15*, 3442–3451.
26. Le Gal, Y.; Lorcy, D.; Jeannin, O.; Barrière, F.; Dorcet, V.; Lieffrig, J.; Fourmigué, M. C=S···I Halogen Bonding Interactions in Crystalline Iodinated Dithiole-2-thiones and Thiazole-2-thiones. *Cryst. Eng. Comm*. **2016**, *8*. 5474–5481.
27. Cauliez, P.; Polo, V.; Roisnel, T.; Llusar, R.; Fourmigué. The Thiocyanate anion as a polydentate halogen bond acceptor. *Cryst. Eng. Comm*. **2010**, *12*, 558–556.
28. Cinčić, D.; Friščić, T.; Joens, W. Experimental and Database Studies of Three-centered Halogen Bonds with Bifurcated Acceptors Present in Molecular Crystals, Cocrystals and Salts. *Cryst. Eng. Comm*. **2011**, *13*, 3224–3231.
29. Goud, N. R.; Bolton, O.; Burgess, E. C.; Matzger. A.J. Unprecedented Size of the σ-Holes on 1,3,5-Triiodo-2,4,6-trinitrobenzene Begets Unprecedented Intermolecular Interactions. *Cryst. Growth Des.* **2016**, *16*, 1765–1771.
30. Pigge, F. C.; Kapadia, P. P.; Swenson, D.C. Halogen Bonded Networks from Pryidyl-substituted Tetraarylethylenes and Diiodotetrafluorobenzenes. *Cryst.Eng. Comm*. **2013**, *15*, 4386–4391.
31. Ravat, P.; Lekshmi, S. S.; Biswas, S. N.; Nandy, P.; Varughese, S. Equivalence of Ethylene and Azo-Bridges in the Modular Design of Molecular Complexes: Role of Weak Interactions. *Cryst. Growth Des.* **2015**, *15*, 2389–2401.
32. Aakeröy, C. B.; Spartz, C. L.; Dembowski, S.; Dwyre, S.; Desper, J. A Systematic Structural Study of Halogen Bonding *versus* Hydrogen Bonding within Competitive Supramolecular Systems. *IUCrJ*. **2015**, *2*, 498–510.
33. Bosch, E.; Kruse, S. J.; Groeneman, R. H. Infinite and Discrete Halogen Bonded Assemblies Based upon 1, 2-Bis(iodoethynyl)benzene. *Cryst. Eng. Comm*. **2019**, *21*, 990–993.
34. Peterson, A.; Kaasik, M.; Metsala, A.; Järving, I.; Adamson, J.; Kanger, T. Tunable chiral triazole-based halogen bond donors: assessment of donor strength in solution with nitrogen-containing acceptors. *RSC Adv*., **2019**, *9*, 11718–11721.

35. Lee, S.; Chen, B.; Fredrickson, D. C.; DiSalvo, F. J.; Lobkovsky, E.; Adams, J. Crystal Structures of (Pyrene)$_{10}$(I_3^-)$_4$(I_2)$_{10}$ and [1, 3, 6, 8-Tetrakis(methylthio)pyrene]$_3$(I_3^-)$_3$(I_2)$_7$: Structural Trends in Fused Aromatic Polyiodides. *Chem. Mater.* **2003**, *15*, 1420–1433.
36. Tamilselvi, A.; Mugesh, G. Interaction of Heterocyclic thiols/thiones eliminated from cephalosporins with iodine and its biological implications. *Bioorg. Med. Chem. Lett.* **2010**, *20* 3692–3697.
37. Mancini, A.; Pala, L.; Aragoni, M. C.; Arca. M.; Devillanova, F. A.; Hursthouse, M. B.; Light, M. E.; Skabara, P. J.; Bricklebank, N. Structural and DFT Studies of Dibromine and Diiodine Adducts of a Sulfur-Rich Thiocarbonyl Donor. *Eur. J. Inorg. Chem.* **2012**, 2373–2380; doi:10.1002/ejic.201101028
38. Eichstaedt, K.; Wasilewska, A.; Wicher, B.; Gdaniec, M.; Połoński. Supramolecular Synthesis Based on a Combination of Se···N Secondary Bonding Interactions with Hydrogen and Halogen Bonds. *Cryst. Growth Des.* **2016**, *16*, 1282–1293.
39. Montis, R.; Arca, M.; Aragoni, M. C.; Bauzá, A.; Demartin, F.; Frontera, A.; Isaia, F.; Lippolis, V. Hydrogen- and Halogen-bond Cooperativity in Determining the Crystal Packing of Dihalogen Charge-transfer Adducts: A Study Case from Heterocyclic Pentatomic Chalcogenone Donors. *Cryst. Eng. Comm*. **2017**, *19*, 4401–4412.
40. Ivolgina, V. A.; Chernov'yants, M. S.; Popov, L. D.; Suslonov, V. V.; Borodkin, G. S.; Luanguzov, N. V.; Avtushenko, N. A. Perspective Anti-thyroid Druy 2-thioxo-5-(3, 4, 5-trimethoxybenzylidene) thiazolidine-4-one: X-ray and Thermogravimetric Characterization of Two Novel Molecular Adducts, Obtained by Interaction with I_2. *J. Mol. Struct*. **2019**, *1180*, 629–635.
41. Sheldrick, G. M. Crystal Structure Refinement with SHELXL. *Acta Cryst*. **2015**, *C71*, 3–8.
42. Van der Lubbe, S. C. C.; Guerra, C. F. The Nature of Hydrogen Bonds: A Delineation of the Role of Different Energy Components on Hydrogen Bond Strengths and Lengths. *Chem. Asian J.* **2019**, *14*, 2760–2769.
43. Bondi, A. van der Waals Volumes and Radii. *J. Phys. Chem.* **1964**, *68*, 441–451.
44. Lommerse, P. M.; Stone, A. J.; Taylor, R.; Allen, F.H. The Nature and Geometry of Intermolecular Interactions Between Halogen and Oxygen or Nitrogen. *J. Am. Chem. Soc*. **1996**, *118*, 3108–3116.
45. Brammer, L.; Bruton, E. A.; Sherwood, P. Understanding the Behavior of Halogens as Hydrogen Bond Acceptors. *Cryst. Growth Des*. **2001**, *1*, 277–290.
46. Zordan, F.; Brammer, L.; Sherwood, P. Supramolecular Chemistry of Halogens: Complementary Features of Inorganic (M-X) and Organic (C-X') halogens Applied to M-X···X'-C Halogen Bond Formation. *J. Am. Chem. Soc.* **2005**, *127*, 5979–5989.
47. Johnson, M. T.; Džolić, Z.; Cetina, M.; Wendt, O. F.; Öhrström, L.; Rissanen, K. Neutral Organometallic Halogen Bond Acceptors: Halogen Bonding in Complexes of PCPPdX (X=Cl, Br, I) with Iodine (I_2), 1,4-Diiodotetrafluorobenzene (F4DIBz), and 1,4-Diiodooctafluorobutane (F8DIBu). *Cryst. Growth Des.* **2012**, *12*, 362–368.
48. Ding, X.; Tuikka, M.; Rissanen, K.; Haukka, M. Extended Assemblies of Ru(bpy)$(CO)_2X_2$ (X=Cl, Br, I) Molecules Linked by 1,4-Diiodotetrafluoro-Benzene (DITFB) Halogen Bond Donors. *Crystals*. **2019**, *9*, 319.
49. Riel, A. M. S.; Jessop, M. J.; Decato, D. A.; Massena, C. J.; Nascimento, V. R.; Berryman, O. B. Experimental Investigation of Halogen-bond Hard-soft Acid-base Complementarity. *Acta Cryst*. **2017**, *B73*, 203–209.
50. Spackman, M. A.; Jayatilaka, D. Hirshfeld Surface Analysis. CrystEngComm, **2009**, *11*, 19–32.
51. Yang, P.; Qin C.; Du, S.; Jia, L.; Qin, Y.; Gong J.; Wu, S.Crystal Structure, Stability and Desolvation of the Solvates of Sorafenib Tosylate. *Crystals*. **2019**, *9*, 367.
52. Turner, M. J.; McKinnon, J. J.; Wolff, S. K.; Grimwood, D. J.; Spackman, M. A. CrystalExplorer Model Energies and Ergy Frameworks: Extension to Metal Coordination Compounds, Organic Salts, Solvates and Open-shell Systems. *ICUrJ*. **2017**, *4*, 547–587.

crystals

MDPI

Supplementary Materials

A Novel Halogen Bond Acceptor: 1-(4-Pyridyl)-4-Thiopyridine (PTP) Zwitterion

Xin Ding, Matti Tuikka and Matti Haukka *

Department of Chemistry, University of Jyväskylä, P.O. Box 35, FI-40014 Jyväskylä, Finland; xin.x.ding@jyu.fi (X.D.); MTU@dinex.fi (M.T.)

* Correspondence: matti.o.haukka@jyu.fi ; Tel.: +358-40-8054666

Received: 7 February 2020; Accepted: 29 February 2020; Published: date

Table of Contents

Table S1. Descriptive statistics of CCDC survey of sp^2-N.

C-N···I	Count	Structure	Minimum/Å	Maximum/Å	Median/Å	Mean/Å
DIST	289	210	2.324	3.529	3.050	3.085

Table S2. Descriptive statistics of CCDC survey of sp^3-S.

C-S···I	Count	Structure	Minimum/Å	Maximum/Å	Median/Å	Mean/Å
DIST	783	349	2.715	3.78	3.668	3.620

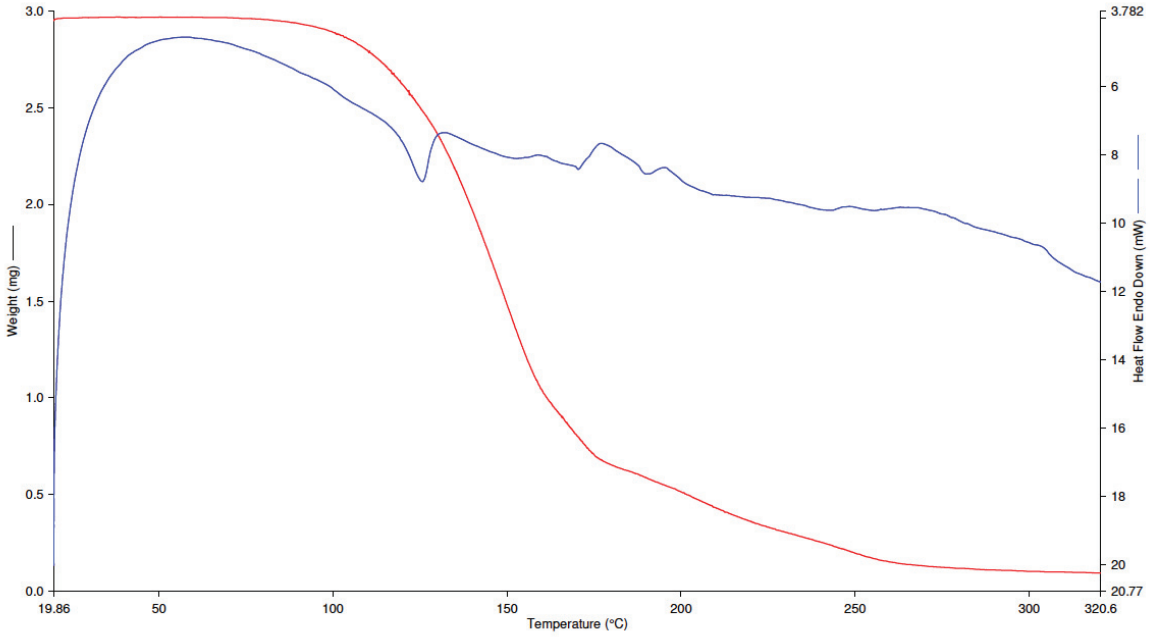

Figure S1. TGA/DSC measurements of cocrystal 1.

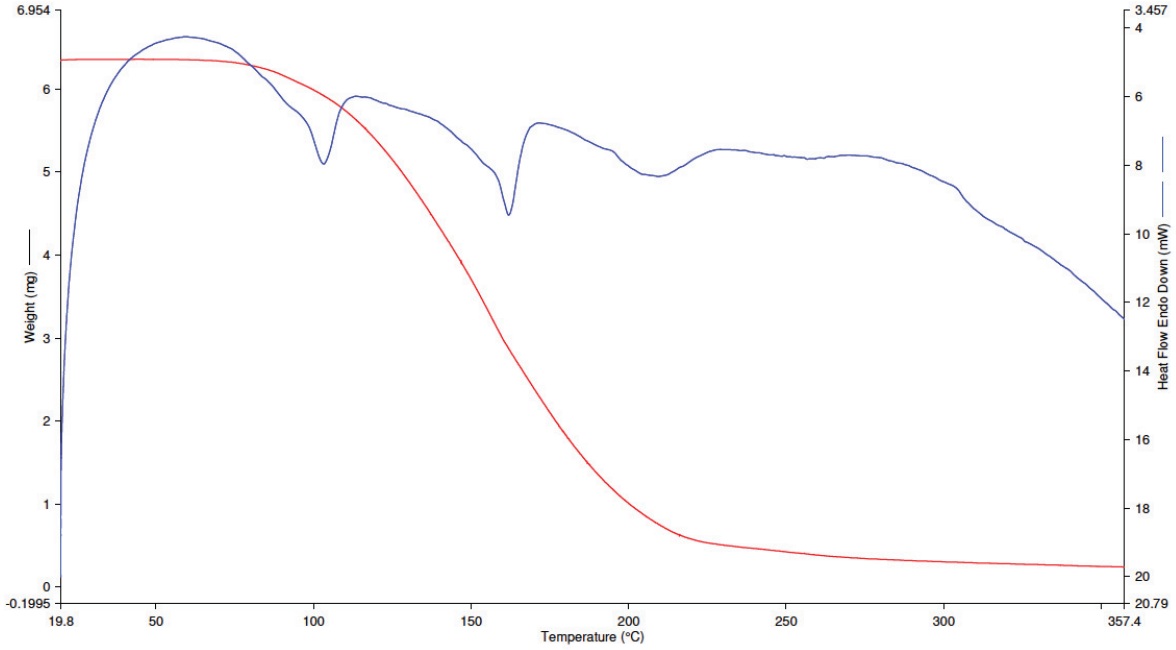

Figure S2. TGA/DSC measurements of cocrystal 2.

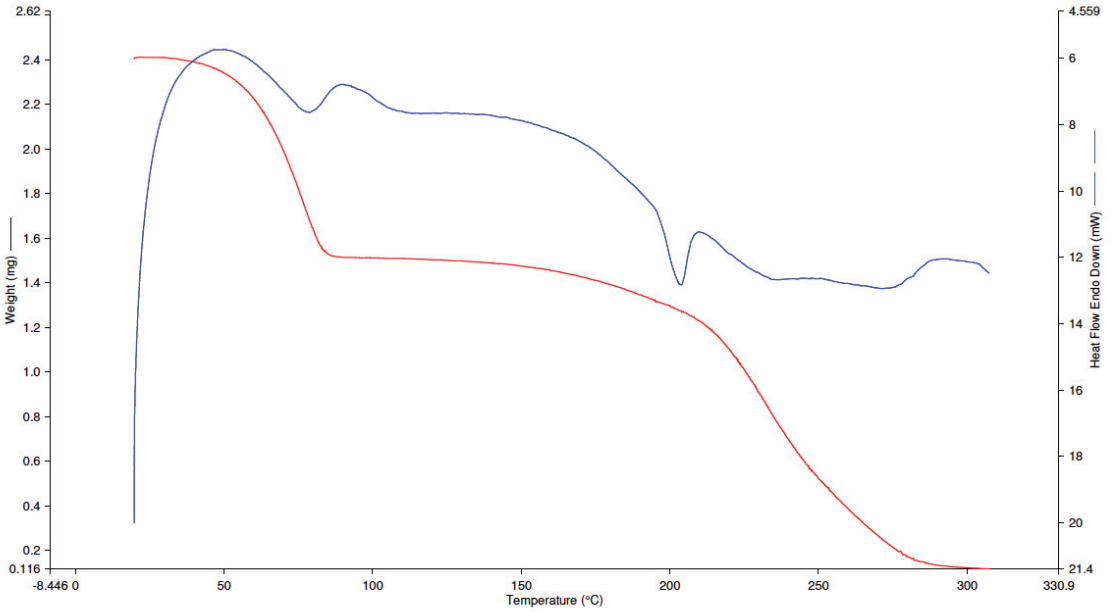

Figure S3. TGA/DSC measurements of cocrystal 3.

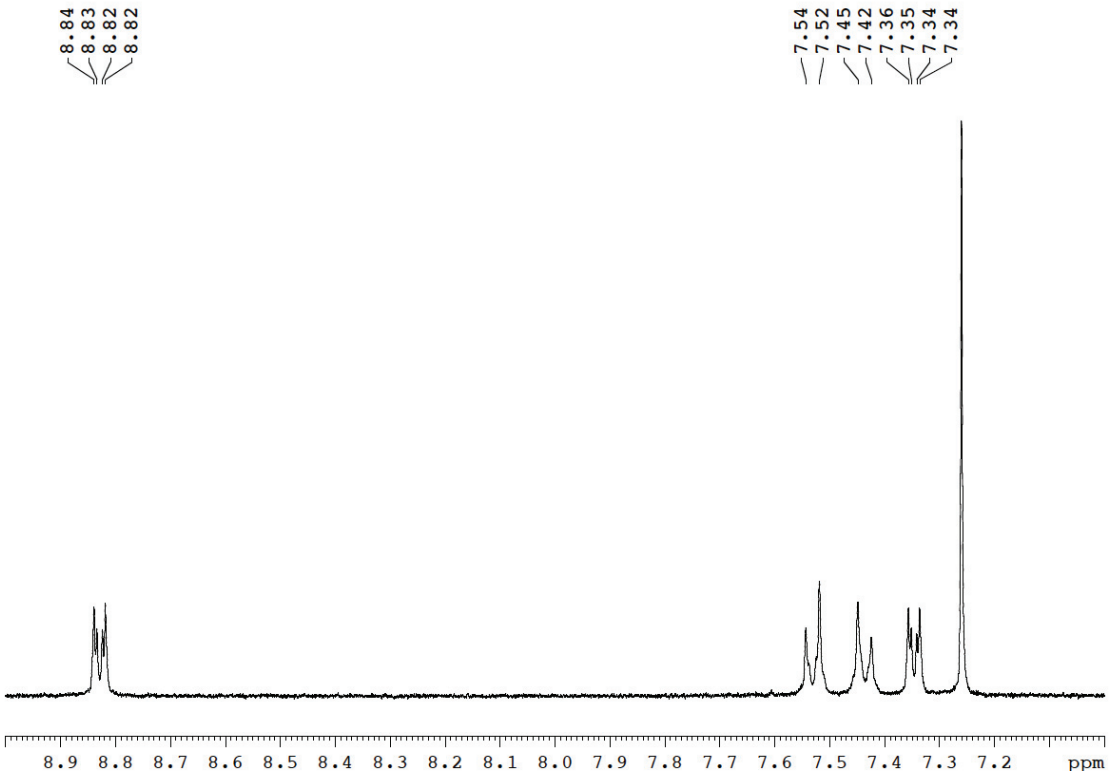

Figure S4. ^{1}H NMR of PTP in $CDCl_3$.

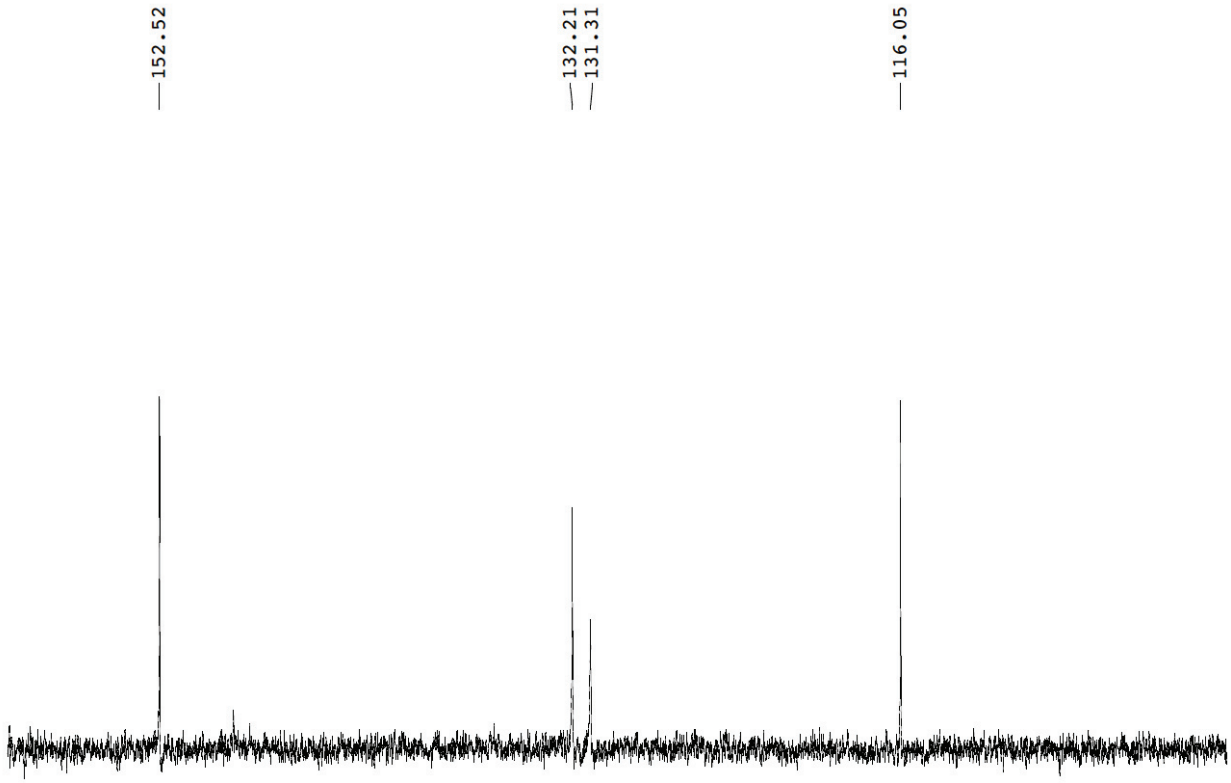

Figure S5. ^{13}C NMR of PTP in $CDCl_3$.

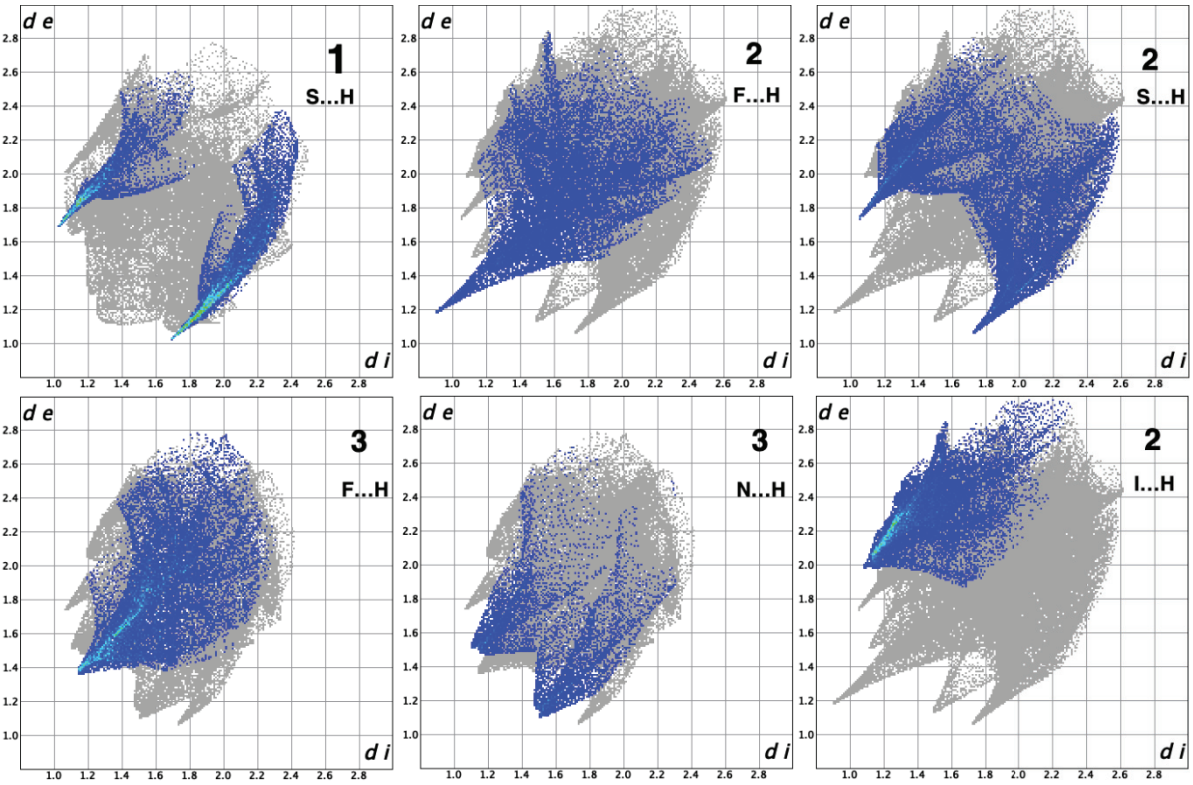

Figure S6. Fingerprint plots resolved in S···H in 1, F···H, S···H an I···H in 2, F···H and N···H in 3. The full fingerprints appear in each plot as grey.

DEPARTMENT OF CHEMISTRY, UNIVERSITY OF JYVÄSKYLÄ
RESEARCH REPORT SERIES

1. Vuolle, Mikko: Electron paramagnetic resonance and molecular orbital study of radical ions generated from (2.2)metacyclophane, pyrene and its hydrogenated compounds by alkali metal reduction and by thallium(III)trifluoroacetate oxidation. (99 pp.) 1976
2. Pasanen, Kaija: Electron paramagnetic resonance study of cation radical generated from various chlorinated biphenyls. (66 pp.) 1977
3. Carbon-13 Workshop, September 6-8, 1977. (91 pp.) 1977
4. Laihia, Katri: On the structure determination of norbornane polyols by NMR spectroscopy. (111 pp.) 1979
5. Nyrönen, Timo: On the EPR, ENDOR and visible absorption spectra of some nitrogen containing heterocyclic compounds in liquid ammonia. (76 pp.) 1978
6. Talvitie, Antti: Structure determination of some sesquiterpenoids by shift reagent NMR. (54 pp.) 1979
7. Häkli, Harri: Structure analysis and molecular dynamics of cyclic compounds by shift reagent NMR. (48 pp.) 1979
8. Pitkänen, Ilkka: Thermodynamics of complexation of 1,2,4-triazole with divalent manganese, cobalt, nickel, copper, zinc, cadmium and lead ions in aqueous sodium perchlorate solutions. (89 pp.) 1980
9. Asunta, Tuula: Preparation and characterization of new organometallic compounds synthesized by using metal vapours. (91 pp.) 1980
10. Sattar, Mohammad Abdus: Analyses of MCPA and its metabolites in soil. (57 pp.) 1980
11. Bibliography 1980. (31 pp.) 1981
12. Knuuttila, Pekka: X-Ray structural studies on some divalent 3d metal compounds of picolinic and isonicotinic acid N-oxides. (77 pp.) 1981
13. Bibliography 1981. (33 pp.) 1982
14. 6^{th} National NMR Symposium, September 9-10, 1982, Abstracts. (49 pp.) 1982
15. Bibliography 1982. (38 pp.) 1983
16. Knuuttila, Hilkka: X-Ray structural studies on some Cu(II), Co(II) and Ni(II) complexes with nicotinic and isonicotinic acid N-oxides. (54 pp.) 1983
17. Symposium on inorganic and analytical chemistry May 18, 1984, Program and Abstracts. (100 pp.) 1984
18. Knuutinen, Juha: On the synthesis, structure verification and gas chromatographic determination of chlorinated catechols and guaiacols occuring in spent bleach liquors of kraft pulp mill. (30 pp.) 1984
19. Bibliography 1983. (47 pp.) 1984
20. Pitkänen, Maija: Addition of BrCl, B_2 and Cl_2 to methyl esters of propenoic and 2-butenoic acid derivatives and ^{13}C NMR studies on methyl esters of saturated aliphatic mono- and dichlorocarboxylic acids. (56 pp.) 1985
21. Bibliography 1984. (39 pp.) 1985
22. Salo, Esa: EPR, ENDOR and TRIPLE spectroscopy of some nitrogen heteroaromatics in liquid ammonia. (111 pp.) 1985

23. Humppi, Tarmo: Synthesis, identification and analysis of dimeric impurities of chlorophenols. (39 pp.) 1985
24. Aho, Martti: The ion exchange and adsorption properties of sphagnum peat under acid conditions. (90 pp.) 1985
25. Bibliography 1985 (61 pp.) 1986
26. Bibliography 1986. (23 pp.) 1987
27. Bibliography 1987. (26 pp.) 1988
28. Paasivirta, Jaakko (Ed.): Structures of organic environmental chemicals. (67 pp.) 1988
29. Paasivirta, Jaakko (Ed.): Chemistry and ecology of organo-element compounds. (93 pp.) 1989
30. Sinkkonen, Seija: Determination of crude oil alkylated dibenzothiophenes in environment. (35 pp.) 1989
31. Kolehmainen, Erkki (Ed.): XII National NMR Symposium Program and Abstracts. (75 pp.) 1989
32. Kuokkanen, Tauno: Chlorocymenes and Chlorocymenenes: Persistent chlorocompounds in spent bleach liquors of kraft pulp mills. (40 pp.) 1989
33. Mäkelä, Reijo: ESR, ENDOR and TRIPLE resonance study on substituted 9,10-anthraquinone radicals in solution. (35 pp.) 1990
34. Veijanen, Anja: An integrated sensory and analytical method for identification of off-flavour compounds. (70 pp.) 1990
35. Kasa, Seppo: EPR, ENDOR and TRIPLE resonance and molecular orbital studies on a substitution reaction of anthracene induced by thallium(III) in two fluorinated carboxylic acids. (114 pp.) 1990
36. Herve, Sirpa: Mussel incubation method for monitoring organochlorine compounds in freshwater recipients of pulp and paper industry. (145 pp.) 1991
37. Pohjola, Pekka: The electron paramagnetic resonance method for characterization of Finnish peat types and iron (III) complexes in the process of peat decomposition. (77 pp.) 1991
38. Paasivirta, Jaakko (Ed.): Organochlorines from pulp mills and other sources. Research methodology studies 1988-91. (120 pp.) 1992
39. Veijanen, Anja (Ed.): VI National Symposium on Mass Spectrometry, May 13-15, 1992, Abstracts. (55 pp.) 1992
40. Rissanen, Kari (Ed.): The 7. National Symposium on Inorganic and Analytical Chemistry, May 22, 1992, Abstracts and Program. (153 pp.) 1992
41. Paasivirta, Jaakko (Ed.): CEOEC'92, Second Finnish-Russian Seminar: Chemistry and Ecology of Organo-Element Compounds. (93 pp.) 1992
42. Koistinen, Jaana: Persistent polychloroaromatic compounds in the environment: structure-specific analyses. (50 pp.) 1993
43. Virkki, Liisa: Structural characterization of chlorolignins by spectroscopic and liquid chromatographic methods and a comparison with humic substances. (62 pp.) 1993
44. Helenius, Vesa: Electronic and vibrational excitations in some

biologically relevant molecules. (30 pp.) 1993

45. Leppä-aho, Jaakko: Thermal behaviour, infrared spectra and x-ray structures of some new rare earth chromates(VI). (64 pp.) 1994
46. Kotila, Sirpa: Synthesis, structure and thermal behavior of solid copper(II) complexes of 2-amino-2- hydroxymethyl-1,3-propanediol. (111 pp.) 1994
47. Mikkonen, Anneli: Retention of molybdenum(VI), vanadium(V) and tungsten(VI) by kaolin and three Finnish mineral soils. (90 pp.) 1995
48. Suontamo, Reijo: Molecular orbital studies of small molecules containing sulfur and selenium. (42 pp.) 1995
49. Hämäläinen, Jouni: Effect of fuel composition on the conversion of fuel-N to nitrogen oxides in the combustion of small single particles. (50 pp.) 1995
50. Nevalainen, Tapio: Polychlorinated diphenyl ethers: synthesis, NMR spectroscopy, structural properties, and estimated toxicity. (76 pp.) 1995
51. Aittola, Jussi-Pekka: Organochloro compounds in the stack emission. (35 pp.) 1995
52. Harju, Timo: Ultrafast polar molecular photophysics of (dibenzylmethine)borondifluoride and 4-aminophthalimide in solution. (61 pp.) 1995
53. Maatela, Paula: Determination of organically bound chlorine in industrial and environmental samples. (83 pp.) 1995
54. Paasivirta, Jaakko (Ed.): CEOEC'95, Third Finnish-Russian Seminar: Chemistry and Ecology of Organo-Element Compounds. (109 pp.) 1995
55. Huuskonen, Juhani: Synthesis and structural studies of some supramolecular compounds. (54 pp.) 1995
56. Palm, Helena: Fate of chlorophenols and their derivatives in sawmill soil and pulp mill recipient environments. (52 pp.) 1995
57. Rantio, Tiina: Chlorohydrocarbons in pulp mill effluents and their fate in the environment. (89 pp.) 1997
58. Ratilainen, Jari: Covalent and non-covalent interactions in molecular recognition. (37 pp.) 1997
59. Kolehmainen, Erkki (Ed.): XIX National NMR Symposium, June 4-6, 1997, Abstracts. (89 pp.) 1997
60. Matilainen, Rose: Development of methods for fertilizer analysis by inductively coupled plasma atomic emission spectrometry. (41 pp.) 1997
61. Koistinen, Jari (Ed.): Spring Meeting on the Division of Synthetic Chemistry, May 15-16, 1997, Program and Abstracts. (36 pp.) 1997
62. Lappalainen, Kari: Monomeric and cyclic bile acid derivatives: syntheses, NMR spectroscopy and molecular recognition properties. (50 pp.) 1997
63. Laitinen, Eira: Molecular dynamics of cyanine dyes and phthalimides in solution: picosecond laser studies. (62 pp.) 1997
64. Eloranta, Jussi: Experimental and theoretical studies on some

quinone and quinol radicals. (40 pp.) 1997

65. Oksanen, Jari: Spectroscopic characterization of some monomeric and aggregated chlorophylls. (43 pp.) 1998
66. Häkkänen, Heikki: Development of a method based on laser-induced plasma spectrometry for rapid spatial analysis of material distributions in paper coatings. (60 pp.) 1998
67. Virtapohja, Janne: Fate of chelating agents used in the pulp and paper industries. (58 pp.) 1998
68. Airola, Karri: X-ray structural studies of supramolecular and organic compounds. (39 pp.) 1998
69. Hyötyläinen, Juha: Transport of lignin–type compounds in the receiving waters of pulp mills. (40 pp.) 1999
70. Ristolainen, Matti: Analysis of the organic material dissolved during totally chlorine-free bleaching. (40 pp.) 1999
71. Eklin, Tero: Development of analytical procedures with industrial samples for atomic emission and atomic absorption spectrometry. (43 pp.) 1999
72. Välisaari, Jouni: Hygiene properties of resol-type phenolic resin laminates. (129 pp.) 1999
73. Hu, Jiwei: Persistent polyhalogenated diphenyl ethers: model compounds syntheses, characterization and molecular orbital studies. (59 pp.) 1999
74. Malkavaara, Petteri: Chemometric adaptations in wood processing chemistry. (56 pp.) 2000
75. Kujala Elena, Laihia Katri, Nieminen Kari (Eds.): NBC 2000, Symposium on Nuclear, Biological and Chemical Threats in the 21st Century. (299 pp.) 2000
76. Rantalainen, Anna-Lea: Semipermeable membrane devices in monitoring persistent organic pollutants in the environment. (58 pp.) 2000
77. Lahtinen, Manu: *In situ* X-ray powder diffraction studies of Pt/C, CuCl/C and Cu_2O/C catalysts at elevated temperatures in various reaction conditions. (92 pp.) 2000
78. Tamminen, Jari: Syntheses, empirical and theoretical characterization, and metal cation complexation of bile acid-based monomers and open/closed dimers. (54 pp.) 2000
79. Vatanen, Virpi: Experimental studies by EPR and theoretical studies by DFT calculations of α-amino-9,10-anthraquinone radical anions and cations in solution. (37 pp.) 2000
80. Kotilainen, Risto: Chemical changes in wood during heating at 150-260 °C. (57 pp.) 2000
81. Nissinen, Maija: X-ray structural studies on weak, non-covalent interactions in supramolecular compounds. (69 pp.) 2001
82. Wegelius, Elina: X-ray structural studies on self-assembled hydrogen-bonded networks and metallosupramolecular complexes. (84 pp.) 2001
83. Paasivirta, Jaakko (Ed.): CEOEC'2001, Fifth Finnish-Russian Seminar: Chemistry and Ecology of Organo-Element Compounds. (163 pp.) 2001
84. Kiljunen, Toni: Theoretical studies on spectroscopy and

atomic dynamics in rare gas solids. (56 pp.) 2001

85. Du, Jin: Derivatives of dextran: synthesis and applications in oncology. (48 pp.) 2001
86. Koivisto, Jari: Structural analysis of selected polychlorinated persistent organic pollutants (POPs) and related compounds. (88 pp.) 2001
87. Feng, Zhinan: Alkaline pulping of non-wood feedstocks and characterization of black liquors. (54 pp.) 2001
88. Halonen, Markku: Lahon havupuun käyttö sulfaattiprosessin raaka-aineena sekä havupuun lahontorjunta. (90 pp.) 2002
89. Falábu, Dezsö: Synthesis, conformational analysis and complexation studies of resorcarene derivatives. (212 pp.) 2001
90. Lehtovuori, Pekka: EMR spectroscopic studies on radicals of ubiquinones Q-*n*, vitamin K_3 and vitamine E in liquid solution. (40 pp.) 2002
91. Perkkalainen, Paula: Polymorphism of sugar alcohols and effect of grinding on thermal behavior on binary sugar alcohol mixtures. (53 pp.) 2002
92. Ihalainen, Janne: Spectroscopic studies on light-harvesting complexes of green plants and purple bacteria. (42 pp.) 2002
93. Kunttu, Henrik, Kiljunen, Toni (Eds.): 4th International Conference on Low Temperature Chemistry. (159 pp.) 2002
94. Väisänen, Ari: Development of methods for toxic element analysis in samples with environmental concern by ICP-AES and ETAAS. (54 pp.) 2002
95. Luostarinen, Minna: Synthesis and characterisation of novel resorcarene derivatives. (200 pp.) 2002
96. Louhelainen, Jarmo: Changes in the chemical composition and physical properties of wood and nonwood black liquors during heating. (68 pp.) 2003
97. Lahtinen, Tanja: Concave hydrocarbon cyclophane π-prismands. (65 pp.) 2003
98. Laihia, Katri (Ed.): NBC 2003, Symposium on Nuclear, Biological and Chemical Threats – A Crisis Management Challenge. (245 pp.) 2003
99. Oasmaa, Anja: Fuel oil quality properties of wood-based pyrolysis liquids. (32 pp.) 2003
100. Virtanen, Elina: Syntheses, structural characterisation, and cation/anion recognition properties of nano-sized bile acid-based host molecules and their precursors. (123 pp.) 2003
101. Nättinen, Kalle: Synthesis and X-ray structural studies of organic and metallo-organic supramolecular systems. (79 pp.) 2003
102. Lampiselkä, Jarkko: Demonstraatio lukion kemian opetuksessa. (285 pp.) 2003
103. Kallioinen, Jani: Photoinduced dynamics of $Ru(dcbpy)_2(NCS)_2$ – in solution and on nanocrystalline titanium dioxide thin films. (47 pp.) 2004
104. Valkonen, Arto (Ed.): VII Synthetic Chemistry Meeting and XXVI Finnish NMR Symposium. (103 pp.) 2004

105. Vaskonen, Kari: Spectroscopic studies on atoms and small molecules isolated in low temperature rare gas matrices. (65 pp.) 2004
106. Lehtovuori, Viivi: Ultrafast light induced dissociation of $Ru(dcbpy)(CO)_2I_2$ in solution. (49 pp.) 2004
107. Saarenketo, Pauli: Structural studies of metal complexing Schiff bases, Schiff base derived *N*-glycosides and cyclophane π-prismands. (95 pp.) 2004
108. Paasivirta, Jaakko (Ed.): CEOEC'2004, Sixth Finnish-Russian Seminar: Chemistry and Ecology of Organo-Element Compounds. (147 pp.) 2004
109. Suontamo, Tuula: Development of a test method for evaluating the cleaning efficiency of hard-surface cleaning agents. (96 pp.) 2004
110. Güneş, Minna: Studies of thiocyanates of silver for nonlinear optics. (48 pp.) 2004
111. Ropponen, Jarmo: Aliphatic polyester dendrimers and dendrons. (81 pp.) 2004
112. Vu, Mân Thi Hong: Alkaline pulping and the subsequent elemental chlorine-free bleaching of bamboo (*Bambusa procera*). (69 pp.) 2004
113. Mansikkamäki, Heidi: Self-assembly of resorcinarenes. (77 pp.) 2006
114. Tuononen, Heikki M.: EPR spectroscopic and quantum chemical studies of some inorganic main group radicals. (79 pp.) 2005
115. Kaski, Saara: Development of methods and applications of laser-induced plasma spectroscopy in vacuum ultraviolet. (44 pp.) 2005
116. Mäkinen, Riika-Mari: Synthesis, crystal structure and thermal decomposition of certain metal thiocyanates and organic thiocyanates. (119 pp.) 2006
117. Ahokas, Jussi: Spectroscopic studies of atoms and small molecules isolated in rare gas solids: photodissociation and thermal reactions. (53 pp.) 2006
118. Busi, Sara: Synthesis, characterization and thermal properties of new quaternary ammonium compounds: new materials for electrolytes, ionic liquids and complexation studies. (102 pp.) 2006
119. Mäntykoski, Keijo: PCBs in processes, products and environment of paper mills using wastepaper as their raw material. (73 pp.) 2006
120. Laamanen, Pirkko-Leena: Simultaneous determination of industrially and environmentally relevant aminopolycarboxylic and hydroxycarboxylic acids by capillary zone electrophoresis. (54 pp.) 2007
121. Salmela, Maria: Description of oxygen-alkali delignification of kraft pulp using analysis of dissolved material. (71 pp.) 2007
122. Lehtovaara, Lauri: Theoretical studies of atomic scale impurities in superfluid ^{4}He. (87 pp.) 2007
123. Rautiainen, J. Mikko: Quantum chemical calculations of structures, bonding, and spectroscopic properties of some sulphur and selenium iodine cations. (71 pp.) 2007
124. Nummelin, Sami: Synthesis, characterization, structural and

retrostructural analysis of self-assembling pore forming dendrimers. (286 pp.) 2008

125. Sopo, Harri: Uranyl(VI) ion complexes of some organic aminobisphenolate ligands: syntheses, structures and extraction studies. (57 pp.) 2008
126. Valkonen, Arto: Structural characteristics and properties of substituted cholanoates and *N*-substituted cholanamides. (80 pp.) 2008
127. Lähde, Anna: Production and surface modification of pharmaceutical nano- and microparticles with the aerosol flow reactor. (43 pp.) 2008
128. Beyeh, Ngong Kodiah: Resorcinarenes and their derivatives: synthesis, characterization and complexation in gas phase and in solution. (75 pp.) 2008
129. Välisaari, Jouni, Lundell, Jan (Eds.): Kemian opetuksen päivät 2008: uusia oppimisympäristöjä ja ongelmalähtöistä opetusta. (118 pp.) 2008
130. Myllyperkiö, Pasi: Ultrafast electron transfer from potential organic and metal containing solar cell sensitizers. (69 pp.) 2009
131. Käkölä, Jaana: Fast chromatographic methods for determining aliphatic carboxylic acids in black liquors. (82 pp.) 2009
132. Koivukorpi, Juha: Bile acid-arene conjugates: from photoswitchability to cancer cell detection. (67 pp.) 2009
133. Tuuttila, Tero: Functional dendritic polyester compounds: synthesis and characterization of small bifunctional dendrimers and dyes. (74 pp.) 2009
134. Salorinne, Kirsi: Tetramethoxy resorcinarene based cation and anion receptors: synthesis, characterization and binding properties. (79 pp.) 2009
135. Rautiainen, Riikka: The use of first-thinning Scots pine (*Pinus sylvestris*) as fiber raw material for the kraft pulp and paper industry. (73 pp.) 2010
136. Ilander, Laura: Uranyl salophens: synthesis and use as ditopic receptors. (199 pp.) 2010
137. Kiviniemi, Tiina: Vibrational dynamics of iodine molecule and its complexes in solid krypton - Towards coherent control of bimolecular reactions? (73 pp.) 2010
138. Ikonen, Satu: Synthesis, characterization and structural properties of various covalent and non-covalent bile acid derivatives of N/O-heterocycles and their precursors. (105 pp.) 2010
139. Siitonen, Anni: Spectroscopic studies of semiconducting single-walled carbon nanotubes. (56 pp.) 2010
140. Raatikainen, Kari: Synthesis and structural studies of piperazine cyclophanes – Supramolecular systems through Halogen and Hydrogen bonding and metal ion coordination. (69 pp.) 2010
141. Leivo, Kimmo: Gelation and gel properties of two- and three-component Pyrene based low molecular weight organogelators. (116 pp.) 2011
142. Martiskainen, Jari: Electronic energy transfer in light-harvesting complexes isolated from *Spinacia oleracea* and from three

photosynthetic green bacteria *Chloroflexus aurantiacus*, *Chlorobium tepidum*, and *Prosthecochloris aestuarii*. (55 pp.) 2011

143. Wichmann, Oula: Syntheses, characterization and structural properties of [O,N,O,X´] aminobisphenolate metal complexes. (101 pp.) 2011
144. Ilander, Aki: Development of ultrasound-assisted digestion methods for the determination of toxic element concentrations in ash samples by ICP-OES. (58 pp.) 2011
145. The Combined XII Spring Meeting of the Division of Synthetic Chemistry and XXXIII Finnish NMR Symposium. Book of Abstracts. (90 pp.) 2011
146. Valto, Piia: Development of fast analysis methods for extractives in papermaking process waters. (73 pp.) 2011
147. Andersin, Jenni: Catalytic activity of palladium-based nanostructures in the conversion of simple olefinic hydro- and chlorohydrocarbons from first principles. (78 pp.) 2011
148. Aumanen, Jukka: Photophysical properties of dansylated poly(propylene amine) dendrimers. (55 pp.) 2011
149. Kärnä, Minna: Ether-functionalized quaternary ammonium ionic liquids – synthesis, characterization and physicochemical properties. (76 pp.) 2011
150. Jurček, Ondřej: Steroid conjugates for applications in pharmacology and biology. (57 pp.) 2011
151. Nauha, Elisa: Crystalline forms of selected Agrochemical actives: design and synthesis of cocrystals. (77 pp.) 2012
152. Ahkola, Heidi: Passive sampling in monitoring of nonylphenol ethoxylates and nonylphenol in aquatic environments. (92 pp.) 2012
153. Helttunen, Kaisa: Exploring the self-assembly of resorcinarenes: from molecular level interactions to mesoscopic structures. (78 pp.) 2012
154. Linnanto, Juha: Light excitation transfer in photosynthesis revealed by quantum chemical calculations and exiton theory. (179 pp.) 2012
155. Roiko-Jokela, Veikko: Digital imaging and infrared measurements of soil adhesion and cleanability of semihard and hard surfaces. (122 pp.) 2012
156. Noponen, Virpi: Amides of bile acids and biologically important small molecules: properties and applications. (85 pp.) 2012
157. Hulkko, Eero: Spectroscopic signatures as a probe of structure and dynamics in condensed-phase systems – studies of iodine and gold ranging from isolated molecules to nanoclusters. (69 pp.) 2012
158. Lappi, Hanna: Production of Hydrocarbon-rich biofuels from extractives-derived materials. (95 pp.) 2012
159. Nykänen, Lauri: Computational studies of Carbon chemistry on transition metal surfaces. (76 pp.) 2012
160. Ahonen, Kari: Solid state studies of pharmaceutically important molecules and their derivatives. (65 pp.) 2012

161. Pakkanen, Hannu: Characterization of organic material dissolved during alkaline pulping of wood and non-wood feedstocks. (76 pp.) 2012
162. Moilanen, Jani: Theoretical and experimental studies of some main group compounds: from closed shell interactions to singlet diradicals and stable radicals. (80 pp.) 2012
163. Himanen, Jatta: Stereoselective synthesis of Oligosaccharides by *De Novo* Saccharide welding. (133 pp.) 2012
164. Bunzen, Hana: Steroidal derivatives of nitrogen containing compounds as potential gelators. (76 pp.) 2013
165. Seppälä, Petri: Structural diversity of copper(II) amino alcohol complexes. Syntheses, structural and magnetic properties of bidentate amino alcohol copper(II) complexes. (67 pp.) 2013
166. Lindgren, Johan: Computational investigations on rotational and vibrational spectroscopies of some diatomics in solid environment. (77 pp.) 2013
167. Giri, Chandan: Sub-component self-assembly of linear and non-linear diamines and diacylhydrazines, formulpyridine and transition metal cations. (145 pp.) 2013
168. Riisiö, Antti: Synthesis, Characterization and Properties of Cu(II)-, Mo(VI)- and U(VI) Complexes With Diaminotetraphenolate Ligands. (51 pp.) 2013
169. Kiljunen, Toni (Ed.): Chemistry and Physics at Low Temperatures. Book of Abstracts. (103 pp.) 2013
170. Hänninen, Mikko: Experimental and Computational Studies of Transition Metal Complexes with Polydentate Amino- and Aminophenolate Ligands: Synthesis, Structure, Reactivity and Magnetic Properties. (66 pp.) 2013
171. Antila, Liisa: Spectroscopic studies of electron transfer reactions at the photoactive electrode of dye-sensitized solar cells. (53 pp.) 2013
172. Kemppainen, Eeva: Mukaiyama-Michael reactions with α-substituted acroleins – a useful tool for the synthesis of the pectenotoxins and other natural product targets. (190 pp.) 2013
173. Virtanen, Suvi: Structural Studies of Dielectric Polymer Nanocomposites. (49 pp.) 2013
174. Yliniemelä-Sipari, Sanna: Understanding The Structural Requirements for Optimal Hydrogen Bond Catalyzed Enolization – A Biomimetic Approach.(160 pp.) 2013
175. Leskinen, Mikko V: Remote β-functionalization of β'-keto esters. (105 pp.) 2014
176. 12th European Conference on Research in Chemistry Education (ECRICE2014). Book of Abstracts. (166 pp.) 2014
177. Peuronen, Anssi: N-Monoalkylated DABCO-Based N-Donors as Versatile Building Blocks in Crystal Engineering and Supramolecular Chemistry. (54 pp.) 2014
178. Perämäki, Siiri: Method development for determination and recovery of rare earth elements from industrial fly ash. (88 pp.) 2014

179. Chernyshev, Alexander, N.: Nitrogen-containing ligands and their platinum(IV) and gold(III) complexes: investigation and basicity and nucleophilicity, luminescence, and aurophilic interactions. (64 pp.) 2014
180. Lehto, Joni: Advanced Biorefinery Concepts Integrated to Chemical Pulping. (142 pp.) 2015
181. Tero, Tiia-Riikka: Tetramethoxy resorcinarenes as platforms for fluorescent and halogen bonding systems. (61 pp.) 2015
182. Löfman, Miika: Bile acid amides as components of microcrystalline organogels. (62 pp.) 2015
183. Selin, Jukka: Adsorption of softwood-derived organic material onto various fillers during papermaking. (169 pp.) 2015
184. Piisola, Antti: Challenges in the stereoselective synthesis of allylic alcohols. (210 pp.) 2015
185. Bonakdarzadeh, Pia: Supramolecular coordination polyhedra based on achiral and chiral pyridyl ligands: design, preparation, and characterization. (65 pp.) 2015
186. Vasko, Petra: Synthesis, characterization, and reactivity of heavier group 13 and 14 metallylenes and metalloid clusters: small molecule activation and more. (66 pp.) 2015
187. Topić, Filip: Structural Studies of Nano-sized Supramolecular Assemblies. (79 pp.) 2015
188. Mustalahti, Satu: Photodynamics Studies of Ligand-Protected Gold Nanoclusters by using Ultrafast Transient Infrared Spectroscopy. (58 pp.) 2015
189. Koivisto, Jaakko: Electronic and vibrational spectroscopic studies of gold-nanoclusters. (63 pp.) 2015
190. Suhonen, Aku: Solid state conformational behavior and interactions of series of aromatis oligoamide foldamers. (68 pp.) 2016
191. Soikkeli, Ville: Hydrometallurgical recovery and leaching studies for selected valuable metals from fly ash samples by ultrasound-assisted extraction followed by ICP-OES determination. (107 pp.) 2016
192. XXXVIII Finnish NMR Symposium. Book of Abstracts. (51 pp.) 2016
193. Mäkelä, Toni: Ion Pair Recognition by Ditopic Crown Ether Based bis-Urea and Uranyl Salophen Receptors. (75 pp.) 2016
194. Lindholm-Lehto, Petra: Occurrence of pharmaceuticals in municipal wastewater treatment plants and receiving surface waters in Central and Southern Finland. (98 pp.) 2016
195. Härkönen, Ville: Computational and Theoretical studies on Lattice Thermal conductivity and Thermal properties of Silicon Clathrates. (89 pp.) 2016
196. Tuokko, Sakari: Understanding selective reduction reactions with heterogeneous Pd and Pt: climbing out of the black box. (85 pp.) 2016
197. Nuora, Piia: Monitapaustutkimus LUMA-Toimintaan liittyvissä oppimisympäristöissä tapahtuvista kemian oppimiskokemuksista. (171 pp.) 2016

198. Kumar, Hemanathan: Novel Concepts on The Recovery of By-Products from Alkaline Pulping. (61 pp.) 2016
199. Arnedo-Sánchez, Leticia: Lanthanide and Transition Metal Complexes as Building Blocks for Supramolecular Functional Materials. (227 pp.) 2016
200. Gell, Lars: Theoretical Investigations of Ligand Protected Silver Nanoclusters. (134 pp.) 2016
201. Vaskuri, Juhani: Oppiennätyksistä opetussuunnitelman perusteisiin - lukion kemian kansallisen opetussuunnitelman kehittyminen Suomessa vuosina 1918-2016. (314 pp.) 2017
202. Lundell Jan, Kiljunen Toni (Eds.): 22nd Horizons in Hydrogen Bond Research. Book of Abstracts. 2017
203. Turunen, Lotta: Design and construction of halogen-bonded capsules and cages. (61 pp.) 2017
204. Hurmalainen, Juha: Experimental and computational studies of unconventional main group compounds: stable radicals and reactive intermediates. (88 pp.) 2017
205. Koivistoinen Juha: Non-linear interactions of femtosecond laser pulses with graphene: photo-oxidation, imaging and photodynamics. (68 pp.) 2017
206. Chen, Chengcong: Combustion behavior of black liquors: droplet swelling and influence of liquor composition. (39 pp.) 2017
207. Mansikkamäki, Akseli: Theoretical and Computational Studies of Magnetic Anisotropy and Exchange Coupling in Molecular Systems. (190 p. + included articles) 2018.
208. Tatikonda, Rajendhraprasad: Multivalent N-donor ligands for the construction of coordination polymers and coordination polymer gels. (62 pp.) 2018
209. Budhathoki, Roshan: Beneficiation, desilication and selective precipitation techniques for phosphorus refining from biomass derived fly ash. (64 pp.) 2018
210. Siitonen, Juha: Synthetic Studies on 1-azabicyclo[5.3.0]decane Alkaloids. (140 pp.) 2018
211. Ullah, Saleem: Advanced Biorefinery Concepts Related to Non-wood Feedstocks. (57 pp.) 2018
212. Ghalibaf, Maryam: Analytical Pyrolysis of Wood and Non-Wood Materials from Integrated Biorefinery Concepts. (106 pp.) 2018

DEPARTMENT OF CHEMISTRY, UNIVERSITY OF JYVÄSKYLÄ
DISSERTATIONS PUBLISHED IN THE JYU DISSERTATIONS RESEARCH SERIES

1. Bulatov, Evgeny: Synthetic and structural studies of covalent and non-covalent interactions of ligands and metal center in platinum(II) complexes containing 2,2′-dipyridylamine or oxime ligands. (58 pp.) 2019. JYU Dissertations 70.
2. Annala, Riia: Conformational Properties and Anion Complexes of Aromatic Oligoamide Foldamers. (80 pp.) 2019. JYU Dissertations 84.
3. Isoaho, Jukka Pekka: Dithionite Bleaching of Thermomechanical Pulp - Chemistry and Optimal Conditions. (73 pp.) 2019. JYU Dissertations 85.
4. Nygrén, Enni: Recovery of rubidium from power plant fly ash. (98 pp.) 2019. JYU Dissertations 136.
5. Kiesilä, Anniina: Supramolecular chemistry of anion-binding receptors based on concave macromolecules. (68 pp.) 2019. JYU Dissertations 137.
6. Sokolowska, Karolina: Study of water-soluble p-MBA-protected gold nanoclusters and their superstructures. (60 pp.) 2019. JYU Dissertations 167.
7. Lahtinen, Elmeri: Chemically Functional 3D Printing: Selective Laser Sintering of Customizable Metal Scavengers. (71 pp.) 2019. JYU Dissertations 175.
8. Larijani, Amir: Oxidative reactions of cellulose under alkaline conditions. (102 pp.) 2020. JYU Dissertations 217.
9. Kolari, Kalle: Metal-metal contacts in late transition metal polymers. (60 pp.) 2020. JYU Dissertations 220.
10. Kauppinen, Minttu: Multiscale computational investigation of catalytic properties of zirconia supported noble metals. (87 pp.) 2020. JYU Dissertations 231.